A SIMPLE CRITERION FOR THREE-DIMENSIONAL FLOW SEPARATION IN AXIAL COMPRESSORS

By

VAI-MAN LEI

B.Eng., Mechanical Engineering, McGill University, 1996
M. Eng., Mechanical Engineering, McGill University, 1998

Submitted to the Department of Aeronautics and Astronautics
in Partial Fulfillment of the Requirements for the Degree of

Doctor of Philosophy

at the

Massachusetts Institute of Technology

February 2006

Author: _____
Department of Aeronautics and Astronautics
September 16, 2005

Certified by: _____
Zoltan S. Spakovszky, Ph.D.
C. S. Draper Associate Professor of Aeronautics and Astronautics
Chair, Thesis Committee

Certified by: _____
Edward M. Greitzer, Ph.D.
H. Nelson Slater Professor of Aeronautics and Astronautics

Certified by: _____
Gerald R. Guenette, Jr., Sc.D.
Principal Research Engineer

Accepted by: _____
Jaime Peraire, Ph.D.
Professor of Aeronautics and Astronautics
Chair, Committee on Graduate Students

A SIMPLE CRITERION FOR THREE-DIMENSIONAL FLOW SEPARATION IN AXIAL COMPRESSORS

By

VAI-MAN LEI

Submitted to the Department of Aeronautics and Astronautics
on September 16, 2005 in Partial Fulfillment of the
Requirements for the Degree of
Doctor of Philosophy

Abstract

Most modern blade designs in axial-flow compressors diffuse the flow efficiently over 20% to 80% of blade span and it is the endwall regions that set the limits in compressor performance. This thesis addresses the estimation, control and mitigation of three-dimensional separation near the hub corner in axial- flow compressors.

A simple method to estimate the onset of hub corner separation in compressor blade passages has been developed. A parameter is defined to quantify the combined effect of adverse pressure gradient and secondary flow which are the two main mechanisms contributing to the formation of three-dimensional flow separation. There is a critical value of the parameter at which the onset of three-dimensional flow separation occurs. Data from existing research and production compressors show the generality of the separation criterion.

The new parameter captures the alleviating effect of boundary layer skew on three-dimensional flow separation. Using this concept, a flow control scheme has been developed to mitigate hub corner separation by injecting spanwise momentum from the blade suction surface. A proof of concept flow control experiment demonstrates a reduction in stagnation pressure loss coefficient of 8% with an injection flow of 0.8% of the cascade mass flow.

Thesis Supervisor: Zoltan S. Spakovszky

Title: C. S. Draper Associate Professor of Aeronautics and Astronautics

My help comes from the Lord, the Maker of heaven and earth.

Acknowledgements

The Ph.D. process at MIT is an eye opening experience. I would like to express my gratitude to the people who offered help during my stay at MIT.

First, I would like to thank my advisor Prof. Zolti Spakovszky for the opportunity of this interesting project and his support throughout the research. I am privileged to have Prof. Edward Greitzer in my thesis committee who pushes things in the right direction with insightful comments and questions. I want to thank Dr. Jerry Guenette for his technical and non-technical advices on different issues. The patience and guidance of the thesis committee is much appreciated. Many thanks to Dr. Yifang Gong and Dr. Ali Merchant for their helpful suggestions, technical assistance and encouragement.

Outside MIT, I would like to thank Dr. Steven Wellborn for his interest in the project, helpful comments on the D parameter and also support by providing data for the analysis. I am grateful to Dr. Anthony Strazisar who provided much help in the fabrication of the actuated blades for the flow control experiment, Dr. Michael Hathaway who provided data of the NASA LSAC and Dr. J. P. Longley for technical information on his hub cavity leakage experiment.

Much gratitude is extended to the staff at the MIT Gas Turbine Lab who make things happen, in particular Viktor Dubrowski who taught me much about the art of machining among many other things, Jimmy Letendre and Jack Costa for their help with the equipments and setup of the experiment, Paul Warren for keeping the computers cool and running, Mary McDavitt and Holly Anderson for taking care of the acquisition of equipments and financial issues, and Lori Martinez for covering the rest so that I can focus on doing research.

I would like to thank Amie Bonner, James Otten, Jeanmarc Freuler for their assistance in the construction of the linear cascade experiment, and especially Nayden Kambouchev who contributed much to the data acquisition system.

The occupants of Room 31-256, Dr. Hyung-Soo Moon, Dr. Boris Sirakov, Juan Castiella, Nathan Fitzgerald, and Jerome Bert are source of technical assistance, friendship and encouragement (especially when I witness your graduation). I want to thank Dr. Duc Vo in particular who gave useful suggestions in critical moments even before I officially started at MIT. Besides my best friends Chiang Juay Teo and Benny Yam, I also want to thank Dong Won Choi and Jinwook Lee for the fun we have in the GTL.

There are many people that I want to thank at MIT: Prof. Earll Murman for serving as my Minor Advisor, Prof. Mark Drela for his time in the general examination, Donald Weiner for his help with the water cutter and Jennifer Craig for reading the thesis manuscript, Dr. C. S. Tan and Parthiv Shah for their helpful comments to my defense presentation, the support and encouragement from my qualifying exam study group with Dr. Vincent Sidwell, Dr. Joe Lee and Sean Bradshaw. I also want to thank my old McGill friends Dr. David Venditti and Giuseppe Alescio who helped me much in my 'back to school' move.

I am deeply indebted to my parents and parents in law for their love and unconditional support. I owe my sister Skylar a big thank you for coming all the way from Calgary to help editing my manuscript and to help with the moving in the most critical period of the thesis writing. I also want to thank my brother in law Tommy for taking care of my hair during the past four years. The sincerest thank you from the bottom of my heart goes to my wife Siu-Mui, who sacrificed much so that I can keep moving forward. I cannot imagine going through the toughest time in the Ph.D. process without her love and support.

This research was funded by NASA Glenn Research Center under grant NAG3-2678 monitored by Dr. Gerard E. Welch whose support is gratefully acknowledged.

Table of Contents

List of Figures

List of Tables

Nomenclature

Symbols

A	area
A	Johnston's A parameter
AR	aspect ratio L/c
B	slope of polar plot associated with boundary layer skewness
c	blade chord length
C_p	static pressure coefficient $(p_2 - p_1)/(1/2\ \rho U_1^2)$
C_{pi}	ideal static pressure coefficient
C_{pt}	stagnation pressure coefficient $(p_{t\,ref} - p_t)/(1/2\ \rho U_1^2)$
D	D parameter
DF	diffusion factor
i	incidence
l	distance along blade camber line measured from the leading edge
L	blade span
$\dot{m}$	mass flow rate
p	static pressure
q	dynamic pressure $\frac{1}{2}\ \rho U^2$
Re	Reynolds number based on chord and average free stream velocity
s	blade pitch
s	entropy
S	S indicator
u	streamwise velocity
U	freestream velocity
v	cross-stream velocity
v_s	characteristic magnitude of secondary flow velocity
v_y	tangential velocity
x	distance in the axial direction
z	distance from endwall in the spanwise direction
α	flow angle
δ	boundary layer thickness
δ^*	displacement thickness
ε	flow turning angle
γ	stagger angle
μ	dynamic viscosity
θ	blade camber angle
θ	momentum thickness
ρ	density
σ	solidity c/s
ζ	streamwise vorticity
ω	loss coefficient $(\overline{p}_{t1}^{\,M} - \overline{p}_{t2}^{\,M})/(1/2\ \rho U_1^2)$
ψ_z	Zweifel loading coefficient based on inlet dynamic pressure
Ω	normal vorticity

Subscripts

1	upstream of blade row
2	downstream of blade row
act	actuation
i	ideal condition with no viscous effect
j	injection or leakage
ref	reference condition
t	stagnation condition
y	tangential direction

Superscripts

-M	mass averaged

Acronyms

HCS	hub corner separation
LE	leading edge
LSAC	low speed axial compressor at the NASA Glenn research center
PS	pressure surface
SS	suction surface
SSS	suction surface separation
TE	trailing edge

Chapter 1 Introduction

Flow separation is detrimental to compressor performance. It decreases efficiency, lowers static pressure rise capability and contributes to instability in compressors. With the demand for higher pressure ratio per stage, prevention of flow separation becomes more challenging. Although current design methodologies enable an almost separation-free flow away from the endwall, three-dimensional flow separation near the endwall regions limits further improvement in performance.

Therefore, it is important to account for the endwall flow behavior as early in the design process as possible. Simple criteria such as the diffusion factor (Lieblein, 1959) are available to evaluate compressor blade designs with respect to two-dimensional flow separation. In contrast, no simple method exists to evaluate the onset of three-dimensional separation near endwalls. As a result, there is motivation to develop a preliminary design criterion for three-dimensional flow separation limits. This dissertation discusses the development and potential applications of such an evaluation criterion.

1.1 Background

This dissertation focuses on separation near the endwall regions where tip leakage is absent: the hub of a rotor, the hub and the casing of a shrouded stator. The objective of this section is to provide the basics of three-dimensional hub region flow separation.

Three-dimensional flow separation in the hub region of an axial compressor is commonly known as hub corner separation or hub corner stall. Hub corner separation which involves flow separation on both the endwall and blade suction surface, is different in nature from two-dimensional flow separation on a blade element. In two-dimensional flow separation, the boundary layer separates from the blade suction surface under the influence of the increasing pressure in the streamwise direction. For hub corner separation, secondary flow contributes in addition to this adverse pressure gradient. The mechanism for secondary flow in a blade passage is as follows. A cross passage pressure gradient $(\partial p / \partial n)$ is developed as the flow follows the curvature of the passage. The cross passage pressure gradient balances with the

centripetal acceleration and since the endwall fluid has a lower velocity but experiences the same pressure gradient as the freestream, the radius of curvature of the endwall streamlines is reduced. The endwall fluid thus accumulates at the hub suction corner region, making it more vulnerable to flow separation (Figure 1.1).

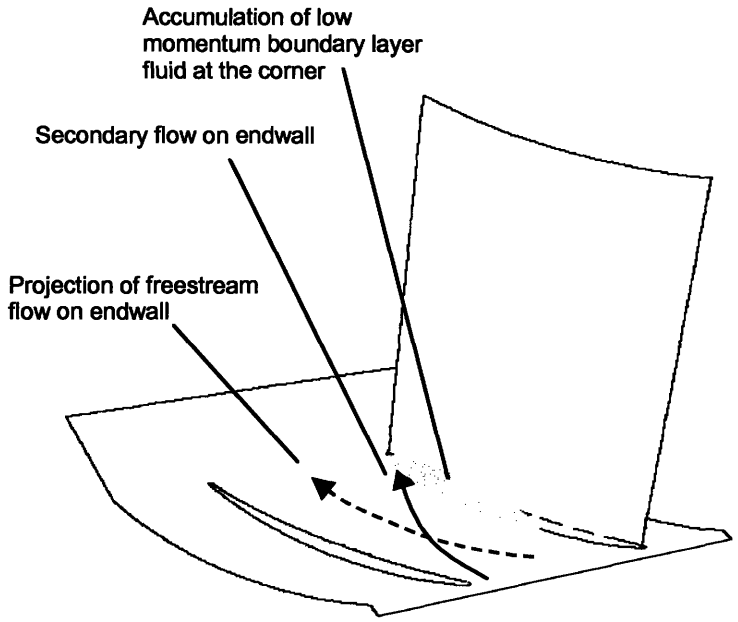

Figure 1.1 Action of secondary flow in a blade passage.

The structure of hub corner separation is different from separation confined to the blade suction surface. Streamlines near solid surfaces, or limiting streamlines, reveal the features of hub corner separation as shown in Figure 1.2. There is a region of three-dimensional flow separation encompassed by separation lines on the blade suction surface and the endwall. The characteristic feature of hub corner separation is a region of flow reversal with a recirculation zone near the endwall. The separation region blocks the blade passage, reducing the flow area and lowering the static pressure rise capability of the compressor.

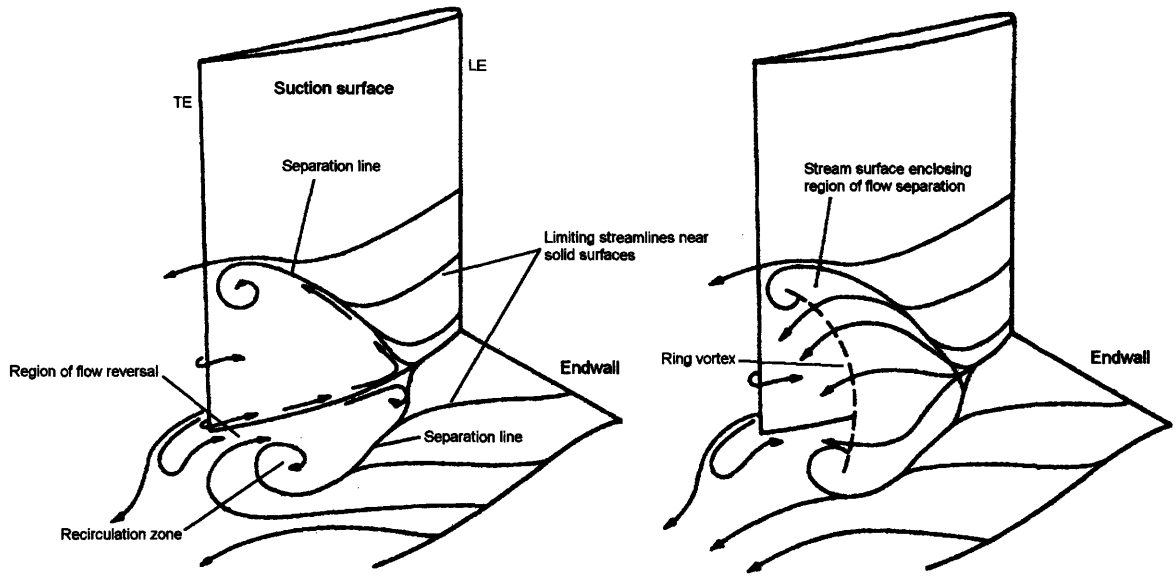

Figure 1.2 Limiting streamlines showing flow features of hub corner separation (left). The separation region behaves as a bluff body that blocks the blade passage (right) (After Schulz et al, 1990).

The influence of hub corner separation on the performance of axial flow compressors can also be seen from stagnation pressure measurements downstream of the separation. Figure 1.3 shows that the onset of hub corner separation increases the size of the high loss region.

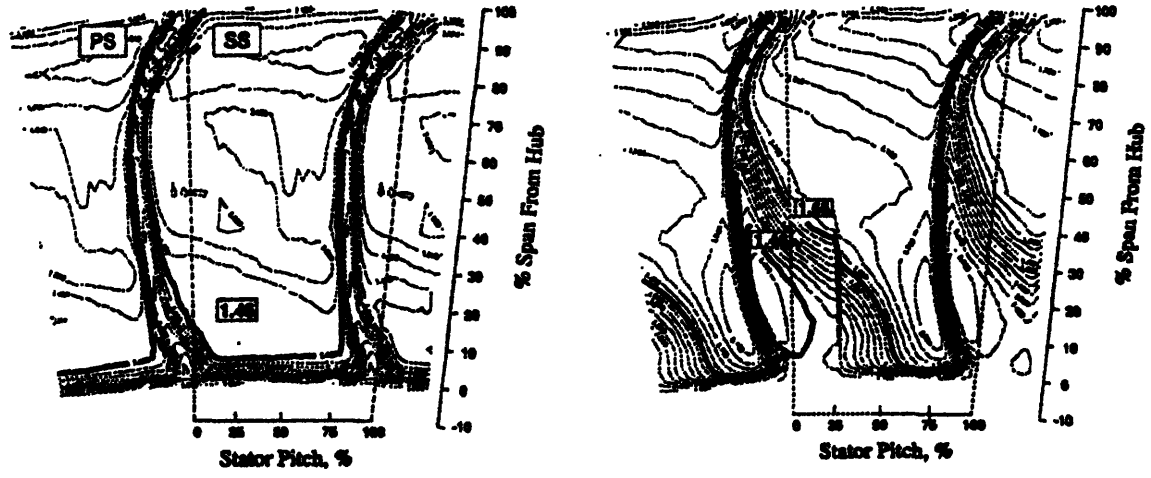

Figure 1.3 Impact of hub corner separation on compressor performance (Barankiewicz and Hathaway 1998). Contours of stagnation pressure coefficient at stator exit are shown. Loading increases from design (left) to near stall (right). The onset of hub corner separation increases the size of the high loss region.

1.2 Previous Work

The basic mechanisms governing the formation of hub corner separation were described over fifty years ago. In a feasibility study of endwall separation control by flow removal, Mertz (1954) proposed that adverse pressure gradient and cross flow in a blade passage are responsible for separation of boundary layer in the endwall region. Based on the results of a series of experimental studies, Horlock et al. (1964) concluded that it is the *combined* effect of adverse pressure gradient and secondary flow that causes hub corner separation. The relevant previous work on hub corner separation is summarized below in four areas:

1. The impact of hub corner separation on compressor performance
2. The topology of hub corner separation
3. The prediction of hub corner separation with numerical methods
4. The mitigation of hub corner separation

1.2.1 Impact of Hub Corner Separation on Compressor Performance

Joslyn and Dring (1985) assessed the impact of hub corner separation on the performance of a two-stage research compressor. Their measurements showed that the growth of three-dimensional flow separation, from the design condition to the near stall condition, increased the loss coefficient near the endwall (from 0 to 5% span) by a factor of two. The blockage associated with the separation reduced the circumferentially averaged axial velocity by 20% over the lower 25% span. They suggested that the blockage effect due to hub corner separation in the rotor increases the incidence on the downstream stator, promoting hub corner separation in the stator. They further argued that this detrimental effect cascades downstream.

Cumpsty commented that the compressor in this experiment was not representative of a commercial compressor and questioned the general validity of the results (Joslyn and Dring, 1985). More

recent studies at NASA Glenn Research Center revealed that hub corner separation does exist in a well-designed and highly efficient compressor (Barankiewicz and Hathaway, 1998). This compressor was designed to simulate the flow field of a representative high speed multistage compressor with blading modeled after that used in General Electric's Energy Efficient Engine (E^3). Despite design features such as end bend and dihedral to reduce loss in the endwall regions, hub corner separation appeared when loading increased beyond the design level. The size of the three-dimensional flow separation increased with the compressor loading as shown in Figure 1.3.

1.2.2 Topology of Hub Corner Separation

Schulz and Gallus (1988) conducted experiments in an annular compressor cascade and identified the characteristic features of the three-dimensional flow separation. These features include a region of flow reversal and a recirculation zone near the endwall as depicted in Figure 1.2.

Schulz et al. (1990) reported measurements of the three-dimensional flow separation in an annular compressor cascade with a moving row of cylinders to simulate the effect of an upstream rotor. They proposed a flow structure of hub corner separation based on measurement and flow visualization results. In the proposed topology, the separation region is closed off from the freestream by a stream surface bounded by the separation lines on the endwall and on the blade suction surface as shown in Figure 1.2. They suggested that a ring vortex emanating from the recirculation zone on the endwall is associated with the flow reversal inside the separation region. Since then, other studies have confirmed the observation of this topology (e.g., Hah and Loellbach, 1997 and Weber et al., 2002).

1.2.3 Prediction of Hub Corner Separation with Numerical Methods

Computational Fluid Dynamics (CFD) provides additional information about the flow field not directly available from experiments. Gallus et al. (1991) used CFD to study the secondary flow and vortex motion associated with the three-dimensional flow separation in an annular cascade. Based on the velocity

vectors computed from the numerical results, a vortex structure inside the separation region was proposed. Hah and Loellbach (1997) analyzed hub corner separation in a subsonic compressor stator and in a transonic compressor rotor. The numerical result confirmed the transportation of low momentum fluid by secondary flow. They also observed the flow topology proposed by Schulz et al (1990).

Research showed that current CFD tools are capable of capturing the essential features of hub corner separation in an axial compressor. Luecke et al. (1996) validated an implicit three-dimensional Navier-Stokes code using the data by Schulz and Gallus (1988). Weber et al. (2002) studied the flow separation in a transonic linear compressor cascade, both numerically and experimentally. The numerical results compared well to the experiment and demonstrated that the code is capable of capturing the characteristic features of hub corner separation, namely a region of flow reversal and a recirculation zone near the endwall. The numerical simulations of Hah and Loellbach (1997) also captured these flow features and agreed well with the experiments by Schulz and Gallus (1988) as depicted in Figure 1.4.

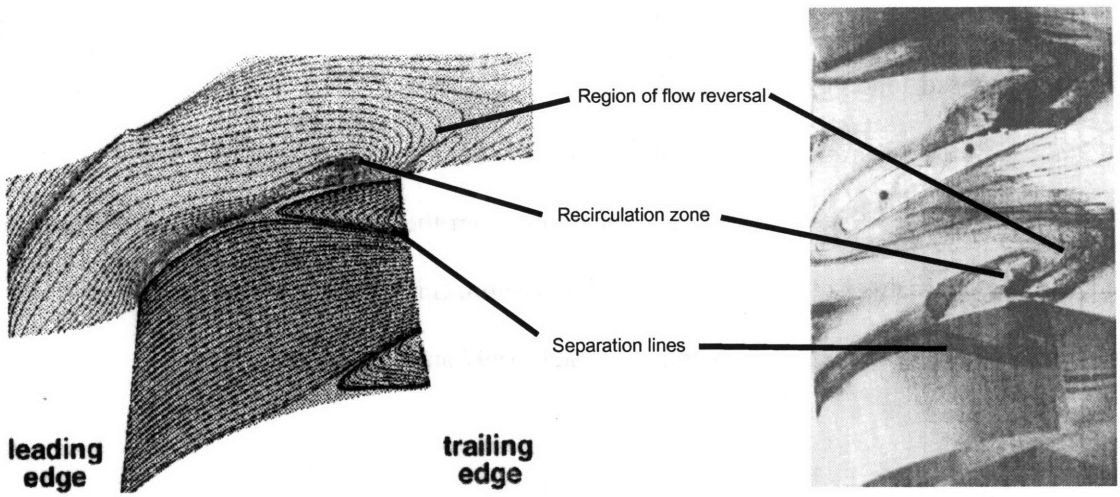

Figure 1.4 CFD tools are capable of capturing the features of hub corner separation. Limiting streamlines from a computation (Hah and Loellbach, 1997) compare well with the experiment (Schulz and Gallus, 1988).

1.2.4 Mitigation of Hub Corner Separation

Hub corner separation is recognized as a source of high loss and blockage that degrades the performance of axial compressors. As a result, strategies have been developed to mitigate the separation. Two major categories of mitigation methods have been reported in the literature: modifications to blade geometry and flow control. These are summarized below.

1.2.4.1 Modifications to Blade Geometry

Dong et al. (1987) experimentally demonstrated the mitigation of hub corner separation with a clearance at the hub end of the stator blade. The leakage from the blade pressure side re-energized the boundary layer on the suction corner and suppressed the separation. A drawback of this method is the degraded structural integrity of the stator blade as cantilevered blades are more susceptible to vibration.

Breugelmans et al. (1984) studied the mitigation of corner separation by introducing dihedral to the blades in a linear compressor cascade. Positive dihedral with the suction surface making an obtuse angle with the endwall set up a pressure gradient in the spanwise direction that suppressed secondary flow and decreased the size of the three-dimensional flow separation. Shang et al. (1993) also demonstrated the mitigation of hub corner separation by introducing dihedral to the blades in a linear cascade. To obtain the benefit of positive dihedral at both endwalls, the blades were bow shaped as shown in Figure 1.5. Weingold et al. (1995) conducted experiments with bowed stator blades which reduced loss due to hub corner separation and raised the efficiency of the compressor by 1%.

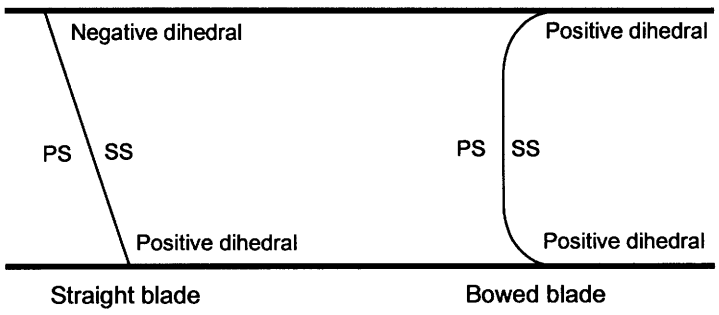

Figure 1.5 Dihedral in a stator with straight blade (left) and bowed blade (right). Positive dihedral can be obtained at both endwalls with a bowed blade.

Tweedt et al. (1986) showed in a two-stage research compressor that leading edge sweep near the hub reduces loss near the endwall region. They explained that the loss reduction is due to the suppression of boundary layer growth as the sweep draws higher momentum fluid to the suction corner. Gümmer et al. (2000) analyzed the combined effects of sweep and dihedral with CFD in an annular compressor cascade and compared the performance of a conventional stator with one featuring sweep and dihedral. The results showed suppression of hub corner separation at the design condition with the latter design. However, at the near stall condition, the three-dimensional separation was mitigated but not completely eliminated.

1.2.4.2 Flow Control

The term flow control is used to refer to the use of fluidic actuation such as suction or injection to change the behavior of a flow field. Lord et al. (2000) discussed the various possibilities for, and potential benefits of, flow control in gas turbine engines. Compressors operate under a wide range of conditions, and the blades are usually designed to operate most efficiently at the design condition. Methods to mitigate hub corner separation with blade geometry modification are less effective at off-design conditions (e.g. Gümmer et al, 2000). With flow control, the amount of actuation can be adjusted to accommodate for different operating conditions and can even be turned off when it is not needed.

Flow control was shown to mitigate hub corner separation by Peacock (1965), who demonstrated that the three-dimensional flow separation could be suppressed by applying boundary layer suction at the corner between hub endwall and blade suction surface. In a linear compressor cascade, Peacock eliminated the hub corner separation by removing 0.32% of the flow.

Stratford (1972) also studied the benefit of boundary layer suction near the endwall corner. He achieved a 25% reduction in loss by removing 1.3% of the flow at the hub corner of a compressor cascade. These ideas were not pursued for application in axial compressors due to the complexity of the pneumatic system involved. Proper location of the suction slot in the stator is also difficult due to restriction in physical access to the hub area.

The most recently published research on the application of flow control to improve compressor performance were by Culley et al. (2003) and Kirtley et al. (2004) who focused on separation control of the blade suction surface in highly loaded axial compressors. Culley et al. (2003) explored the benefit of unsteady blowing on the suction surface while Kirtley et al. (2004) applied steady blowing. Culley et al. (2003) reported 25% reduction in loss based on the stagnation pressure difference across the blade row with injection of 1% of the compressor through flow, and Kirtley et al. (2004) demonstrated 1% improvement in stage efficiency using an injection rate of 1% of the compressor flow. The results also suggest that the effect of blowing from the suction surface is relatively small on the endwall flow.

1.3 Research Objectives

The primary goal of this research is to develop a simple method that allows a designer to quickly evaluate a blade passage design in terms of the onset of hub corner separation. The proposed evaluation method consists of a parameter that measures the tendency of a blade passage to three-dimensional separation, and a separation criterion that indicates the onset of flow separation.

The second goal is to develop a flow control strategy to mitigate three-dimensional flow separation suitable for axial flow compressor applications where physical access to the hub area is limited.

The specific technical objectives of this research are to:

- Develop a parameter that captures and quantifies the effects of the mechanisms that contribute to three-dimensional flow separation in axial flow compressors,
- Develop a parameter that measures the size and strength of hub corner separation,
- Identify a criterion for hub corner separation and assess its generality,
- Design and experimentally demonstrate a flow control strategy suitable for mitigating hub corner separation in axial compressors.

1.4 Technical Approach

To achieve the primary objective of this research, three-dimensional, steady CFD tools were used to simulate the flow field of a large number of geometries spanning the design space with and without hub corner separation. The data was processed to identify a criterion for three-dimensional flow separation, with the aid of two metrics which quantify the size of the separation and the strength of the governing mechanisms respectively. Data from available literature were then used to assess the generality of this criterion.

A flow control strategy to mitigate hub corner separation was developed from the separation criterion. With this, a flow control device was designed and built, and its effectiveness was assessed experimentally in a linear compressor cascade facility.

1.5 Thesis Organization

The identification of a criterion for three-dimensional flow separation is discussed in Chapter 2. Two parameters important to the identification of the criterion are introduced: the S indicator which quantifies the size and strength of hub corner separation, and the D parameter which characterizes the physical mechanisms leading to separation. The validity of the assumptions that are made to simplify the analysis is assessed after the criterion is identified. Chapter 3 evaluates the generality of the separation criterion with experimental data. A discussion on the limitations of the proposed criteria is also presented. Chapter 4 discusses the possibility of using the injection of spanwise momentum as a flow control strategy to mitigate hub corner separation in axial compressors. The effectiveness of this concept is demonstrated with a linear cascade experiment. Chapter 5 summarizes the findings of this research. Recommendations on how to make the separation criterion more suitable for compressor design applications are proposed.

1.6 Thesis Contributions

The major contributions of the research documented in this dissertation are:

- A new method to quantify the size and strength of hub corner separation in axial compressors,
- A new parameter to quantify the tendency of a blade design to three-dimensional flow separation,
- A simple criterion for three-dimensional flow separation in axial compressors,
- A novel flow control idea to mitigate hub corner separation which is suitable for axial flow compressor applications.

Chapter 2 A New Criterion for Three-Dimensional Flow Separation in Axial Compressors

This chapter introduces a simple method to evaluate compressor blade designs in terms of three-dimensional flow separation. The method consists of a parameter (the D parameter) that quantifies the tendency of a blade design to hub corner separation. A criterion for three-dimensional flow separation is proposed based on this method and an indicator that quantifies the size and strength of three-dimensional flow separation (the S indicator).

The S indicator quantifies the size and strength of the flow separation based on the loss in blade loading associated with the flow separation. The D parameter characterizes the tendency towards hub corner separation from the combined effect of adverse pressure gradient and secondary flow. It is hypothesized that the onset of three-dimensional flow separation is signified by an abrupt drop in blade loading as indicated by the S indicator when a critical value of D is reached. Analysis of blade passages with different values of D by numerically solving the steady three-dimensional Reynolds Averaged Navier-Stokes equations shows that a critical D does exist, and it is suggested to be a criterion for hub corner separation.

The first section of this chapter defines the S indicator and the D parameter and discusses their physical significance. An analysis on blade passages with different values of D that leads to the identification of the separation criterion is then described. The applicability and limitation of the separation criterion is then evaluated in terms of endwall boundary layer thickness, Reynolds number, blade aspect ratio and endwall boundary layer skew. The potential application of the D parameter for the design of flow control is also discussed.

2.1 Indicator to Quantify the Size of Hub Corner Separation

The development of a simple method to evaluate compressor blade design in terms of the onset of hub corner separation involves three steps:

- Step 1: Formulation of a method to quantify the severity of the separation.
- Step 2: Formulation of a method to quantify the tendency of a blade design towards hub corner separation.
- Step 3: Identification of a criterion for three-dimensional separation with the aid of steps 1 and 2.

The first step, quantifying the size and strength of hub corner separation, is elucidated in the following section. The flow is assumed to be incompressible, steady and fully turbulent in all that follows.

Most data in the literature related to the size and strength of hub corner separation are qualitative in nature. Flow visualizations from experiments and CFD simulations are often used to depict the severity of the separation. Although this topological approach provides details of the flow field (e.g. Schulz et al., 1990), a metric to quantify the severity of the separation is necessary to facilitate the analysis of compressor blade designs in terms of the separation.

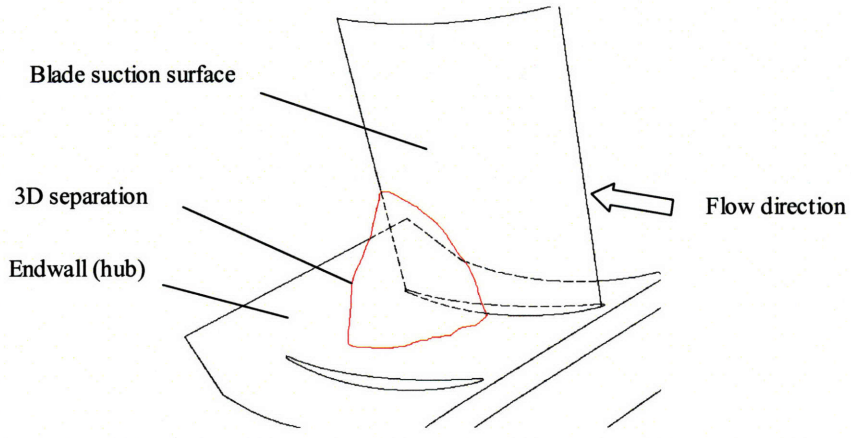

Figure 2.1 Schematic of hub corner separation in an axial compressor blade passage.

One distinct feature of the flow field of hub corner separation is the increase in the chordwise extent of the separation as the distance from the endwall decreases (Figure 2.1). The consequence is a decrease in blade loading from midspan to the hub. The idea, therefore, is to quantify the severity and extent of the three-dimensional separation using the reduction in blade loading.

At midspan, the flow is assumed to be free of separation. Taking this loading as a reference, the reduction in loading due to three-dimensional flow separation can be measured. An indicator that quantifies the size and strength of hub corner separation is thus defined as

$$S(z) = \frac{\left(\int_{LE}^{TE}(p_{ps} - p_{ss})dl\right)_{L/2} - \left(\int_{LE}^{TE}(p_{ps} - p_{ss})dl\right)_{z}}{\frac{1}{2}\rho U_1^{\,2} c}. \qquad (2.1)$$

The S indicator is essentially the difference in blade loading between midspan (z = L/2) and a location at a distance z from the endwall. The difference in loading is normalized by the inlet dynamic pressure and the blade chord. The S indicator can be compactly represented in terms of the Zweifel loading coefficient defined as

$$\psi_z = \frac{\int_0^1 (p_{ps} - p_{ss})d(x/c)}{p_{t1} - p_2}. \qquad (2.2)$$

The Zweifel coefficient compares the actual blade loading to the ideal blade loading as shown in Figure 2.2.

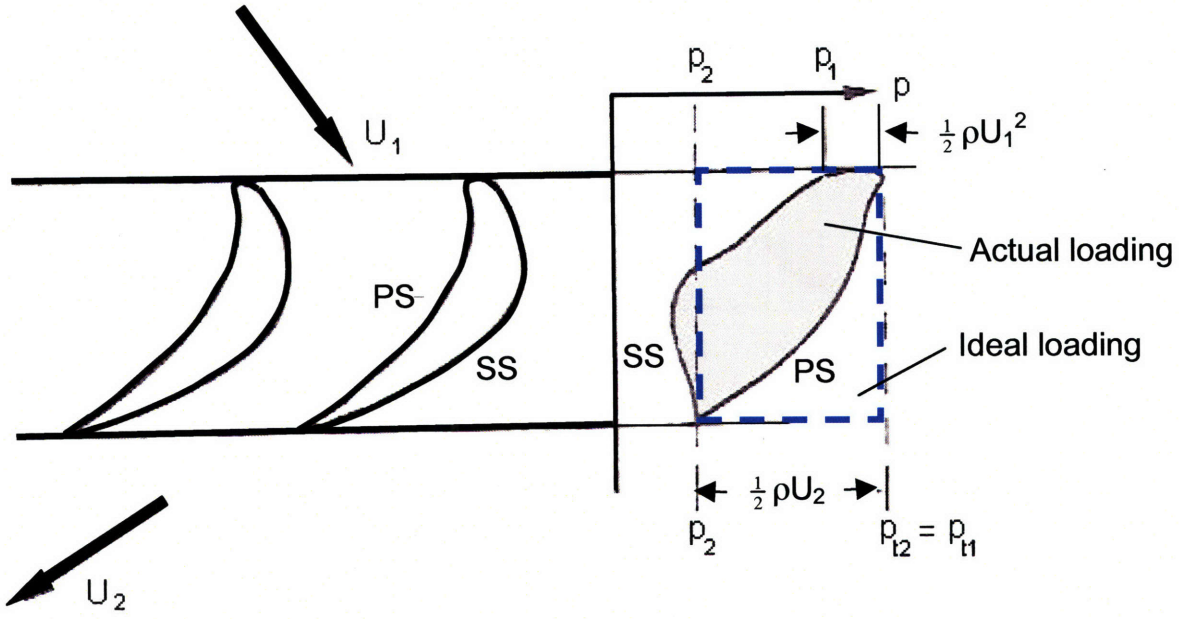

Figure 2.2 Definition of the Zweifel loading coefficient. It compares the actual loading (area shaded in grey) to the ideal loading (area enclosed by the dotted rectangle) (Adopted from Dixon, 1978).

Here, this coefficient is modified to compare the blade loading to the difference between the stagnation pressure and the static pressure at the inlet

$$\psi_z = \frac{\int_0^1 (p_{ps} - p_{ss}) d(x/c)}{p_{t1} - p_1}. \tag{2.3}$$

For incompressible flow, the denominator is the upstream dynamic pressure

$$\psi_z = \frac{\int_0^1 (p_{ps} - p_{ss}) d(x/c)}{\frac{1}{2}\rho U_1^2}. \tag{2.4}$$

The S parameter can thus be written in terms of the modified Zweifel coefficient as

$$S(z) = \psi_z\big|_{L/2} - \psi_z\big|_z. \tag{2.5}$$

The magnitude of S is a function of the distance z from the endwall. Figure 2.3 depicts the extent of the three-dimensional separation on the suction surface with limiting streamlines calculated using CFD. The S indicator of the flow field versus distance from the endwall is shown on the right.

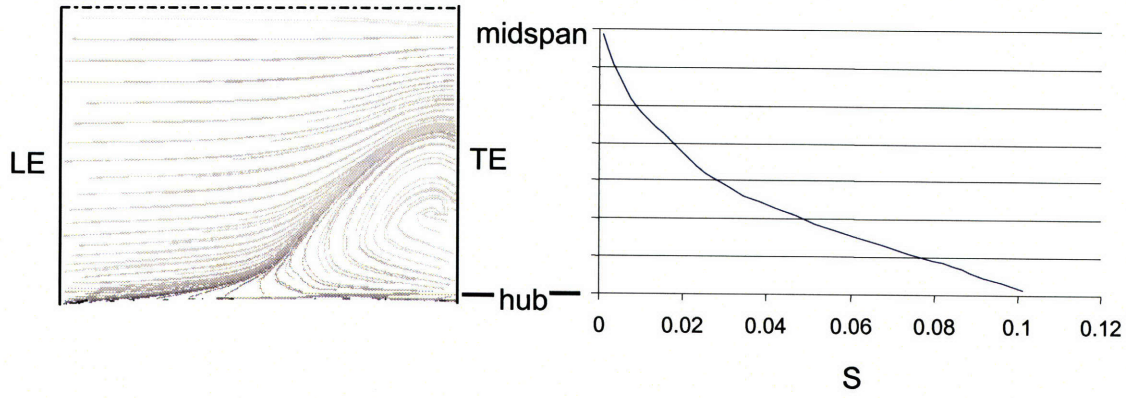

Figure 2.3 Limiting streamlines showing the extent of hub corner separation on the suction surface (left) and the corresponding distribution of the S indicator (right). Blade passage has aspect ratio 1.36, stagger angle 30°, camber 42° and solidity of 1.

The size and strength of hub corner separation can now be quantified using the S parameter. From a practical point of view, it is desirable to characterize the separation with a single S indicator instead of representing the entire three-dimensional separation by the distribution of S as shown in Figure 2.3. To use a single S value, the following questions must be addressed: 1) At what distance from the endwall should S be calculated to ensure appropriate comparison of S between different blade designs[1]? 2) Is there any limitation on the choice of spanwise location to calculate S?

To make the S parameters comparable for different blade designs, the endwall distance should be specified non-dimensionally. The choice of length scale is the blade chord as it scales the physical extent of three-dimensional flow separation. The distribution of S in z/c, of two geometrically similar blades with different chord lengths, are shown in Figure 2.4. The data collapse suggests the S indicator be calculated at consistent z/c for appropriate comparison. The specific value of z/c to be used in the calculation of S is related to the second question from above which is discussed next.

[1] The integral of the S indicator was also evaluated but it did not correlate well with the D parameter introduced later.

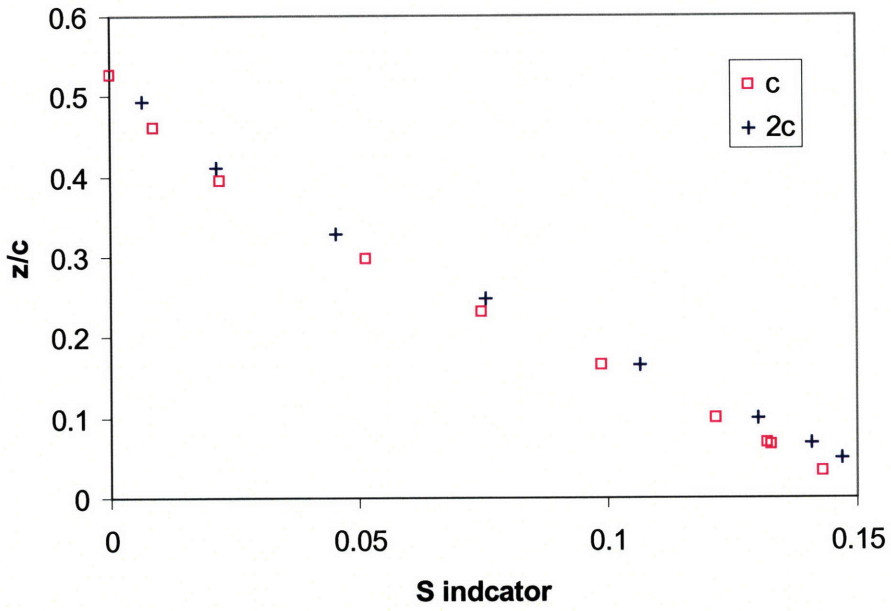

Figure 2.4 S indicator as a function of z/c for two geometrically similar blades with different chord lengths.

Recall that the S indicator measures the size and strength of hub corner separation as indicated by the change in Zweifel coefficient with respect to the reference value at midspan. From Figure 2.3, the value of S increases from zero at midspan to a maximum at the endwall. It would be desirable to calculate S as close to the endwall as possible. However, if one gets too close to the endwall, S picks up the loading change due to flow turning from the endwall to the suction surface. This effect is not a consequence of separation and misrepresents the size and strength of three-dimensional separation indicated by S.

In the blade passage, boundary layer fluid overturns toward the blade suction surface due to the effect of secondary flow. Upon reaching the suction surface, the boundary layer fluid turns a second time as it travels from the endwall to the suction surface. The pressure gradient associated with this change in flow direction, which is shown in Figure 2.5, influences the local blade loading and hence affects the value of S. For larger turning (e.g. higher camber), this effect is stronger and hence has a greater effect on the S indicator.

Examination of the flow field of hub corner separation from numerical simulation reveals that the spanwise influence of the pressure gradient due to this turning effect is about half the thickness of the incoming endwall boundary layer. It is thus recommended to calculate the S indicator at a distance of at least half the thickness of the incoming boundary layer from the endwall.

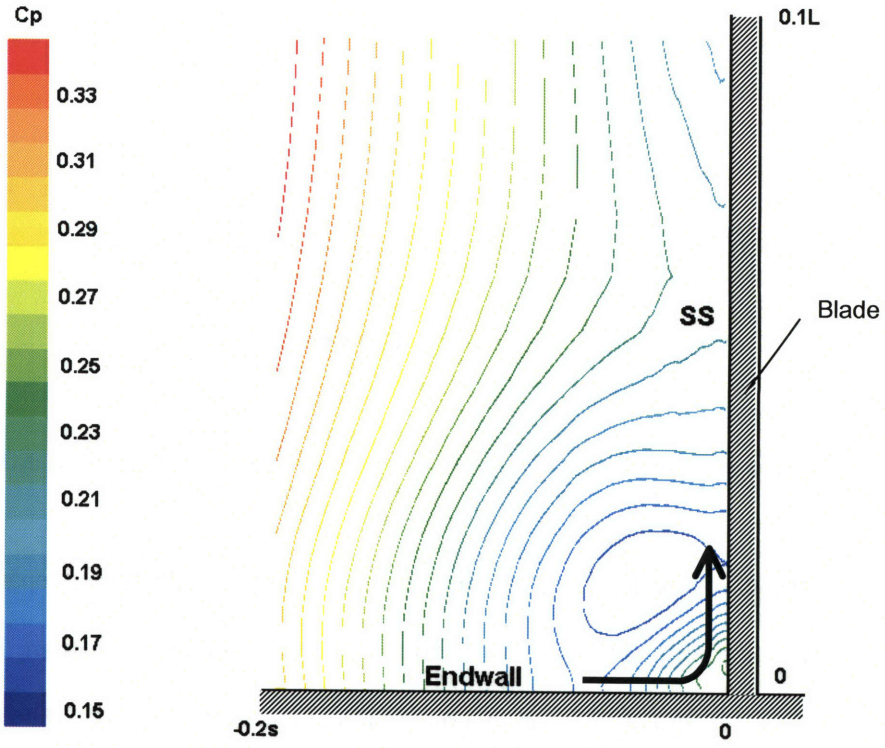

Figure 2.5 Pressure field associated with secondary flow. Axial view of a blade passage near the hub corner is shown. The arrow indicates direction of secondary flow.

Summarizing the discussion above, the S indicator should be evaluated at a consistent z/c for appropriate comparison between different blade designs. Moreover, the S parameter should be evaluated at a minimum distance of half the thickness of the incoming endwall boundary layer in order to avoid the influence of the flow turning effect due to secondary flow. To obtain a standard z/c for the calculation of the S indicator throughout this dissertation, the NASA Low Speed Axial Compressor (LSAC), a representative axial compressor design featuring end bend and dihedral, is used as a reference. At the near stall condition, the thickness of the endwall boundary layer is 7% of chord (Wellborn, 1996). The non-

dimensional spanwise location z/c of 0.1 is used in the calculation of the S indicator. In this dissertation, the S indicator is thus defined as follows unless otherwise specified.

$$S = \psi_z\big|_{z/L=0.5} - \psi_z\big|_{z/c=0.1} \tag{2.6}$$

With this definition, S measures the size and strength of hub corner separation with the difference in loading between two spanwise locations, namely at midspan and at 10% of chord from the endwall.

2.2 Parameter to Quantify the Governing Mechanisms of Hub Corner Separation

In a blade passage where the flow is incompressible, steady and fully turbulent, the parameters that are relevant to the size of hub corner separation are upstream velocity (U), density (ρ), viscosity (μ), chord (c), blade pitch (s), camber angle (θ), stagger angle (γ), inlet (α_1) and exit (α_2) flow angles, and blade span (L). There are three non-dimensional groups in addition to the angles:

$$\mathrm{S} = \mathrm{S}\left(\frac{\rho v c}{\mu}, \frac{s}{c}, \frac{L}{c}, \theta, \gamma, \alpha_1, \alpha_2\right). \tag{2.7}$$

The first group is the Reynolds number based on chord, the second group is the inverse of the solidity and the third group is the blade aspect ratio. Examination of the separation flow field with CFD shows that Reynolds number (for fully turbulent flow) and aspect ratio have little effect on the physical size of the separation over the range of parameters examined (the influence of Reynolds number and aspect ratio will be further discussed in Sections 2.4). With this information, the functional form of the S indicator for the size of hub corner separation becomes

$$\mathrm{S} = \mathrm{S}\left(\frac{1}{\sigma}, \theta, \gamma, \alpha_1, \alpha_2\right). \tag{2.8}$$

The next step is to quantify the physical mechanisms that govern the size and strength of the separation with the independent variables. The objective is to obtain a single parameter that indicates how close a blade design is to three-dimensional flow separation.

In an axial compressor, the function of the stator is to deswirl and to diffuse the flow from the upstream rotor. It is thus suggested to decompose the blade passage into a rectangular diffuser and a curved channel. This decomposition also facilitates the analysis since the physical mechanisms governing hub corner separation are adverse pressure gradient and secondary flow as identified previously. Characterization of the governing mechanisms as represented by these two components is examined next.

In a planar diffuser, the static pressure of the flow rises as the flow area increases. The static pressure rise coefficient is defined as

$$C_p = \frac{p_2 - p_1}{\frac{1}{2}\rho U_1^2}. \tag{2.9}$$

Using Bernoulli's equation and continuity, the ideal static pressure rise coefficient can be expressed in terms of the inlet to exit area ratio

$$C_{pi} = 1 - \left(\frac{A_1}{A_2}\right)^2. \tag{2.10}$$

For two-dimensional flow, the ratio of inlet to exit area can be expressed in terms of the flow angles such that the ideal static pressure rise coefficient can be written as

$$C_{pi} = 1 - \left(\frac{\cos\alpha_1}{\cos\alpha_2}\right)^2. \tag{2.11}$$

The inlet angle is defined by the upstream condition while the exit angle depends on a number of factors in addition to inlet angle. The exit flow does not always follow the blade surface and deviates from the blade exit angle due to viscous effects. For this analysis, it is assumed that the flow always follows the blade surface and viscous effects in the diffuser are negligible such that the static pressure rise coefficient is ideal. Assuming that the camber line is circular, the exit angle is

$$\alpha_2 = \gamma - \frac{\theta}{2}. \tag{2.12}$$

The isentropic static pressure rise coefficient thus becomes

$$C_{pi} = 1 - \left(\frac{\cos \alpha_1}{\cos\left(\gamma - \frac{\theta}{2} \right)} \right)^2 . \tag{2.13}$$

Rather than the level of static pressure rise, the distance over which the static pressure rise occurs (i.e. the adverse pressure gradient) is the parameter that governs the flow separation. Using the chord as the characteristic length over which the pressure rise occurs, a pressure gradient can be defined as

$$\frac{dC_{pi}}{dx} = \frac{1 - \left(\frac{\cos \alpha_1}{\cos\left(\gamma - \frac{\theta}{2} \right)} \right)^2}{c} . \tag{2.14}$$

The second functional component of a blade passage is a curved channel. As identified previously, secondary flow accumulates low momentum boundary layer fluid near the hub corner and worsens the condition of the boundary layer. To measure this effect, the strength of secondary flow in the blade passage needs to be quantified. From inviscid secondary flow theory, vortex filaments in the boundary layer entering a curved channel are tilted such that streamwise vorticity is developed. Secondary flow theory (Squire and Winter, 1950) suggests that the strength of the secondary vorticity is proportional to the product of the flow turning angle and the width of the channel.

This result is readily applicable to a blade passage where flow turning is the difference between inlet and exit flow angles, and the channel width is the blade pitch. A parameter that characterizes the strength of secondary flow (v_s) in the blade passage can then be defined as

$$v_s = s(\alpha_1 - \alpha_2). \tag{2.15}$$

With the assumptions of a circular camber line and zero deviation, the parameter becomes

$$v_s = s\left(\alpha_1 - \gamma + \frac{\theta}{2} \right). \tag{2.16}$$

The next step is to find a parameter that quantifies the combined effect that governs the formation of hub corner separation. The term dC_{pi}/dx has the dimension of one over length while v_s has the dimension of length. A power law analysis described in Appendix A suggests multiplication of the two parameters to form a non-dimensional parameter that quantifies the combined effect:

$$D = \frac{\left(1-\left(\frac{\cos\alpha_1}{\cos\left(\gamma-\frac{\theta}{2}\right)}\right)^2\right)\left(\alpha_1-\gamma+\frac{\theta}{2}\right)}{\sigma}, \tag{2.17}$$

or more compactly,

$$D = \frac{C_{pi}\varepsilon}{\sigma} \tag{2.18}$$

where $\varepsilon = (\alpha_1-\gamma+\theta/2)$ is the flow turning term.

The D parameter is non-dimensional, and it is a simple parameter that can be readily calculated from the blade row geometry. It is hypothesized that the size and strength of hub corner separation as measured by the S indicator given in equation (2.6) correlates with the D parameter. It is also conjectured that a critical value of the D parameter indicates whether three-dimensional flow separation is present in a blade passage. If these hypotheses are correct, the D parameter gives a simple method to determine whether hub corner separation exists.

2.3 Assessment of the S Indicator and D Parameter

Two parameters important for the identification of a criterion for hub corner separation in axial compressors have been introduced. The S indicator defined as

$$S = \psi_z\big|_{z/L=0.5} - \psi_z\big|_{z/c=0.1} \tag{2.6}$$

measures the size of hub corner separation with the loss in blade loading caused by the separation. The D parameter

$$D = \frac{C_{pi}\varepsilon}{\sigma} \tag{2.18}$$

quantifies the combined effect of adverse pressure gradient and secondary flow in the blade passage which govern the formation of hub corner separation. It is hypothesized that the tendency to hub corner separation increases with the D parameter, and at the onset of three-dimensional flow separation, an abrupt drop in blade loading, indicated by the change in the S indicator, is anticipated. In this section, the validity of this hypothesis and the existence of a criterion for three-dimensional flow separation in axial compressors are examined.

2.3.1 Outline of the CFD Analysis

To establish a three-dimensional separation criterion, it is necessary to populate the S indicator versus D parameter space with various geometries including cases that are free of hub corner separation and also cases that exhibit separations of different size and strength. Simulations of the flow fields with a wide variety of geometries have been performed to achieve this. Prismatic blades with modified NACA 65 thickness distribution on circular camber lines were used. The airfoil chosen is similar to that used in the NASA LSAC compressor in terms of profile and pressure distribution. Figure 2.6 compares a typical airfoil used in this analysis to the airfoil at 20% span of the LSAC stator. The application of the NACA 65 family airfoil with a circular camber line in axial compressor research is well established (Cumpsty, 1989). The cascade geometries allowed rapid and reliable grid generation without sacrificing the physics relevant to hub corner separation. The generality and limitation of the result based on the NACA 65 cascade analysis will be discussed in Chapter 3.

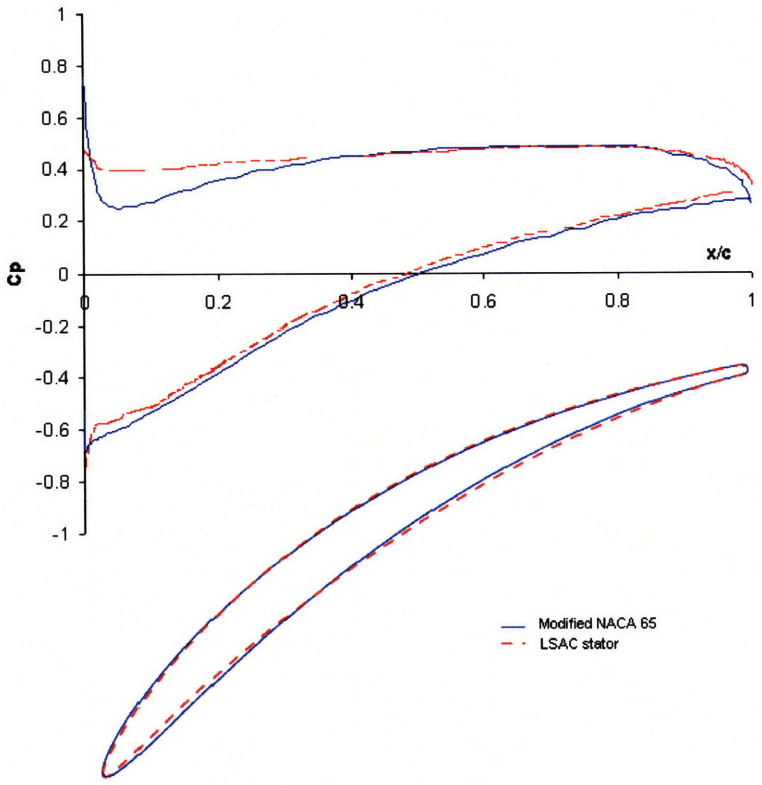

Figure 2.6 Comparison of the modified NACA 65 airfoil and the NASA LSAC airfoil. The airfoil shown has 42° camber and 38° stagger. The airfoil profiles are shown with pressure coefficient calculated using two-dimensional CFD.

The blade camber and stagger angle are the two important variables that determine the geometry of a blade passage. They also determine C_{pi} and ε in the D parameter. Figure 2.6 depicts the combinations of camber and stagger used in the analysis. Basically three different levels of camber at roughly 20°, 40° and 60° created the framework of the matrix. The stagger angles were varied for each level of camber to produce blade passage geometries with different levels of C_{pi} ranging from 0.3 to 0.7. The combination of blade camber and stagger angles covers a wide variety of geometries such as guide vanes with high turning and low C_{pi} and highly loaded blades with moderate turning and high C_{pi}. A case with 90° camber and 5° stagger was also included to examine the combined effect of strong secondary flow and low C_{pi}. For reference, the rectangle in the chart encloses the range of camber and stagger that exists in the literature on hub corner separation.

The solidity in most modern compressors ranges from unity to about 1.5. For the NASA LSAC compressor, the solidity in the rotor varies from 1.05 at the casing to 1.3 at the hub and in the stator the solidity ranges from 1.3 to 1.5. Using this as a reference range for solidity, three levels of solidity at 1.0, 1.5 and 2.0 were chosen for the analysis. The three levels of solidity were applied to each of the geometries shown in Figure 2.7.

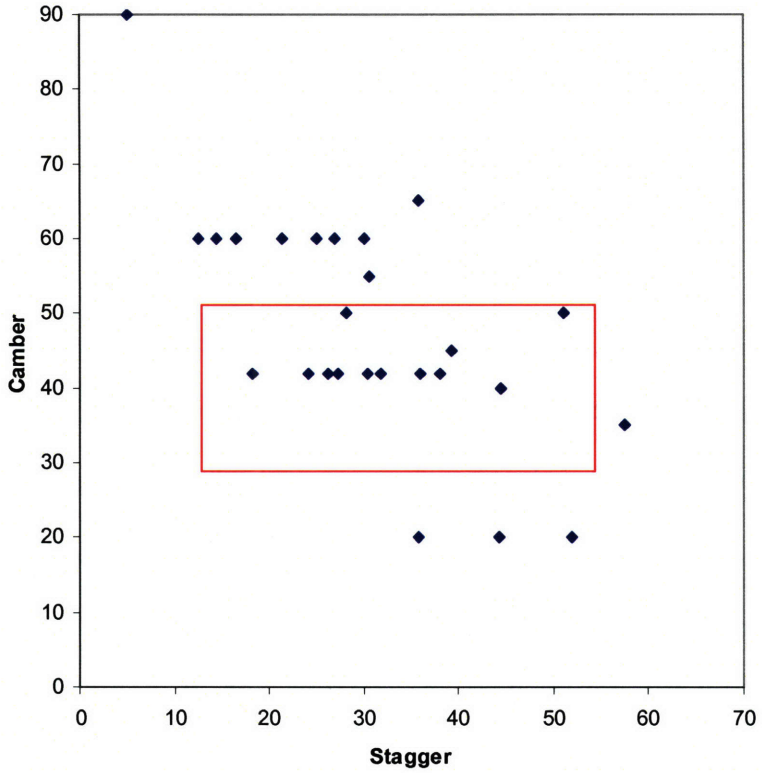

Figure 2.7 Combinations of camber and stagger angle used in the analysis. Angles are shown in degrees. The red rectangle encompasses the range of stagger and camber used in the literature for the study of hub corner separation.

The other variable in the D parameter that was varied in the analysis is the upstream flow angle. For blade profile with a circular camber line, the upstream flow angle can be expressed as

$$\alpha_1 = i + \theta/2 + \gamma \tag{2.19}$$

where i is the incidence angle. Zero incidence means the flow far upstream is aligned to the camber line at the leading edge, and is solely determined by the camber and stagger angles. Since the camber and stagger angles were specified per Figure 2.7, α_1 was changed by varying the incidence. Incidences for

geometries with no hub corner separation were increased by 3° to 5° in an attempt to stall the endwall. On the other hand, incidences for geometries with hub corner separation were reduced by 3° to 6° to reduce the size of the separation.

Since it was hypothesized that Reynolds number and blade aspect ratio have negligible effect on hub corner separation, these two parameters were kept constant in the baseline analysis. The Reynolds number based on chord in a typical compressor is on the order of 10^5 or higher (Cumpsty, 1989). In the NASA LSAC compressor, the average Reynolds number is around 2.5×10^5 and this value was selected as the baseline value. As for the blade aspect ratio, a value of 1.36 based on the LSAC stator was chosen as the baseline value. The effects of Reynolds number and blade aspect ratio will be further discussed in Section 2.4

The typical thickness of endwall boundary layer in an axial compressor is on the order of 10% of chord (Smith, 1970). Taking the NASA LSAC compressor as an example, the thickness of the endwall boundary layer for both the stator and rotor at the increased loading condition is 7% of chord (Wellborn, 1996). A recent experiment by Leishman et al. (2004) on the effect of bleed rate on endwall flow used inlet boundary layer with thickness of 11.2% of chord. So the value of 10% of chord was chosen as a representative value for this analysis. Table 2.1 summarizes the design parameters used in the baseline CFD analysis.

Parameter	Range
Camber	20° – 90°
Stagger	5° – 57°
Solidity	1.0, 1.5, 2.0
Incidence	-6°, -3°, 0°, +3°, +5°
Reynolds number	2.5×10^5
Blade aspect ratio	1.36
Endwall boundary layer	10% of chord

Table 2.1 The design parameters used in the baseline analysis

2.3.2 Description of Numerical Tools used in the CFD Analysis

The numerical tools used in the analysis were commercial CFD packages by Fluent Inc. The GAMBIT CFD preprocessor was used for geometry and grid generation. The FLUENT flow modeling software was used to simulate the flow field and for post-processing the numerical results. This section provides details on how these numerical tools were employed.

FLUENT employs finite-volume numerical methods to solve the governing integral equations for the conservation of mass and momentum. A coupled-implicit solver with second order discretization schemes was chosen because of its robustness and improved accuracy. For turbulence modeling, a k-ε model was employed for its robustness and lesser demand on computing resources compared to the other turbulence models available in FLUENT. All calculations were three-dimensional, incompressible, steady and fully turbulent.

A MATLAB program was written to generate the coordinates of the NACA 65 airfoils. GAMBIT was then used to create the numerical model of the cascade using the blade profile. The endwall region of the cascade was first meshed using quadrilateral and triangular elements with the mesh size refined near solid surfaces to resolve the flow field in the boundary layer. The mesh in the inlet and exit regions was structured while that in the blade passage was unstructured. Figure 2.8 shows the mesh of a typical cascade used in the analysis. The endwall mesh was extruded in the spanwise direction such that the entire computation domain was meshed with hexahedral and wedge elements. The extrusion rate was controlled such that the mesh was more refined near the solid surfaces to resolve the endwall boundary layer. For each computation, only one blade passage was modeled with periodic boundary conditions as depicted in Figure 2.8.

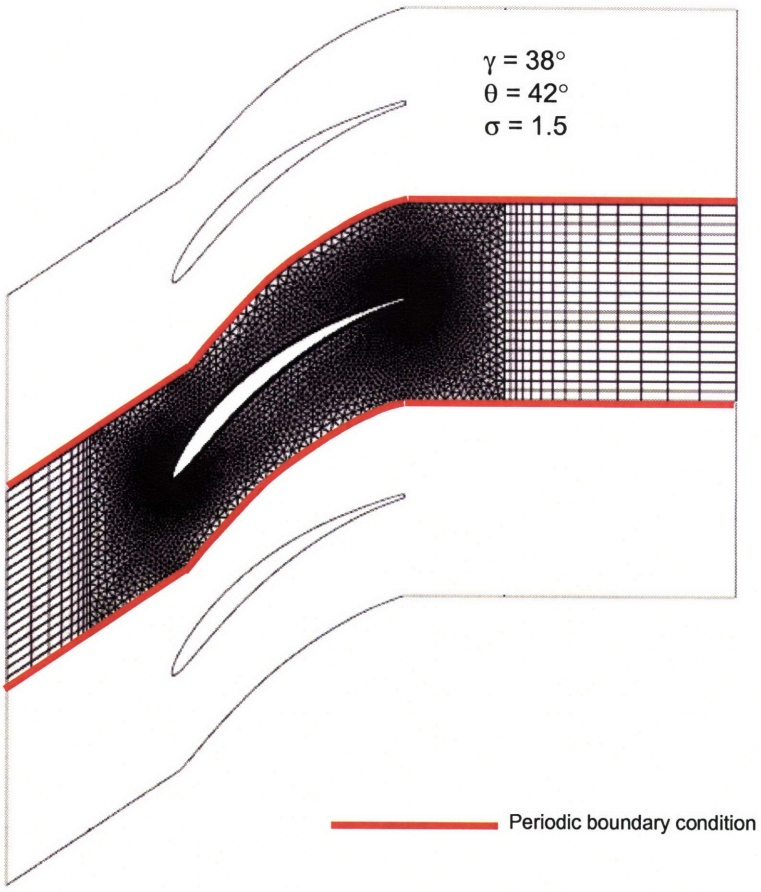

Figure 2.8 The mesh of a cascade with θ = 42°, γ = 38°, σ = 1.5.

To study the effect of computational grid density on the flow field solution, a cascade geometry with 42° camber angle, 38° stagger angle, a solidity of 1.5 and an aspect ratio of 1.36 was examined for three levels of grid density. The three meshes are denoted as coarse, baseline and fine. The maximum number of elements allowed for any given geometry was limited by the memory capacity of the computing system and the fine grid was on the verge of exceeding this limit. The number of elements in the baseline grid was roughly half of that in the fine grid and twice of that in the coarse grid.

Numerical simulations of the flow field at Reynolds number of 2.5×10^5 based on chord length were performed using the three meshes. The numerical solutions with all three meshes revealed hub corner separation. However, the size of the separation regions was slightly different for each case. To compare the performance of the three meshes quantitatively, the S indicator measuring the size and

strength of the separation were calculated. In addition to the S indicators, the mass averaged loss coefficients (ω) were also calculated and compared. The results are tabulated in Table 2.2.

Grid Density	Element Count	S	ω
Coarse	419000	0.08816	0.0728
Baseline	873860	0.1086	0.0855
Fine	1708400	0.1085	0.0849

Table 2.2 CFD calculation of S and ω with grids of different density.

Using the fine mesh as a reference, the S indicator and ω computed using the coarse mesh are 18.7% and 13.6% below the reference values respectively. With the baseline mesh, S and ω are within 0.1% and 0.3% of the reference values respectively. The results indicate that the solution does not change much for element count greater than about 870000. The baseline grid density was thus used in the analysis. Since the mesh in the blade passage was unstructured, the total number of elements varied depending on the geometry, but it remained on the order of 9×10^5.

2.3.3 Correlation Between the S Indicator and the D Parameter, and the D Separation Criterion

In a linear cascade, the static pressure coefficient on the pressure surface only changes slightly from midspan to hub as shown in Figure 2.9. The S indicator can thus be calculated using only the pressure of the suction surface to simplify the computation.

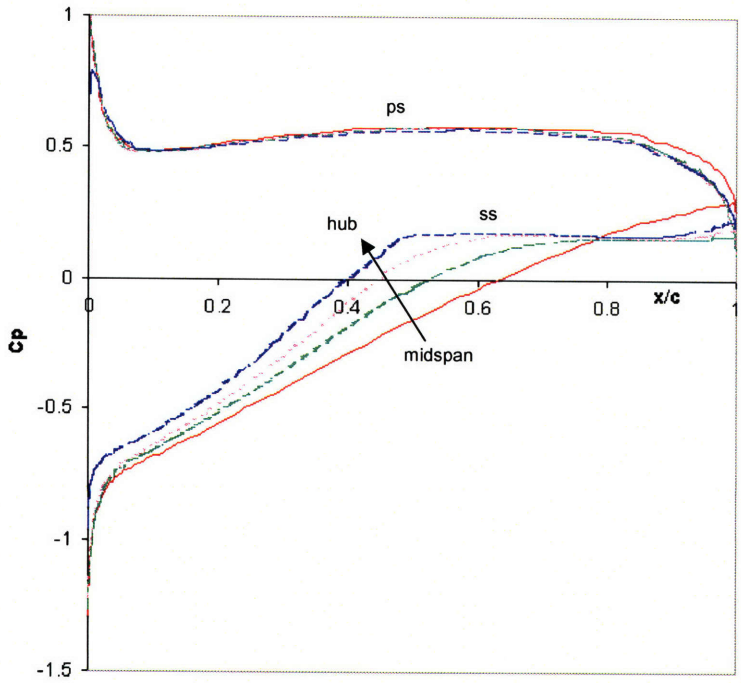

Figure 2.9 Static pressure coefficient at different spanwise locations of a blade passage with hub corner separation. C_p only changes slightly on the pressure surface.

The S indicators from the numerical simulations are plotted against the D parameter for the geometries summarized in Table 2.1. Two distinctive branches can be identified from the plot of S versus D in Figure 2.10. A branch with lower values of S begins at D = 3 with S increases roughly linearly with D up to D = 25. The branch at higher values of S starts at D = 20 and increases linearly with D.

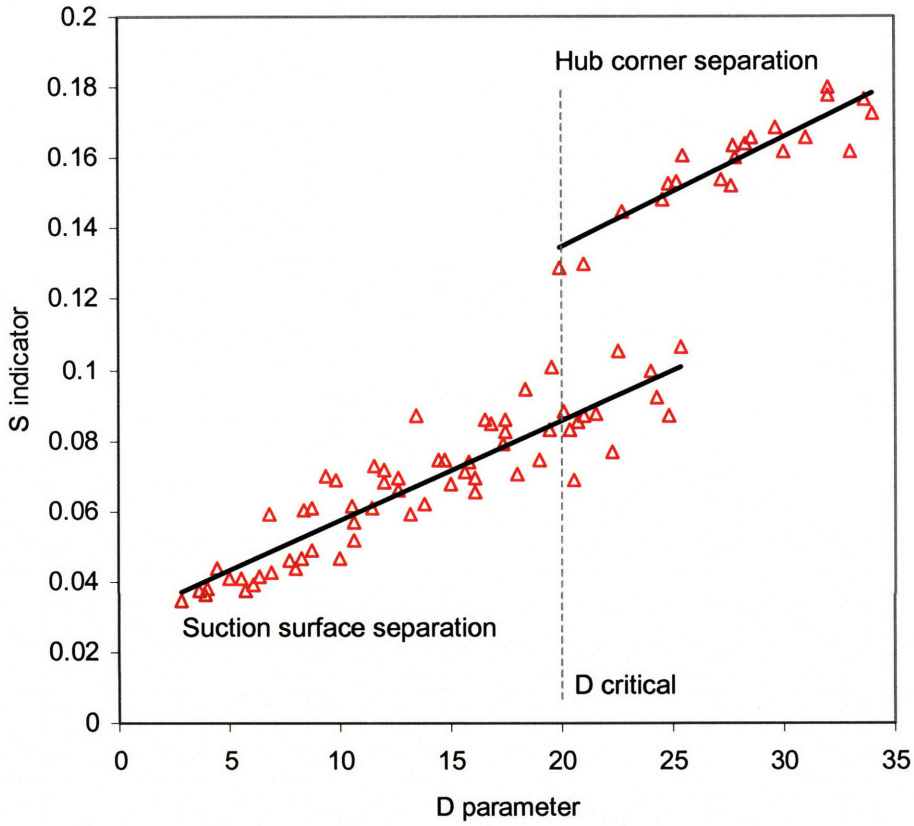

Figure 2.10 The S indicator as a function of the D parameter. CFD data are shown in triangles with best fit lines.

Examination of the cascade flow fields reveals the physical significance of the two branches. The cascades in the lower branches are all free of hub corner separation. The flow field of a cascade in the lower branch, with D = 8, is shown in Figure 2.11. Limiting streamlines from CFD indicate that the flow is attached on the endwall while there is a small region of separation on the suction surface near the blade trailing edge. As the D parameter increases, the size of the separation region on the suction surface increases but the endwall flow remains attached. Figure 2.12 shows the limiting streamlines of a cascade with a D parameter of 18. The size of the separation on the suction surface has grown considerably compared to Figure 2.11. The limiting streamline show that the endwall remains free of separation. Flow separation in the lower branch is confined to the blade suction surface.

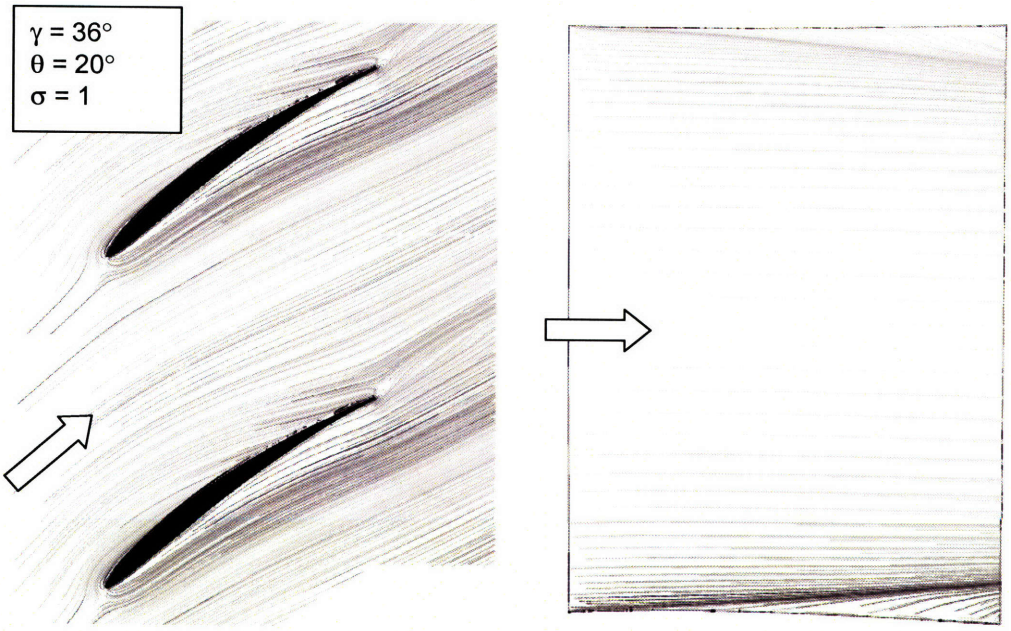

Figure 2.11 Limiting streamlines indicate a separation free endwall (left) and flow separation on the *suction* surface (right) of a cascade with D = 8. Arrow indicates flow direction.

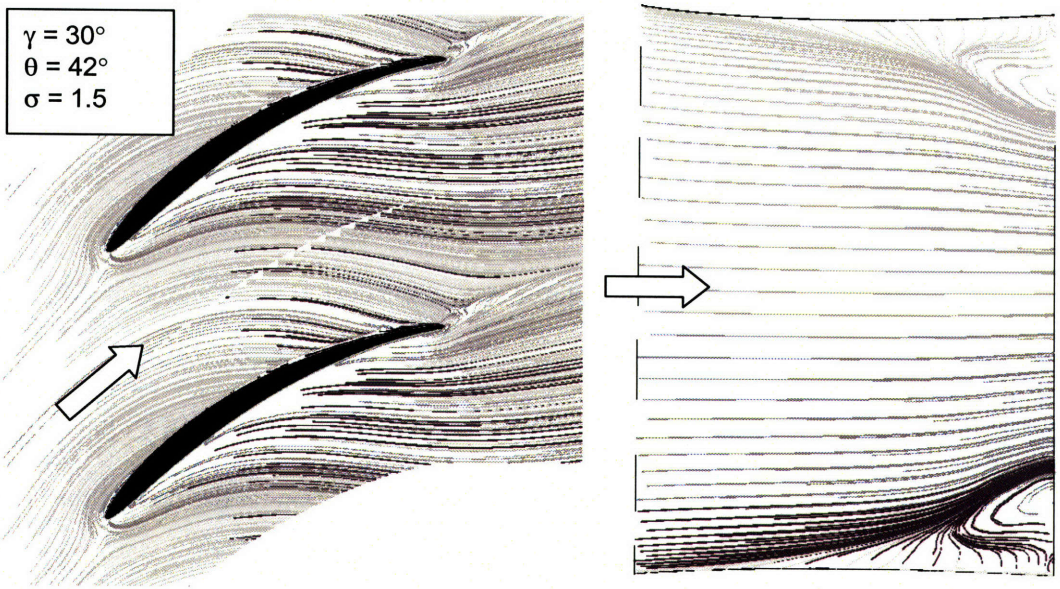

Figure 2.12 Limiting streamlines indicate a separation free endwall (left) and flow separation on the suction surface (right) of a cascade with D = 18. Arrow indicates flow direction.

While cascade geometries of the lower branch are free of endwall separation, hub corner separation is present in all the cases of the upper branch. Flows on both the suction surface and endwall of

a compressor cascade with D = 25 of the upper branch are separated as shown in Figure 2.13. The characteristic features of hub corner separation, namely a region of flow reversal at the endwall with a recirculation zone can be seen in Figure 2.13. The flow field shown in Figure 2.13 is typical for all cascades of the upper branch of Figure 2.10.

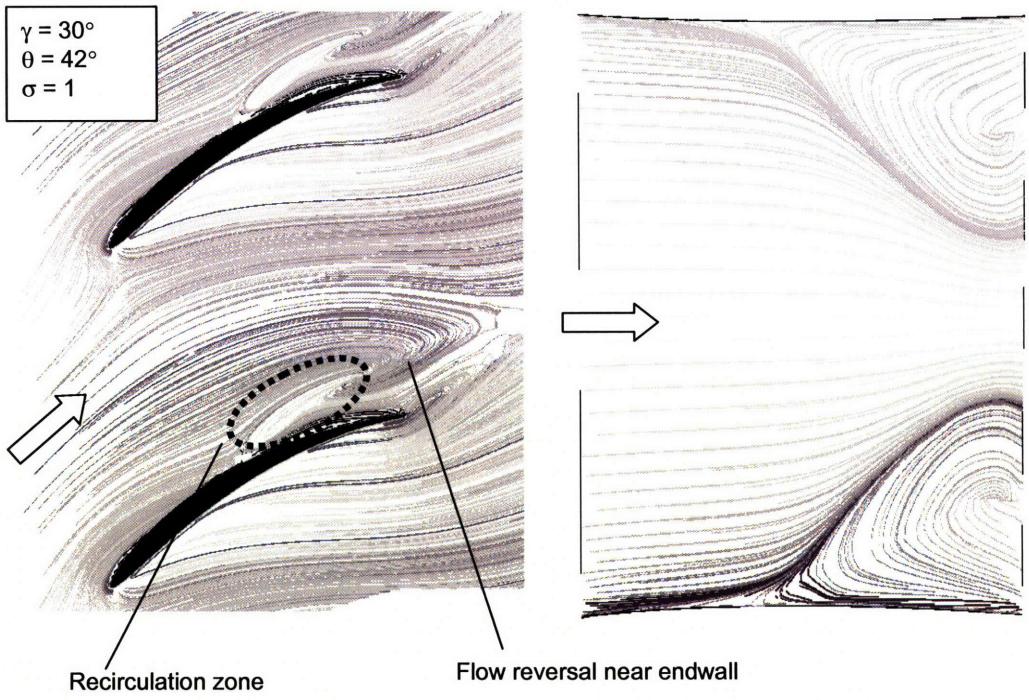

Figure 2.13 Limiting streamlines on the endwall and suction surface of a cascade (D = 25) of the upper branch with hub corner separation. Arrow indicates flow direction. Flow near the endwall is separated with a recirculation zone.

Summarizing the results of the CFD analysis, for compressor cascades of the lower branch shown in Figure 2.10, the flow separation is confined to the blade suction surface. The lower branch is hence referred to as the Suction Surface Separation (SSS) branch. Flow separation in the upper branch involves separation on *both* the endwall and suction surface, and the upper branch is therefore referred to as the Hub Corner Separation (HCS) branch.

These results demonstrate some important properties of the S indicator and the D parameter. The S indicator does not only quantify the size and strength of hub corner separation, but also measures the severity of the suction surface separation. The fact that the value of S increases with D confirms the ideas

that D captures the mechanisms that govern flow separation. Furthermore, it quantifies the tendency of a blade passage to hub corner separation.

The results of the CFD analysis further suggest the existence of a criterion for hub corner separation. The size of the suction surface separation increases with the D parameter for the lower branch. As D reaches a value of 20, there is a discontinuity between the SSS branch and the HCS branch, due to loss in loading from the onset of hub corner separation, that separates the two flow separation regimes (see Figure 2.10). A D value of 20 is therefore suggested to be a criterion for hub corner separation in the blade passage.

The D parameter provides a simple method to evaluate a blade passage in terms of the onset of hub corner separation. It is recommended that the D parameter be kept below 20 to avoid hub corner separation. The D parameter can also guide the design of flow control strategies to mitigate hub corner separation as will be discussed in Section 2.4.4 and Chapter 4.

2.4 Validity of the D Criterion with Additional Effects

In the development of the D parameter, there are flow effects that are either neglected or not accounted for. The objective of this section is to investigate the impact of these effects on the flow separation criterion in terms of the D parameter. The assessment is necessary in order to establish the credibility of the separation criterion for conditions outside that described in Section 2.3.1. The effects that are discussed are

1. Effect of incoming boundary layer thickness
2. Reynolds number effect
3. Blade aspect ratio effect
4. Effect of endwall boundary layer skew

2.4.1 Effect of Incoming Boundary Layer Thickness

In Section 2.3.1, the criterion for three-dimensional flow separation based on the D parameter was developed for an endwall boundary layer with thickness of 10% of chord. The generality of the criterion was also assessed using a thicker endwall boundary layer with a thickness of 20% of chord. Cases on the SSS branch and the HCS branch at different D were chosen, and the results are shown in Figure 2.14 with the baseline data from Figure 2.10 for a reference.

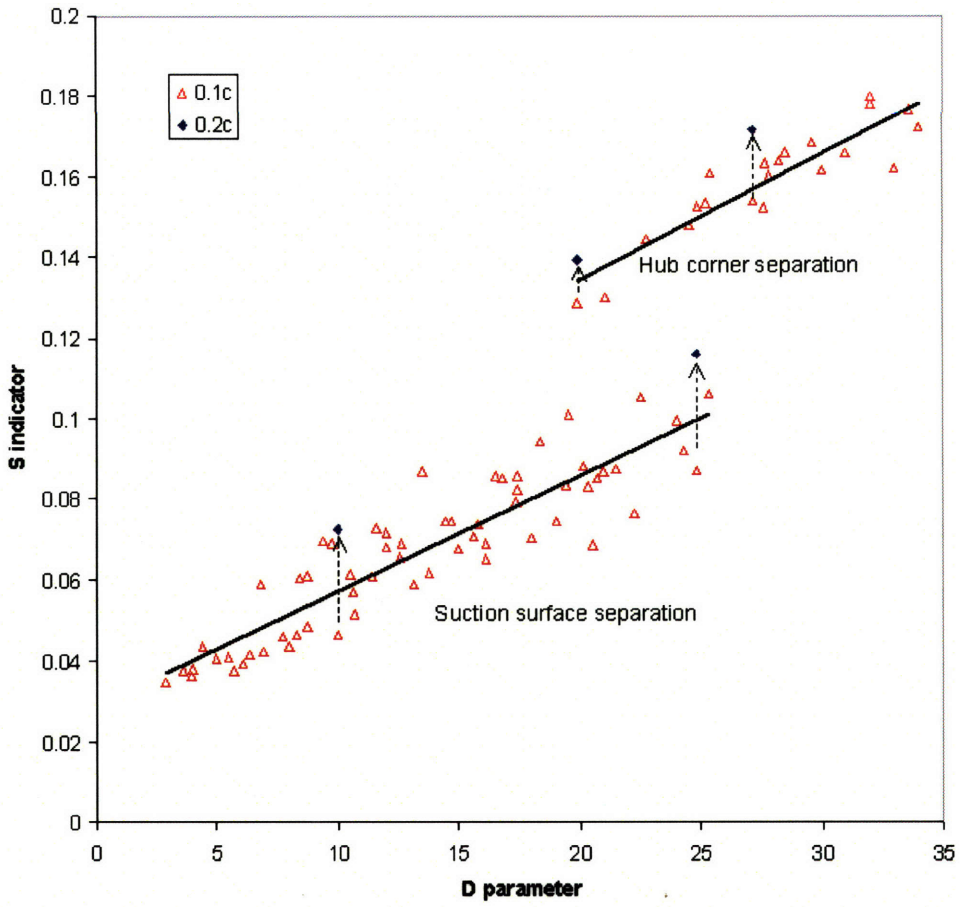

Figure 2.14 The S indicator versus the D parameter for endwall boundary layers of different thicknesses. The dotted arrows indicate the effect of increasing boundary layer thickness. Baseline data are shown as the red triangles. The best fit is indicated by the black lines.

Examination of the flow field reveals that the endwall for the cases on the SSS branch remains free of separation and hub corner separation is present for the cases on the HCS branch. The results suggest that the D separation criterion is also valid for endwall boundary layers with thickness of 20% of chord. Since the size of the separation keeps increasing with the thickness of the incoming boundary layer, it is speculated that the suction surface separation on the SSS branch may turn into hub corner separation at some critical value of boundary layer thickness. The D criterion should thus be applied with discretion in situations involving endwall boundary layers with thickness above 20% of chord.

2.4.2 Reynolds Number Effect

The D criterion developed in the previous section was based on analysis using the baseline Reynolds number of 2.5×10^5 with the NASA LSAC compressor as a reference. The calculations were fully turbulent such that effect of transition from laminar to turbulent flow was not considered. The validity of the D criterion at Reynolds number range representative of axial compressor is assessed in this section.

The range of Reynolds number in multistage compressors reported by Koch (1981) was used as a reference. With this, geometries with different values of D on both the SSS and HCS branches were further analyzed with Reynolds numbers of 2.5×10^4 and 2.5×10^6. The results are shown in Figure 2.15.

Figure 2.15 indicates that for fully turbulent flow, Reynolds number effects in the range considered does not cause suction surface separation to develop hub corner separation. Similarly, hub corner separation does not become suction surface separation with changes in Reynolds number. The examination of the flow fields reveals that all the cases in the SSS branch are free of endwall separation, and hub corner separation is present in all the cases in the HCS branch. For fully turbulent flow, the separation criterion holds in the range of Reynolds numbers considered.

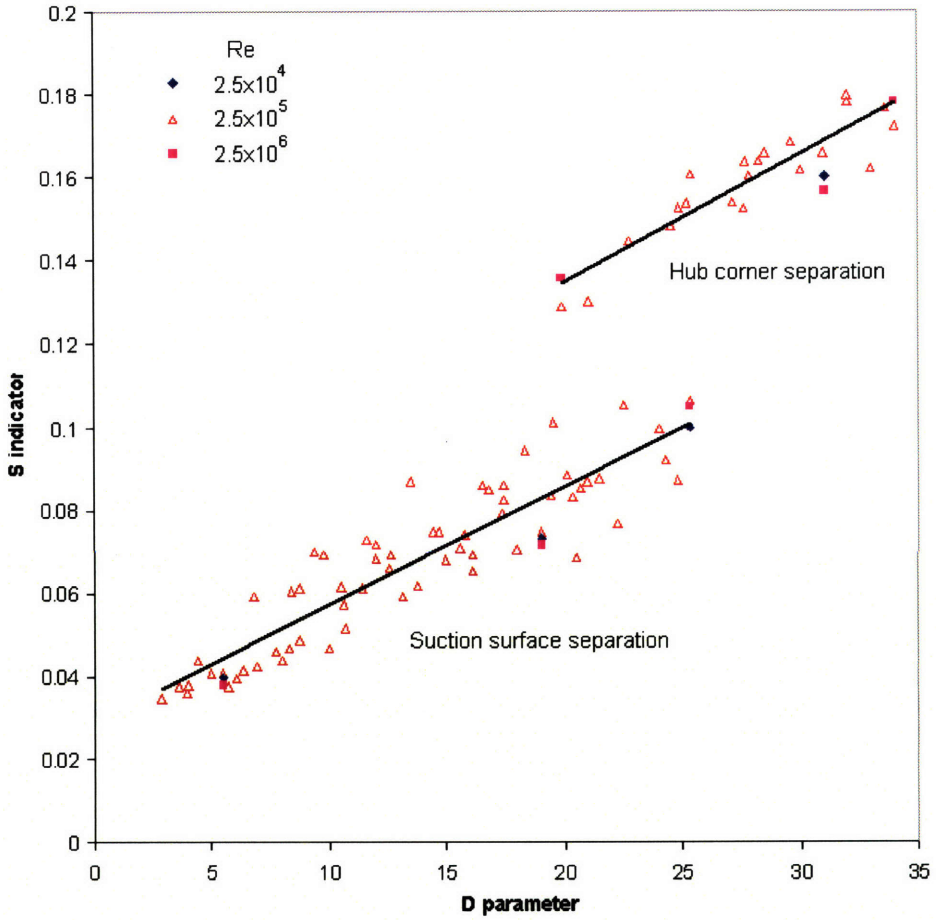

Figure 2.15 S indicator at selected values of D with various Reynolds numbers for fully turbulent flow. The data of the baseline cases with Re = 2.5×10^5 are shown in red triangles with best fit lines.

The results were further examined in terms of the effect of Reynolds number on the size of flow separation. Although the value of S varies with Reynolds number, the sensitivity of S to Reynolds number is small. One way to quantify the sensitivity is to examine the ratio of the percentage change in S to the percentage change in Reynolds number. From the data shown in Figure 2.15, the maximum sensitivity calculated is 0.006. The insensitivity of the size of the separation to Reynolds number is also evident from the limiting streamlines near the blade suction surface given in Figure 2.16. The physical size of the separation remains roughly unchanged for an order of magnitude increase in Reynolds number.

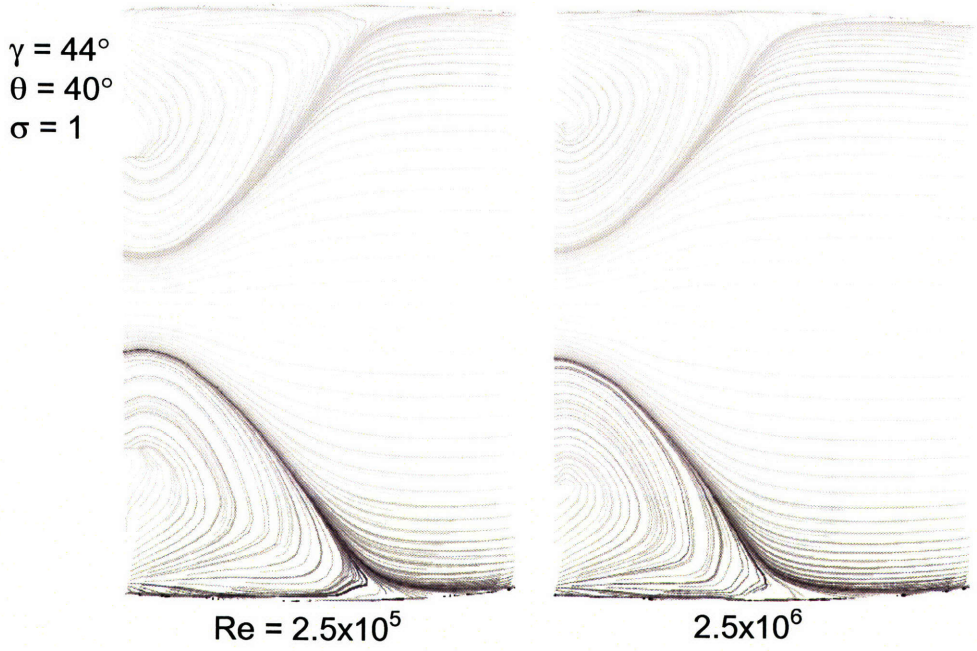

Figure 2.16 Limiting streamlines depicting the extent of flow separation on the suction surface of a cascade with D = 31 at Re = $2.5x10^5$ (left) and $2.5x10^6$ (right).

2.4.3 Effect of Aspect Ratio

In the definition of the D parameter, the effect of blade passage aspect ratio on the size of hub corner separation was not considered and the analysis in Section 2.3.1 was performed with a constant aspect ratio of 1.36. The effect of aspect ratio on the D separation criterion is assessed in this section.

Blade passages with different values of D from the SSS and HCS branches were selected and analyzed with different aspect ratios. A representative range of aspect ratios of range 0.5 to 5 was used (Koch, 1981). It is speculated that the separation regime may change from SSS to HCS at low aspect ratio such that suction surface separation near both endwalls merge at midspan and three cases with aspect ratio below 1 on the SSS branch were considered to examine this argument. For cases with hub corner separation, reducing the aspect ratio below the baseline value of 1.36 causes the flow to separate at midspan. For these cases, the S indicator is no longer applicable, and hence the data is not shown. Results of the analysis are shown in Figure 2.17.

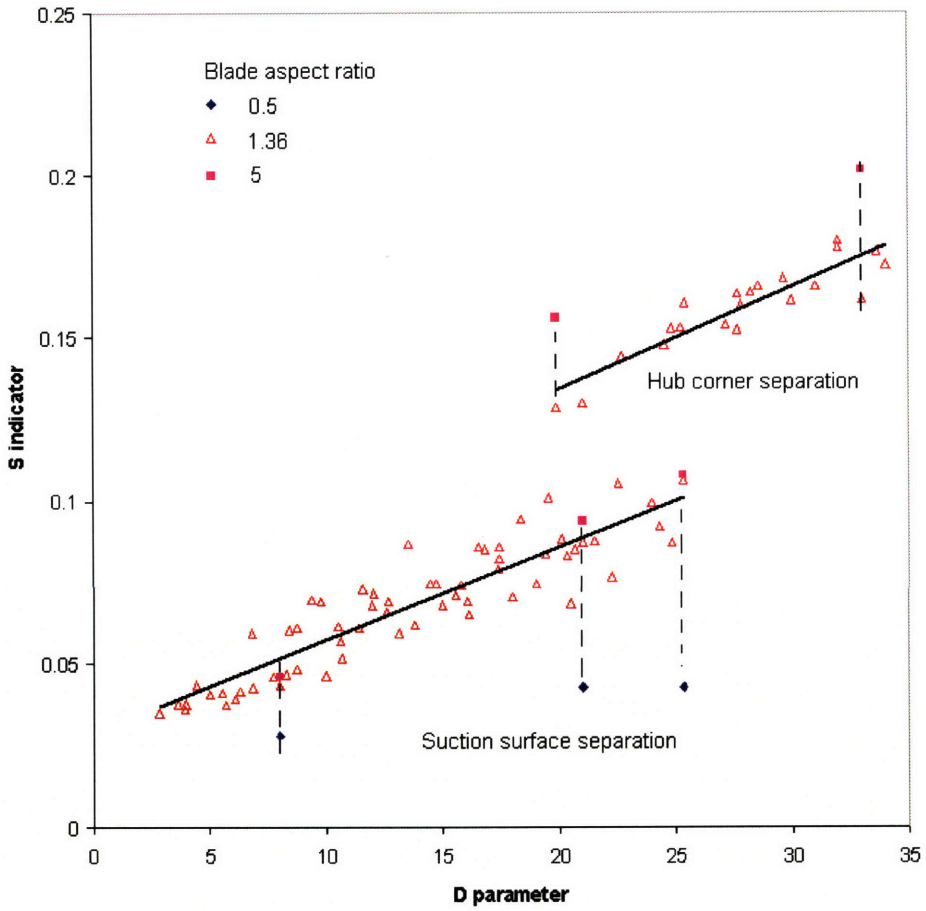

Figure 2.17 Effect of blade aspect ratio on the S indicator and the D separation criterion. The data of the baseline cases with AR = 1.36 are shown in red triangles.

From Figure 2.17, blade aspect ratio in the range considered does not cause suction surface separation to turn into hub corner separation. Similarly, hub corner separation does not become suction surface separation with changes in blade aspect ratio. All the cases on the SSS branch are free of endwall separation, and hub corner separation is present in all the cases on the HCS branch. Based on the result, blade aspect ratio has no effect on the onset of hub corner separation and the D separation criterion holds in the range of aspect ratios considered.

From Figure 2.17, the size of separation on the SSS branch as measured by the S indicator decreases as aspect ratio is reduced. Examination of the flow field, as shown in Figure 2.18, reveals that the apparent change in S is not due to the change in physical size of the separation, but the change in

influence of the separation on the flow at midspan. By definition, S measures the size of the separation by the reference loading at midspan. As aspect ratio decreases, the influence of the separation on the midspan flow increases, leading to a reduction in the reference loading. The consequence is a decrease in S as observed in Figure 2.17.

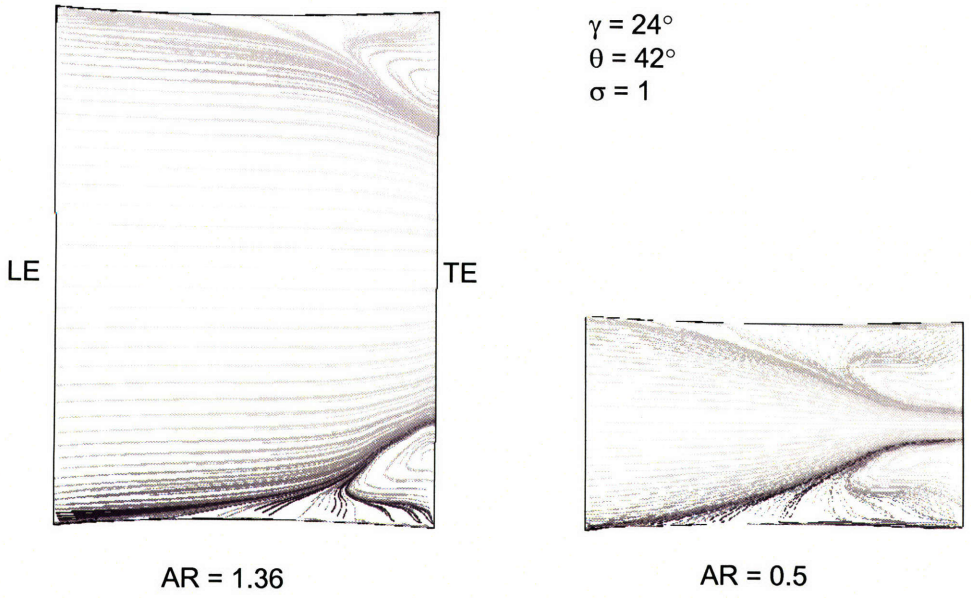

Figure 2.18 Limiting streamlines on the suction surface of two blades with identical D of 21 but different aspect ratios. The physical size of separation is not sensitive to blade aspect ratio.

2.4.4 Effect of Endwall Boundary Layer Skew

In the previous sections, the validity of the D criterion for hub corner separation under the influence of various effects that were not considered in the definition of the D parameter was assessed. A modification to the D parameter to account for the effect of boundary layer skew is introduced in this section. The capability of this modified D parameter to capture the effect of boundary layer skew on hub corner separation is then assessed using numerical experiments.

The modification of the D parameter to include effect of boundary layer skew from upstream is motivated by two reasons:

1. Skewing of the endwall boundary layer is common in axial compressors. Examples of skewed endwall boundary layers can be found on a stator endwall downstream of a rotor as shown in Figure 2.19. Hub cavity leakage in a shrouded stator also causes the endwall boundary layer to skew and it was shown that the size of hub corner separation is closely related to the leakage (see Demargne and Longley, 2000 for details).
2. The modified D parameter that captures the effect of skewed endwall boundary layer has a potential application in the design of flow control schemes to mitigate hub corner separation.

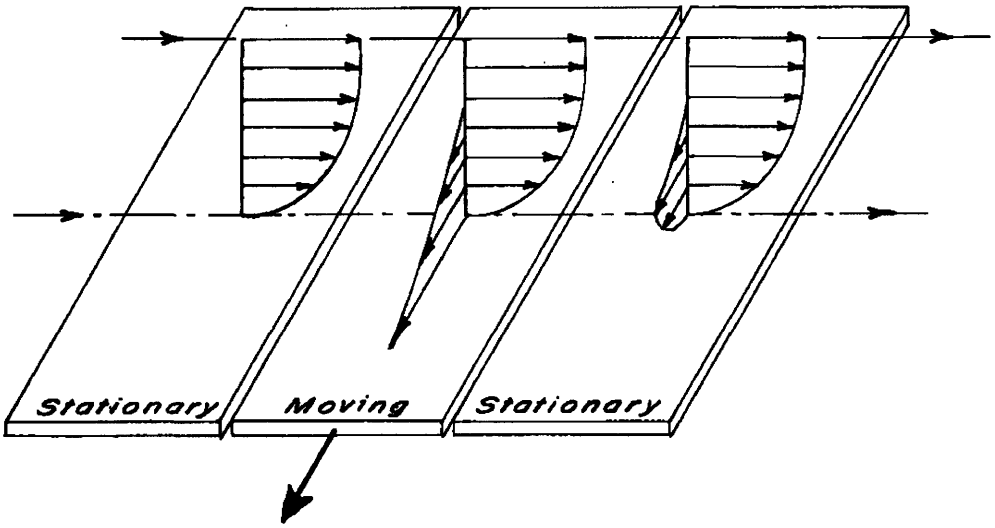

Figure 2.19 The skewing of endwall boundary layer by action of rotor motion (adopted from Hinck, 1959).

Demargne and Longley (2000) and Wellborn and Okiishi (1996) showed that the skewing of endwall boundary layer due to hub cavity leakage alters the size of hub corner separation. Demargne and Longley (2000) used a momentum thickness argument to explain the effect of leakage flow on the hub corner separation. They suggested that the strength of secondary flow in the blade passage (and hence the size of hub corner separation) is proportional to the momentum thickness of the incoming endwall boundary layer as observed in their experiment and CFD calculation. Hub cavity leakage changes the

momentum thickness of the endwall boundary layer causing a change in size of the separation. Wellborn and Okiishi (1996) proposed that hub cavity leakage changes the capability of the low momentum endwall fluid to travel against the cross passage pressure gradient. As hub cavity leakage with low momentum increases, momentum of the endwall fluid is reduced and worsens the condition of the boundary layer near the blade suction surface, thus leading to a bigger separation.

In this dissertation, a secondary flow approach was used to establish a link between the skewing of endwall boundary layer and the size of the hub corner separation. The idea behind the D parameter modification is to quantify the skewness of the boundary layer associated with the secondary vorticity, and to cast it to an equivalent turning to modify the ε term in the D parameter (see equation 2.18).

The idea of the ε term modification can be illustrated by examining the polar plot of a skewed boundary layer. Figure 2.20 shows the polar plot of a typical skewed boundary layer as first proposed by Johnston (1957).

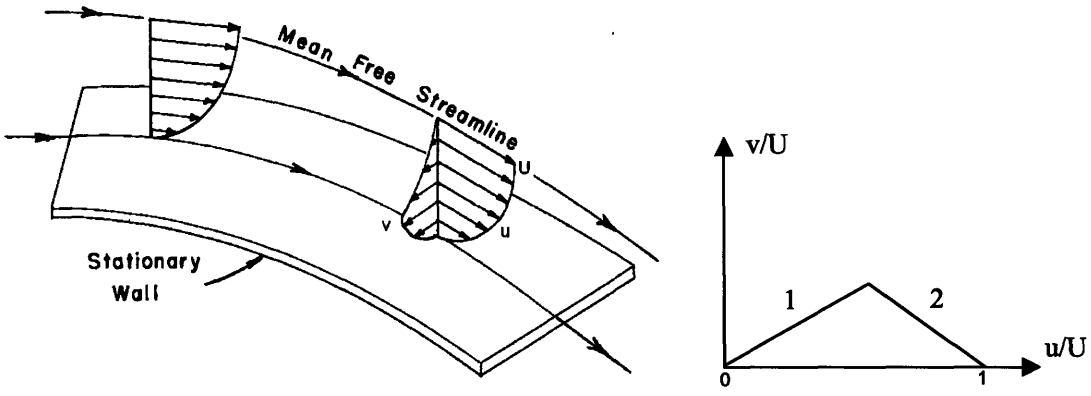

Figure 2.20 A skewed boundary layer and its representation by Johnston's polar plot (adopted from Hinck, 1959).

Figure 2.20 plots the nondimensional cross-stream velocity component (v/U) against the velocity component in the freestream direction (u/U) for a skewed boundary layer. The skewed boundary layer can be modeled as a triangle with two legs. Leg 1 is associated with the portion of the boundary layer close to the endwall where viscous effects dominate. Leg 2 is associated with the portion away from the endwall

where the effect of viscosity is not significant. Strictly speaking, the *net* streamwise vorticity in a skewed boundary layer (i.e. streamwise vorticity associated with both legs 1 and 2) is zero. In the current analysis, the term streamwise vorticity refers to the stremwise vorticity associated with leg 2 of the polar plot, i.e. the vorticity in the region which behaves in an inviscid manner. The slope of leg 2 is a measure of the skewness of the skewed boundary layer and it is equivalent to the ratio of streamwise vorticity to normal vorticity. For a skewed boundary layer generated by turning of the freestream, the slope of leg 2 is two times the turning angle ε as in Squire and Winter's (1951) formula $\zeta = 2\Omega\varepsilon$, where ζ is the streamwise vorticity and Ω is the normal vorticity of the initially collateral boundary layer. In Johnston's notation this is

$$\frac{v}{U} = A\left(1 - \frac{u}{U}\right), \tag{2.19}$$

where $A = 2\varepsilon$ for an initially collateral boundary layer with freestream turning through an angle ε. With reference to the original D formulation in Section 2.2, $\varepsilon = A/2$. For any given skewed boundary layer,

$$\frac{v}{U} = B\left(1 - \frac{u}{U}\right), \tag{2.20}$$

where B is the slope of leg 2 from the polar plot of the skewed boundary layer. If this skewed boundary layer is turned by an angle ε in a blade passage, the combined effect gives

$$\frac{v}{U} = (A + B)\left(1 - \frac{u}{U}\right). \tag{2.21}$$

The additional turning effect for the term ε is thus B/2, where B measures the initial skewness of the boundary layer. For a skewed boundary layer generated by hub cavity leakage, B is a function of the leakage flow properties.

2.4.4.1 Assessment of the modified D parameter

Numerical experiments in linear cascades with skewed boundary layers were carried out to assess the D parameter formulated in Section 2.4.4. Hub cavity leakage was chosen as the source of skewness to the

initially collateral boundary layer. The choice was based on the fact that a shrouded stator with hub cavity is a common feature in modern axial compressor. The known response of hub corner separation to hub cavity leakage (Demargne and Longley, 2000) guides the prescription of the leakage. In a real compressor environment, the leakage properties depend on the pressure difference across the stator and the rotational speed of the spool. However, in the numerical experiments they can be specified independently. The hub cavity leakage can thus be regarded as a means of flow control with potential application to the mitigation of the three-dimensional flow separation.

A cascade on the HCS branch with D = 25 was selected with a hub cavity slot modeled as shown in Figure 2.21.

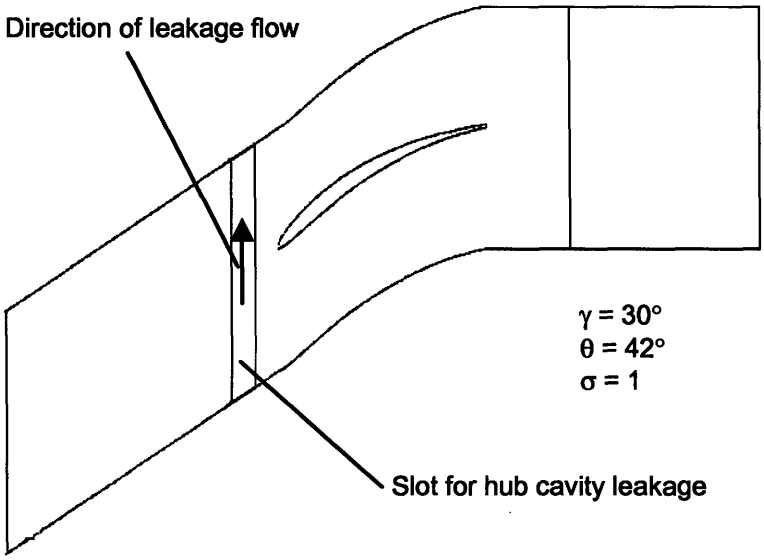

Figure 2.21 Outline of cascade geometry at D = 25 with upstream slot for hub cavity leakage.

The slot width was 10% of chord and was located at a distance of 10% axial chord upstream of the blade leading edge. According to Demargne and Longley (2000), the effect of the leakage on hub corner separation is predominantly determined by two parameters, the ratio of leakage mass flow rate to

the freestream flow rate denoted by $\dot{m}_j / \dot{m}$, and the ratio of leakage velocity to the freestream tangential velocity denoted by v_j / v_y. With reference to the experiment of Demargne and Longley (2000), three levels of $\dot{m}_j / \dot{m}$ at 0.35%, 0.7% and 0.84% representing low, nominal and deteriorated seal leakage fraction were used in the numerical experiments. Demargne and Longley (2000) proposed that the size of the high loss region associated with hub corner separation is related to the change in tangential momentum thickness of the endwall boundary layer ($\Delta\theta_y$) as given by

$$\frac{\Delta\theta_y}{L} = \frac{\dot{m}_j}{\dot{m}}\left(1 - \frac{v_j}{v_y}\right) \tag{2.22}$$

where L is the blade span. According to equation (2.22), $v_j / v_y < 1$ promotes hub corner separation while $v_j / v_y \geq 1$ mitigates separation. To study the effect of tangential velocity ratio on the size of the separation, five levels of v_j / v_y at 0.5, 0.75, 1, 1.25 and 1.5 were chosen.

The effect of hub cavity leakage on the size of hub corner separation, as indicated by the size of the high loss region, is shown in Figure 2.22. The size of the high loss region decreases as v_j / v_y increases and the trend agrees qualitatively with the results of Demargne and Longley (2000).

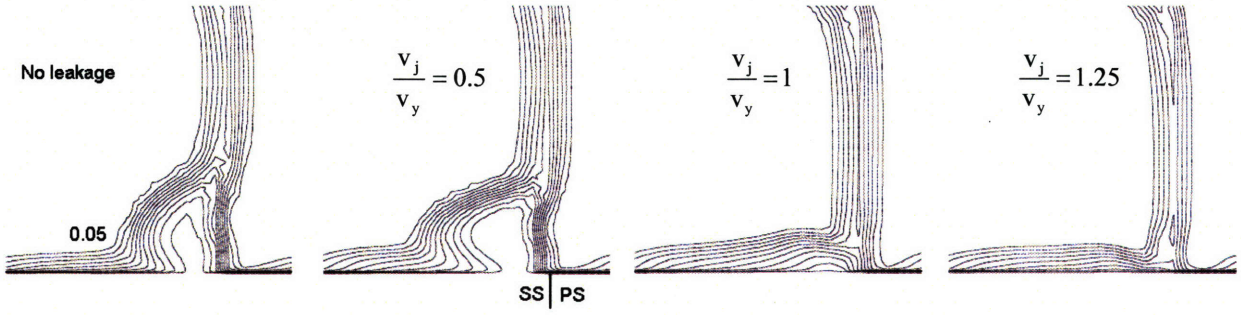

Figure 2.22 Effect of hub cavity leakage on hub corner separation. Contours of stagnation pressure coefficient at blade row exit are show in intervals of 0.05. The leakage fraction is 0.7% of the freestream.

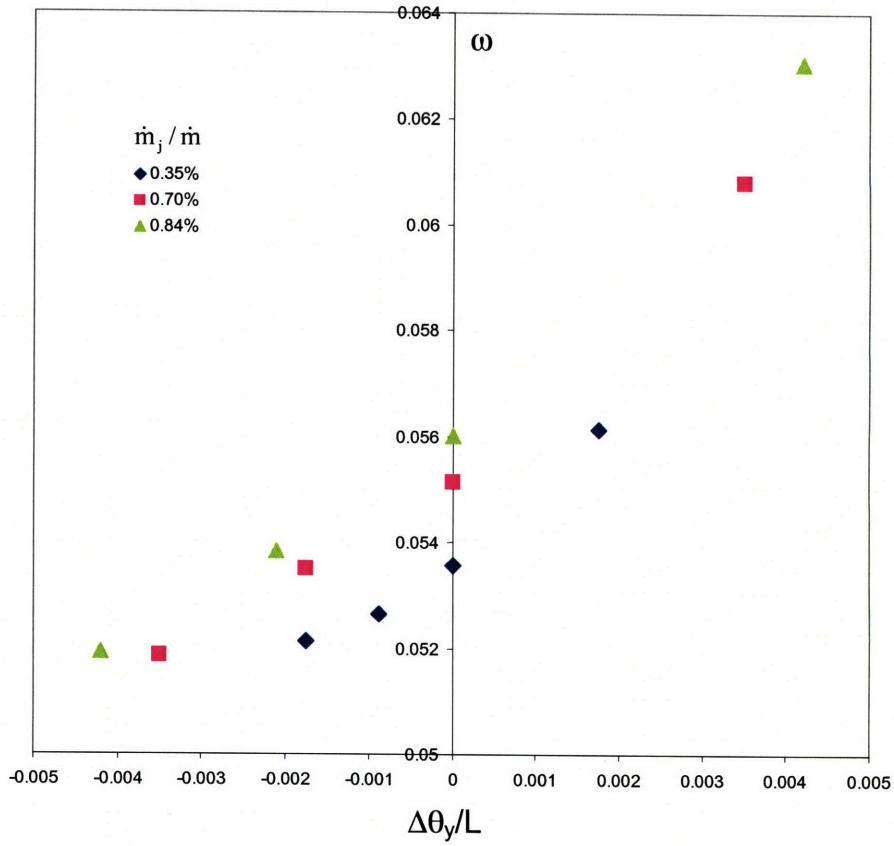

Figure 2.23 Loss coefficient as a function of the change in tangential momentum thickness of the endwall boundary layer as proposed by Demargne and Longley (2000).

Using the stagnation pressure loss coefficient (ω) as a metric for the size and strength of hub corner separation, the size of the separation roughly increases with $\Delta\theta_y/L$ as shown in Figure 2.23. This further confirm that the result of the numerical experiment concurs with that reported by Demargne and Longley (2000). The scattering of the data due to different $\dot{m}_j / \dot{m}$ suggests that the parameter $\Delta\theta_y/L$ does not fully capture the effect of hub cavity leakage on hub corner separation.

The B coefficient of the skewed boundary layer downstream of the leakage slot was determined from the polar plots based on the numerical results and the modified D parameter was calculated as described in Section 2.4.4. The S indicator versus the D parameter with effect of boundary layer skew is shown in Figure 2.24. The baseline cases with no leakage are also shown for reference.

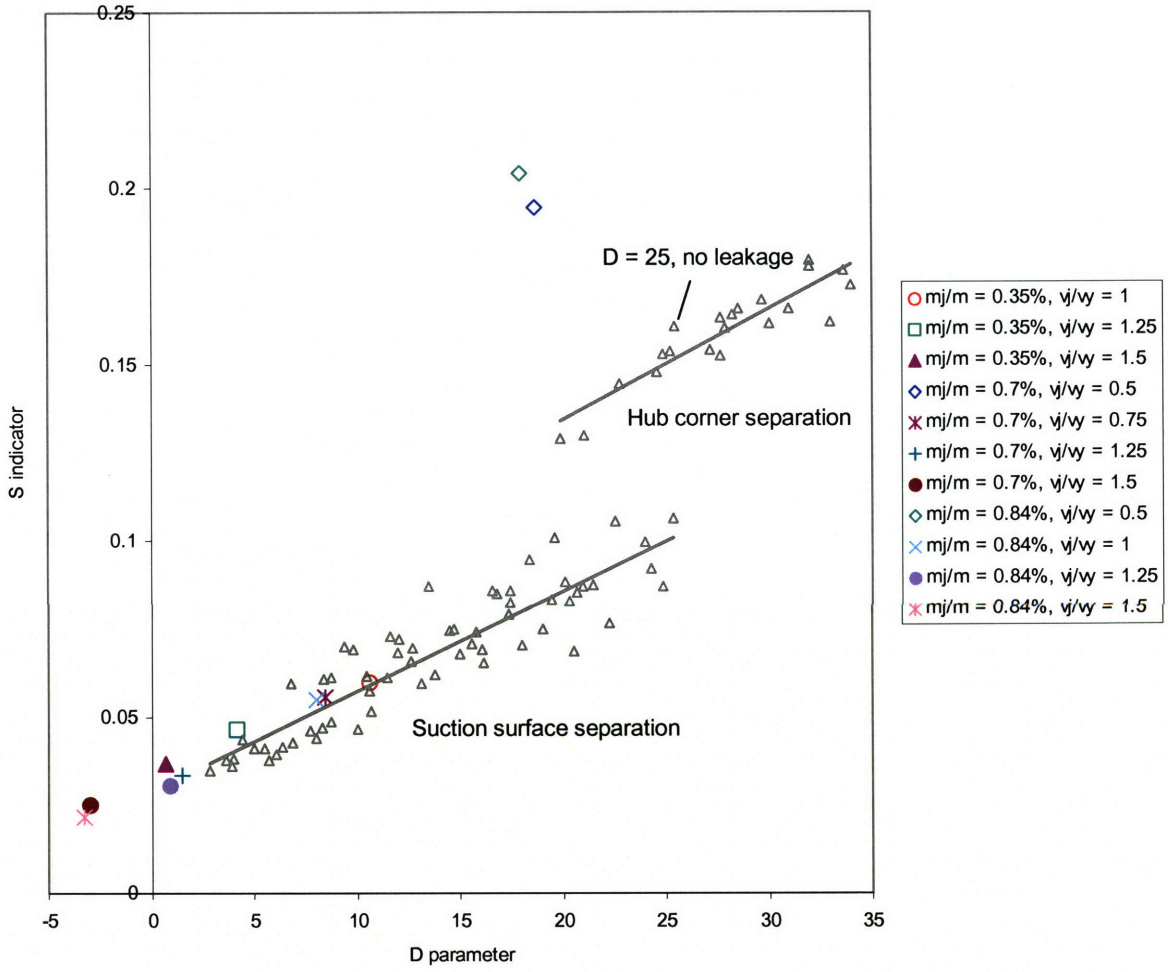

Figure 2.24 The D parameter with hub cavity leakage effect. Results of the baseline analysis are show in grey.

As shown in Figure 2.24, hub cavity leakage can either promote or mitigate hub corner separation. Regardless of the leakage mass fraction, leakage with tangential velocity ratio above 0.5 always helps to mitigate the three-dimensional separation. The direction of cross-stream momentum associated with the skewed boundary layer due to hub leakage is opposite to the direction of the naturally developed streamwise vorticity from flow turning. The D parameter with hub cavity leakage is thus always smaller than that without hub leakage effect.

The modified D parameter seems to capture the mitigating effect of hub cavity leakage on the three-dimensional flow separation. The result suggests that cross-stream momentum introduced to the

flow in a direction opposite to the blade passage secondary vorticity can mitigate hub corner separation. On the other hand, the D parameter does not capture the deteriorating effect of leakage on the separation. At a tangential velocity ratio of 0.5, the leakage flow lowers the streamwise momentum of the boundary layer, making it more vulnerable to separation under the influence of adverse pressure gradient in the blade passage. This situation is reflected by an increase in boundary layer shape factor from 1.4 without leakage to 2.1 with leakage at a tangential velocity ratio of 0.5. This effect it is not captured by the D parameter.

The capability of the D parameter to capture the effect of hub cavity leakage for cases that mitigate hub corner separation suggests a potential application of the modified D parameter to flow control design. Given a geometry of D >20 with three-dimensional flow separation, flow control can be used to reduce the D parameter below the critical value to mitigate the separation. The necessary reduction in D to achieve this objective can thus be viewed as the flow control requirement. To design a flow control scheme using hub cavity leakage, it is necessary to determine the leakage property from the flow control requirement. To achieve this goal in the preliminary design process without using CFD tools, a first principle based model that predicts the B coefficient associated with the skewed boundary layer as a function of the leakage property is needed. A leakage model based on a control volume analysis that estimates the modified D parameter is described in Appendix B. The model captures the effect of hub cavity leakage on hub corner separation in terms of trend. However, the magnitude of the D parameter calculated using the model deviates from that calculated with CFD data by as much as 100%. Further investigations, as suggested in Appendix B, is necessary such that the model can be used in flow control application. A flow control strategy to reduce the D parameter, and hence to mitigate hub corner separation, using the concept of boundary layer skew will be discussed in Chapter 4.

2.5 Additional Remarks on the S indicator and the D parameter

In practice, stagnation pressure loss coefficient (ω) and static pressure rise coefficients (C_p) are metrics commonly used to assess blade row performance. Since hub corner separation is a source of loss and blockage, these parameters may also be used to quantify the size of the separation. The S indicator was compared to the mass averaged ω and C_p computed using the data in Section 2.3 and the result is shown in Figure 2.25.

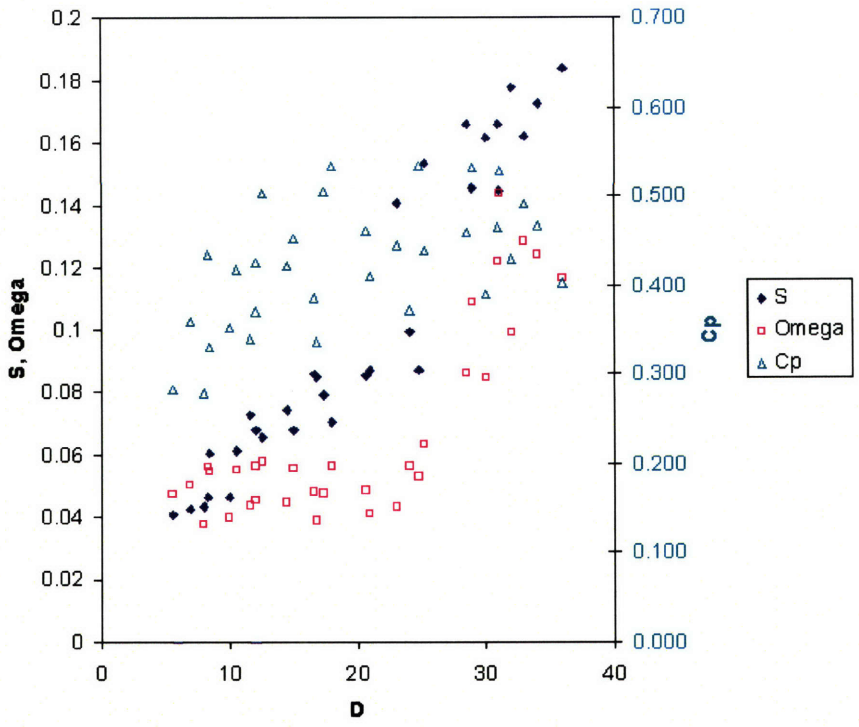

Figure 2.25 The S parameter, stagnation pressure loss coefficient and static pressure coefficient as a function of the D parameter. (Only baseline cases with zero incidence are shown for clarity)

Figure 2.25 shows that there is no distinct correlation between C_p and the D parameter. It is not obvious to identify the onset of hub corner separation with C_p since the data are almost evenly distributed in the range of D parameter considered. On the other hand, interesting trends are observed with the stagnation pressure loss coefficient. On the SSS branch prior to the onset of three-dimensional flow separation, ω is nearly constant with D and is not sensitive to the size of suction surface separation. A

discernable rise in the level of losses is observed after the onset of hub corner separation. Although ω can also be used to identify the criterion of three-dimensional separation by a steep increase in loss, it is less sensitive to the D parameter. On the HCS branch, the loss goes up in general with the size of the three-dimensional flow separation due to the fact that a larger separation gives a larger high loss region. Results from Figure 2.25 suggest that the S indicator captures the sizes of both suction surface separation and hub corner separation better than C_p and ω.

At the beginning of the chapter, it was suggested that a criterion for three-dimensional flow separation analogous to Lieblein's diffusion factor (DF) provides a simple way to assess compressor blade design. The diffusion factor is commonly used in compressor design to quantify the tendency of a blade row towards two-dimensional flow separation. A diffusion factor of 0.6 is usually considered as the critical value for flow separation on the blade suction surface and a typical choice of diffusion factor in design is around 0.45. Since it was shown that the D parameter could be used to assess a blade row design in terms of hub corner separation, it is useful to examine whether the diffusion factor, which was originally formulated for two-dimensional flow separation, can be applied to three-dimensional flow separation.

For incompressible flow with constant axial velocity through the blade row, the diffusion factor can be written as

$$DF = \left(1 - \frac{\cos\alpha_1}{\cos\alpha_2}\right) + \frac{\cos\alpha_1}{2\sigma}\left(\tan\alpha_1 - \tan\alpha_2\right). \tag{2.23}$$

The diffusion factor for the cases shown in Figure 2.10 was calculated using the formula above with the assumption of zero deviation and is shown in Figure 2.26 with the S indicator.

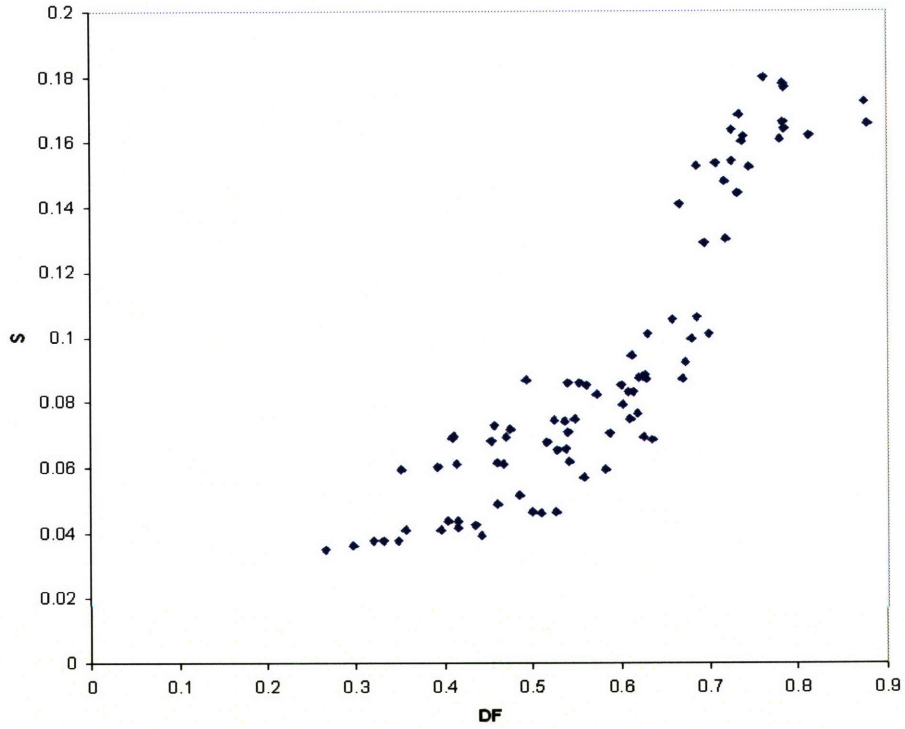

Figure 2.26 The S indicator as a function of Lieblein's diffusion factor

The size of flow separation as measured by the S indicator increases with the diffusion factor. At a diffusion factor between 0.67 and 0.73, there is an abrupt increase in S which indicates the onset of hub corner separation. The trend is similar to that shown in Figure 2.10 with the D parameter. It thus appears that the diffusion factor may also be used to assess blade row design in terms of hub corner separation.

It is interesting that the diffusion factor and the D parameter which are formulated for different purposes and developed with different approaches behave similarly in terms of capturing the mechanism governing the onset of hub corner separation. The diffusion factor was originally defined as the ratio of maximum velocity at the suction surface to velocity at the blade row exit for a two-dimensional cascade (Lieblein, 1959). Lieblein later showed that the diffusion factor could be expressed in terms of the area ratio and the flow turning through the blade row. These two effects are explicitly modeled in the D parameter to account for the effects of adverse pressure gradient and secondary flow in the blade passage. This explains the similarity between the diffusion factor and the D parameter. The major difference

between the two parameters is that the D parameter was modeled to capture the effect of endwall boundary layer skew. Data of the numerical experiment with the effect of hub leakage as shown in Figure 2.24 is plotted using the diffusion factor in Figure 2.27. The diffusion factor remains unchanged as it does not contain any information on the endwall boundary layer skew associated with the hub leakage.

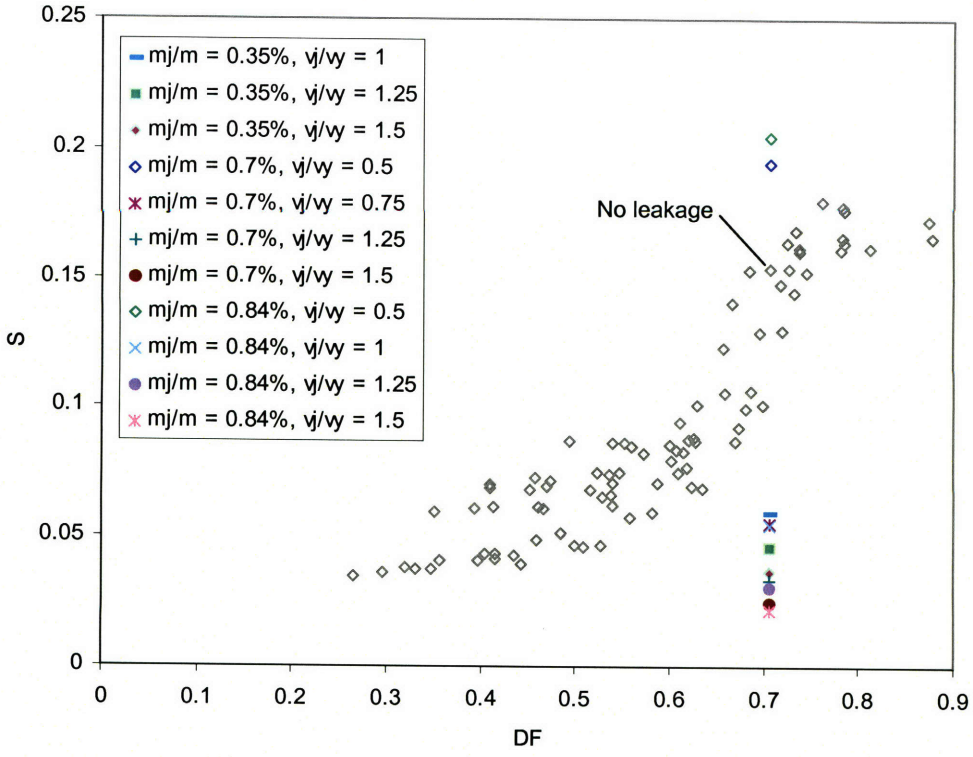

Figure 2.27 The S indicator for cases with hub leakage as a function of the diffusion factor. The baseline data with no leakage are shown in grey diamonds. The diffusion factor does not capture the effect of endwall boundary layer skew.

2.6 Summary

Two new parameters, the S indicator that quantifies the size of hub corner separation and the D parameter that quantifies the governing mechanisms of the three-dimensional flow separation were developed. The S indicator measures the size and strength of the separation with the loss in blade loading caused by flow separation. The D parameter captures and quantifies the combined effects of the adverse pressure gradient and the secondary flow in a blade passage that govern the size and strength of hub corner separation.

Incompressible, steady, and fully turbulent numerical simulations have been carried out on linear cascades with wide range of design parameters. The data was analyzed using the S indicator and the D parameter. The results suggest the onset of hub corner separation when the D parameter is greater than 20. The flow separation criterion in terms of the D parameter provides a simple means of evaluating whether hub corner separation exists in a blade row. The criterion was also scrutinized against flow effects that were not considered in the definition of the D parameter. The separation criterion is valid for Reynolds numbers between 2.5×10^4 and 2.5×10^6, blade aspect ratios between 0.5 and 5, incoming endwall boundary layer with thickness up to 20% of chord.

A modification to the D parameter to capture the effect of endwall boundary layer skew was proposed. Numerical experiments with hub cavity leakage demonstrated that the D parameter is capable of capturing the effects of endwall boundary layer skew that mitigates hub corner separation.

Chapter 3 Assessment of the New Criterion for Hub Corner Separation

A simple criterion for three-dimensional separation in axial compressor was proposed in Chapter 2. With this criterion, the onset of three-dimensional separation occurs in a blade passage when the D parameter is between 20 and 25. The objective of this chapter is to scrutinize the applicability of the criterion to blade rows other than the linear cascades previously examined. In this section, annular cascades and compressor stages are also considered.

3.1 Evaluation of the D Separation Criterion with Data from the Literature

Research data that satisfied the following requirements were chosen for the evaluation:

1. The data reported provide sufficient detail for the calculation of the D parameter.
2. The data substantiate whether hub corner separation is present.

Unlike the linear cascades considered in Chapter 2, in an annular cascade or an axial compressor stage the D parameter can vary with blade span. Since the D parameter is proposed to be an endwall separation parameter, it is to be evaluated at the hub for blades with spanwise variation in geometry. The evaluation of the generality of the separation criterion using data from the literature is presented in the following sections.

Barankiewicz and Hathaway (1998) and Wellborn and Okiishi (1996):

Barankiewicz and Hathaway reported hub corner separation in the third stage stator of the NASA LSAC compressor when it was operated at an increased loading condition with a flow coefficient of 0.35. Wellborn and Okiishi provided details of the stator geometry and flow measurements at the increased loading condition. Using the data from Wellborn and Okiishi, the D parameter at the hub was found to be

23.5 which is greater than the critical value of 20. With the presence of hub corner separation, the separation criterion is valid in this compressor.

Dong et al. (1987):

Dong et al. examined the three-dimensional flow field in a single stage research compressor. The compressor was constructed using twisted blades with C4 profiles on circular camber lines. No separation was reported for the rotor hub while hub corner separation was observed in the downstream stator. Using the blade geometry and velocity measurement in the report, the D parameters for the rotor and stator were calculated at the hub with D = 19.7 (<20) for the rotor and D = 26.4 (>20) for the stator. The separation criterion holds for both the stator and the rotor.

Gbadebo et al. (2004):

Gbadebo et al. examined the topology of flow separation in two linear compressor cascades with numerical and experimental methods. One cascade featured NACA 65 airfoils and the other was designed with prescribed velocity distribution (PVD) blades. Although Gbadebo et al. described the flow separations as three-dimensional, these were not hub corner separation as defined in Chapter 1. Since flow visualizations at the endwall did not show the flow reversal and recirculation reported by Schulz and Gallus (1988) (Figure 1.2 in Chapter 1), the separations were thus not hub corner separation. The flow visualization from Gbadebo et al. is reproduced in Figure 3.1 for reference. Judging from the endwall flow pattern, the hub was free of flow separation and the flow separation was confined to the blade suction surface. The flow separation reported was suction surface separation (SSS) according to the definition in Section 2.3.3. Based on the data from Gbadebo et al., the D parameter for both cascades are less than 14. The separation criterion thus holds for the two linear cascades.

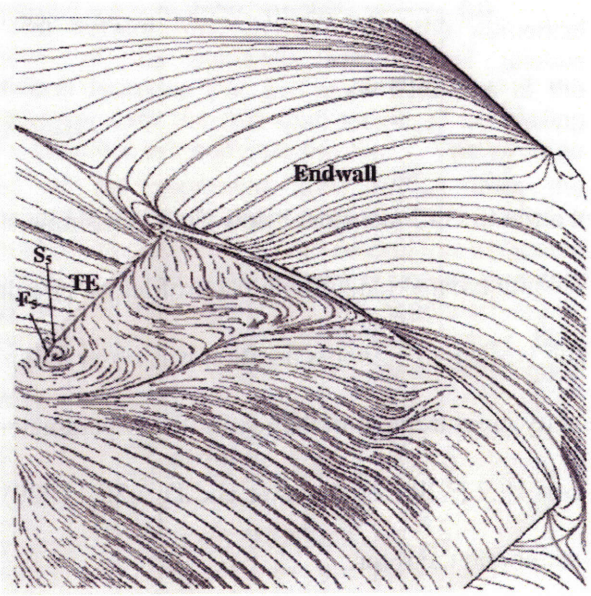

Figure 3.1 Limiting streamlines near the endwall and blade suction surface of the linear cascade from the experiment of Gbadebo et al (2004). Notice the lack of flow reversal and recirculation zone at the endwall.

Horlock et al. (1964):

Hub corner separation was reported in the linear cascade experiment of Horlock et al. The calculated D parameter using the cascade parameters in the report is 18.7. The separation criterion (D=20) is missed by 6.5%. It is not clear what causes the low value of the D parameter as the blade design was not reported.

Joslyn and Dring (1985):

Joslyn and Dring studied the three-dimensional flow in a two-stage research compressor. Hub corner separation in the stator was reported based on flow visualization near the endwall. Since the blade geometry was only described at midspan, the D parameter was calculated based on estimates of the geometry from the imprints of the blade profile in the endwall flow visualization. With an assumption of zero incidence, the D parameter at the hub was estimated to be 23.5 and the separation criterion holds.

Shang et al. (1993):

Shang et al. examined the effect of dihedral on endwall flows with linear cascade experiments. The blades in the compressor linear cascade had NACA65-24A_{10}-10 profile. In their baseline experiment with no dihedral, the endwall flow was free of separation. The D parameter calculated with the cascade parameters is 10.2. The separation criterion in terms of the D parameter holds. However, experiment in the same cascade with 25° negative dihedral indicated hub corner separation. Dihedral introduces a spanwise pressure gradient that affects secondary flow. This effect is not captured in the definition of the D parameter and this particular limitation will be further discussed in Section 3.2.

Kang and Hirsch (1991):

Kang and Hirsch studied the structure of the three-dimensional flow in a linear cascade experiment. The linear compressor cascade was constructed with NACA65-1810 airfoils. Static pressure measurements indicated the endwall was free of separation. The D parameter calculated based on the cascade geometry is 8.6 and the separation threshold was not exceeded.

Schulz and Gallus (1988):

Schulz and Gallus investigated the three-dimensional flow in an annular compressor cascade of untwisted blades. Despite the presence of hub corner separation in the blade passage, the D parameter calculated using the cascade geometry data is only 9.3. It first appeared that the D criterion of three-dimensional flow separation was violated. However, close examination of the blade profile provides an explanation of the exceptionally low D value.

Figure 3.2 illustrates the blade profile in the experiment conducted by Schulz and Gallus. This blade profile has an almost flat pressure surface and most of the curvature in the blade passage is provided by the suction surface. It is conjectured that the reported camber of 29° from which the D parameter was

calculated does not reflect the actual flow turning. The estimated turning provided by the suction surface is in excess of 60° and a flow turning of 45° can yield a D parameter close to the critical value of 20. The blade camber may not be the most appropriate way to characterize the bulk turning of the flow for this particular blade profile.

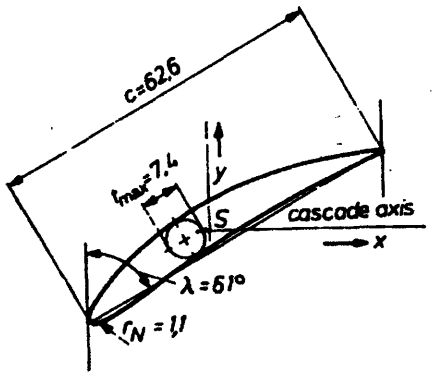

Figure 3.2 Profile of the airfoil in the annular cascade experiment of Schulz and Gallus (1988).

Geometries with no hub corner separation

Reference	Geometry description	D
Dong et al, 1987	Rotor of a single stage compressor with twisted blades	19.7
Gbadebo et al, 2004	Linear compressor cascade	13.6
	Linear compressor cascade	13.2
Kang and Hirsch, 1991	Linear compressor cascade	8.6
Shang et al, 1993	Linear compressor cascade	10.2

Geometries with hub corner separation

Reference	Geometry description	D
Barankiewicz and Hathaway (1998) and Wellborn and Okiishi (1996)	Stator of a four-stage compressor	23.5
Dong et al, 1987	Stator of a single stage compressor with twisted blades	26.4
Horlock et al, 1964	Linear compressor cascade	*18.7*
Joslyn and Dring, 1985	Stator of a two-stage compressor	23.5
Schulz and Gallus, 1988	Annular compressor cascade	*9.3 (31)*[2]

Table 3.1 Summary of the D parameter analysis with data from the literature.

[2] The D parameter is 31 based on a flow turning angle of 60° estimated from the blade geometry.

The data presented in this section are summarized in Table 3.1. The separation criterion in terms of the D parameter appears to work well for geometries with no hub corner separation. For geometries with hub corner separation, there are two exceptions with D less than 20. The unusually low value of the D parameter for the annular cascade of Schulz and Gallus may be explained by the blade profile that features a highly curved suction surface and a flat pressure surface. This particular blade profile renders the choice of camber underestimating the flow turning and thus a D parameter below 20. Another exception is the linear cascade in the experiment of Horlock et al. with a D parameter of 18.7, which is slightly below the critical value of 20. It is not clear what causes the low value of the D parameter as further information on the design of the experiment is not available. The results provide additional confidence in the applicability of the criterion to different geometries.

3.2 Statistical Analysis of the D Parameter

To further evaluate the generality of the separation criterion, a statistical analysis with aero-engine compressor data from industry provided by Wellborn (2005) was conducted. The data provide information on the loading level of modern compressors as measured with the D parameter, and allows an indirect assessment of the D criterion of three-dimensional flow separation.

The D parameters at the endwall were evaluated for five production and research multistage compressors ranging from 5 to 14 stages. Only endwalls with no tip leakage, i.e. rotor hub, stator casing and stator hub of shrouded stator were analyzed. A total of 49 rotor endwalls and 71 stator endwalls were sampled and the occurrence of the D parameter in percentage of the sample population is shown in Figure 3.3.

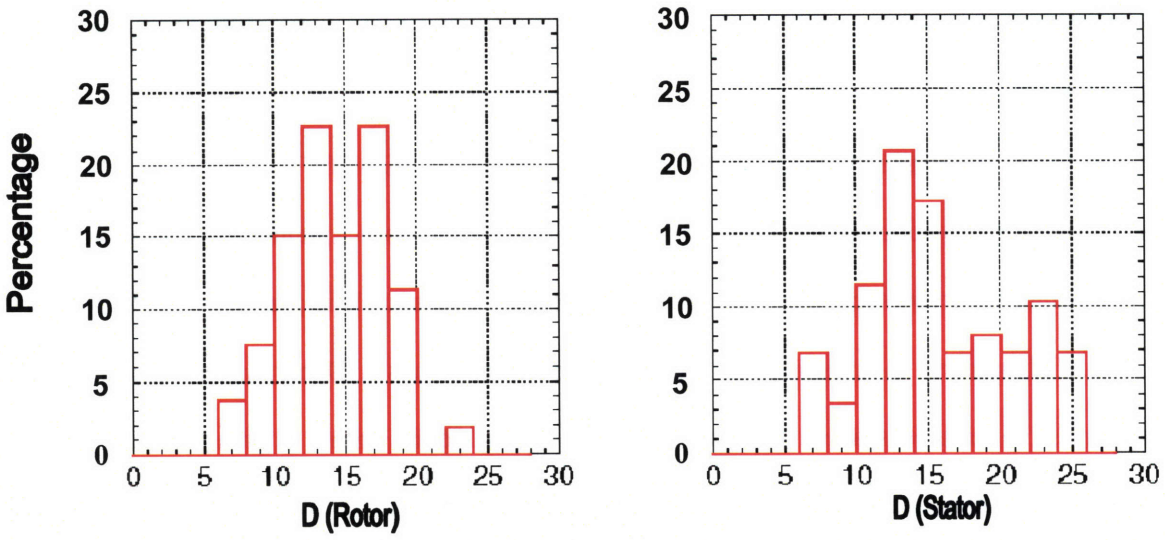

Figure 3.3 Occurrence of the D parameter in the rotors and stators sampled (courtesy of Wellborn).

The majority of the rotors (61%) are designed with the D parameter between 13 and 17. The D parameters for 98% of the rotors are below 20. The remaining 2% represent a compressor design featuring three-dimensionally shaped blades to prevent hub corner separation. With all the rotors reported to be free of endwall flow separation, the rotor data suggests the validity of the D separation criterion for 98% of the data sampled. For the stators, the occurrence peaks at D = 12 to 14. About 24% of the design has D above the critical value of 20. Within this 24% of data, some designs are outlet guide vanes with hub corner separation, while the others feature three-dimensional designs to mitigate hub corner separation. The exact number of cases with hub corner separation could not be determined from the data provided. The statistical analysis for the stators suggests at least 76% of the designs satisfy the criterion of three-dimensional flow separation in terms of the D parameter.

3.3 Effect of Dihedral and Sweep on Hub Corner Separation

Experiments conducted by Shang et al. (1993) demonstrated that negative dihedral could cause hub corner separation to an endwall which was originally free of separation. The dihedral introduced affects the secondary flow such that three-dimensional separation occurs. The current formulation of the D

parameter does not contain any information on the stacking of the blade profiles and hence it does not capture the effects of dihedral or sweep.

The effect of dihedral and sweep on the separation criterion was further investigated with flow field data from numerical simulations provided by Wellborn (2005). Six stators representative of an embedded stage of a low pressure compressor, with different levels of sweep and dihedral, were analyzed at the design operating condition. The stator blades were constructed with identical airfoil sections and were stacked to provide different levels of sweep and dihedral. The D parameters for the stators are thus identical under the same upstream flow condition. The configuration varies from positive dihedral and positive sweep in stator A to negative dihedral and negative sweep in stator F as shown in Figure 3.4 and Figure 3.5.

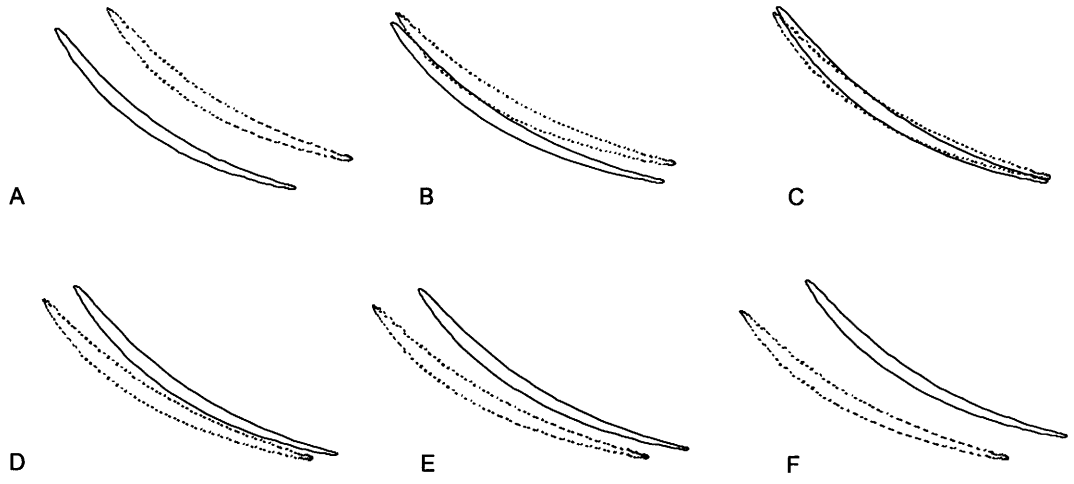

Figure 3.4 Stacking of stators A through F. Solid line: endwall profile. Dotted line: midspan profile. Sweep changes from positive in stator A to negative in stator F.

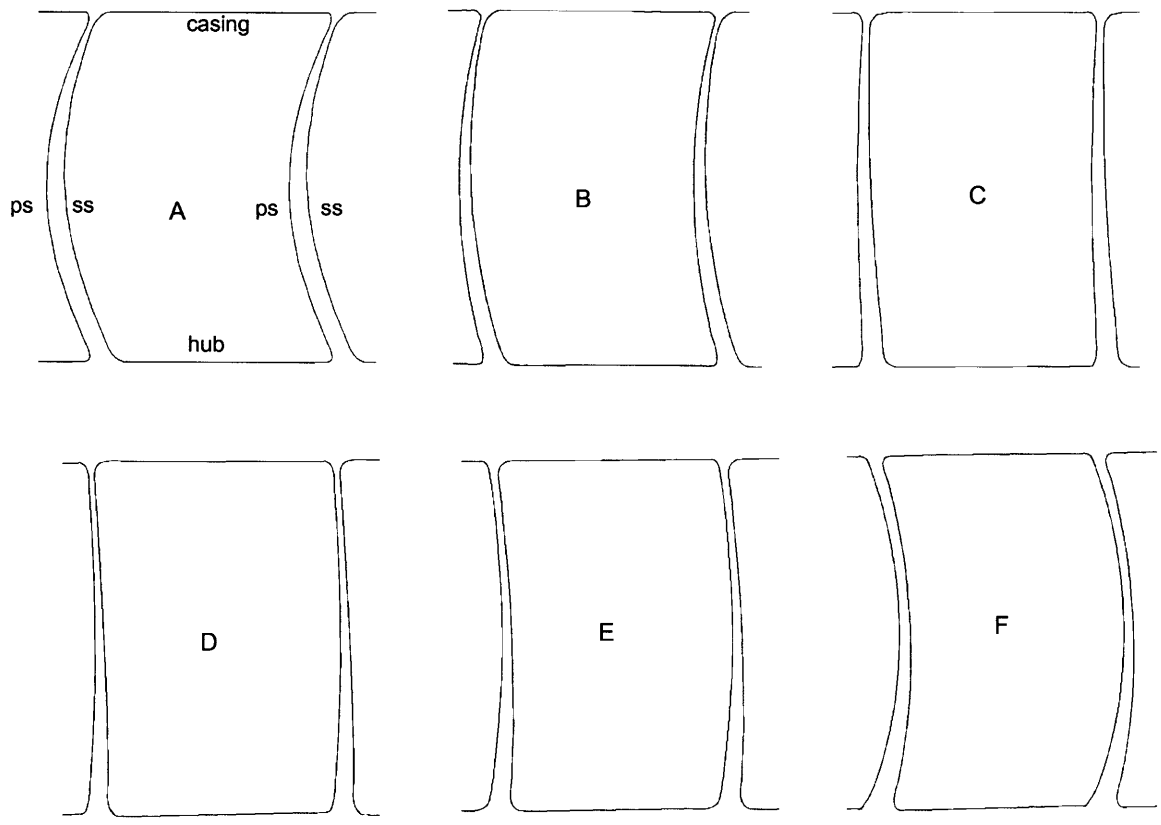

Figure 3.5 Axial view of the blade passage of stators A through F. Dihedral changes from positive in stator A to negative in stator F.

The S indicators are plotted with the D parameters evaluated at the hub in Figure 3.6. The baseline result from section 2.3.3 is also plotted for reference. The D parameters of the stators are roughly 15 with slight variation due to difference in upstream flow condition. The CFD simulations show that for stators A through E, the endwalls are free of separation and the size of the suction surface separation as indicated by the S indicator only changes slightly. The critical D value of 20 is not exceeded and the separation criterion holds for these cases.

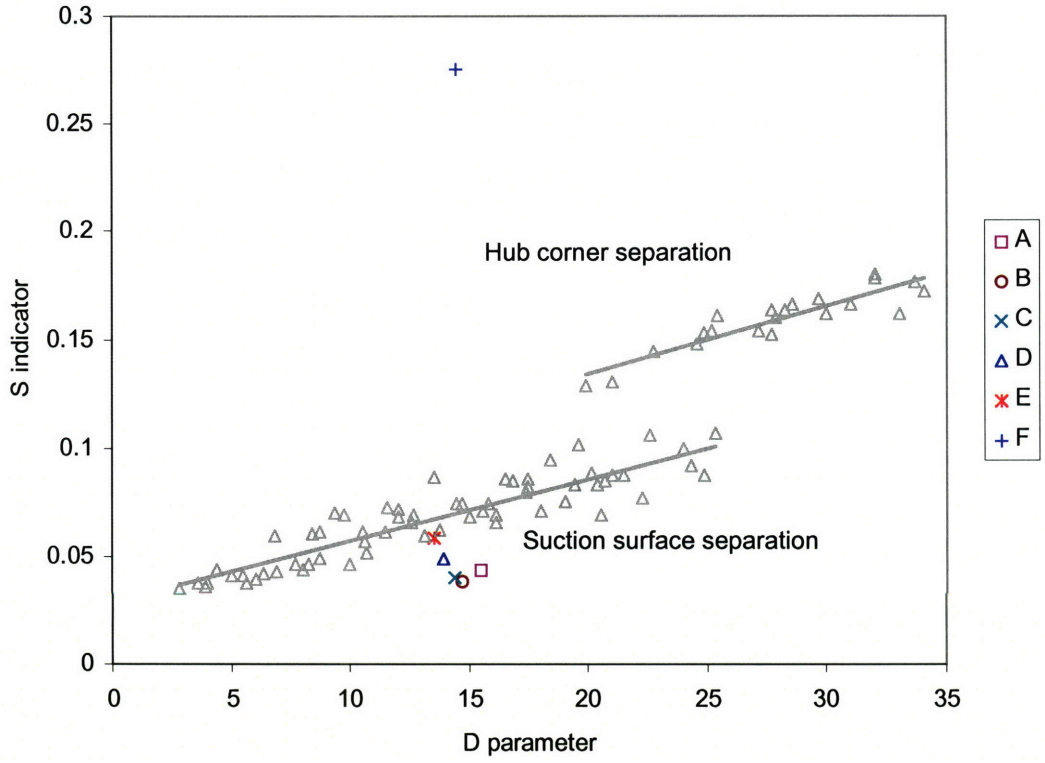

Figure 3.6 The S indicator and D parameter of Stators A through F. Baseline data from Section 2.3.3 are shown in grey.

Negative sweep and negative dihedral promote endwall secondary flow (Tweedt et al, 1986, Breugelmans et al, 1984 and Shang et al, 1993). Weingold et al. (1995) proposed that negative dihedral converges streamtubes near the endwall, increasing the endwall diffusion and hence promoting flow separation. In stator F, the combination of sweep and dihedral causes severe hub corner separation although the D parameter is below the critical value of 20. This reveals a limitation of the D parameter that calls for further investigation.

Summarizing the numerical results of stators A through F, the flow separation criterion should be applied with caution to blade designs with sweep or dihedral. Further investigation is needed to quantify the effects of sweep and dihedral on the onset of hub corner separation such that the D parameter can be redefined to capture these effects.

3.4 Summary

The D criterion for three-dimensional flow separation proposed in Chapter 2 was developed from the analysis of linear cascades with NACA 65 blades using CFD. The applicability of the criterion to other geometries was assessed with blade passage data available from the literature and from the industry. The geometries considered include linear compressor cascades, annular compressor cascades, compressor rotors and compressor stators. The separation criterion in terms of the D parameter with $D > 20$ for hub corner separation and $D < 20$ for suction surface separation holds for the majority of the designs analyzed. The result suggests that the D criterion is applicable to axial compressor design applications. One shortcoming of the D parameter is that it does not capture the effect of dihedral or sweep on endwall secondary flow. Further investigation is necessary to redefine the D parameter such that the effects of blade stacking are captured.

Chapter 4 Flow Control to Mitigate Hub Corner Separation

In Chapter 2, the idea of using hub cavity leakage to mitigate hub corner separation was discussed. The idea of mitigating hub corner separation by introducing momentum in a direction opposite to the secondary vorticity is further explored in this chapter. A flow control concept that produces the necessary momentum to mitigate hub corner separation using injection from the blade suction surface was examined. To gain further confidence in the flow control scheme designed using CFD tools, an actuated blade was fabricated and the effectiveness of the actuation scheme was assessed experimentally in a linear cascade test.

4.1 A New Flow Control Concept to Mitigate Hub Corner Separation

It was demonstrated in Section 2.4.4 that one feasible way of reducing the D parameter of a blade passage to a level below the three-dimensional separation threshold is by introducing cross-stream momentum into the blade passage with hub cavity leakage. Apart from cross-stream momentum, spanwise momentum imparted by suction surface injection can also alleviate secondary flow as shown in Figure 4.1. The hub cavity leakage that causes the skewing of endwall boundary layer studied in Section 2.4.4 can be considered as a form of flow control. However, in an axial compressor, control over the hub cavity leakage is limited. Injection slots necessary for flow control purposes may be located on the endwall but physical access to the area (especially the hub) to deliver the actuation flow is difficult. Delivery of actuation from the suction surface thus appears to be a more feasible alternative.

Flow control strategies with actuation from the suction surface have been experimentally studied by Culley et al. (2003) and Kirtley et al. (2004). These schemes were successful in reducing the loss associated with the flow away from the endwall but the endwall regions, particularly the hub, benefit little

from the actuation. Instead of installing additional flow control devices on the endwall to improve the endwall flow, the concept of mitigating hub corner separation by means of injection from the suction surface has the potential to enhance the existing strategies.

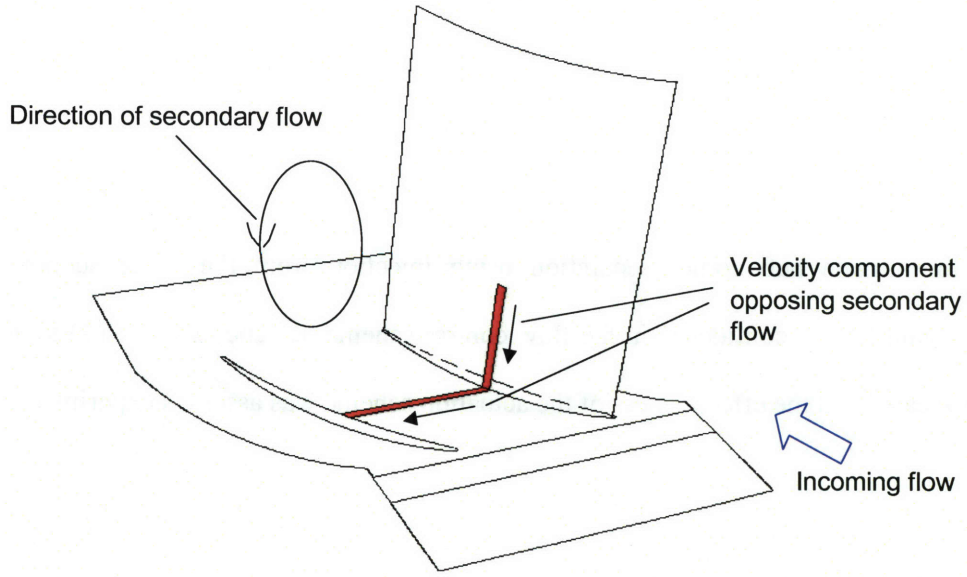

Figure 4.1 Flow control idea to alleviate secondary flow with cross-stream or spanwise momentum injection.

4.1.1 Actuated Blade Concept with Embedded Cavity

Figure 4.2 is a schematic of a typical axial compressor stage with a shrouded stator. It illustrates how the actuation flow can be delivered to a stator blade from the casing where physical access is not as limited as the hub. A similar arrangement has been reported by Culley et al. (2003) and Kirtley et al. (2004).

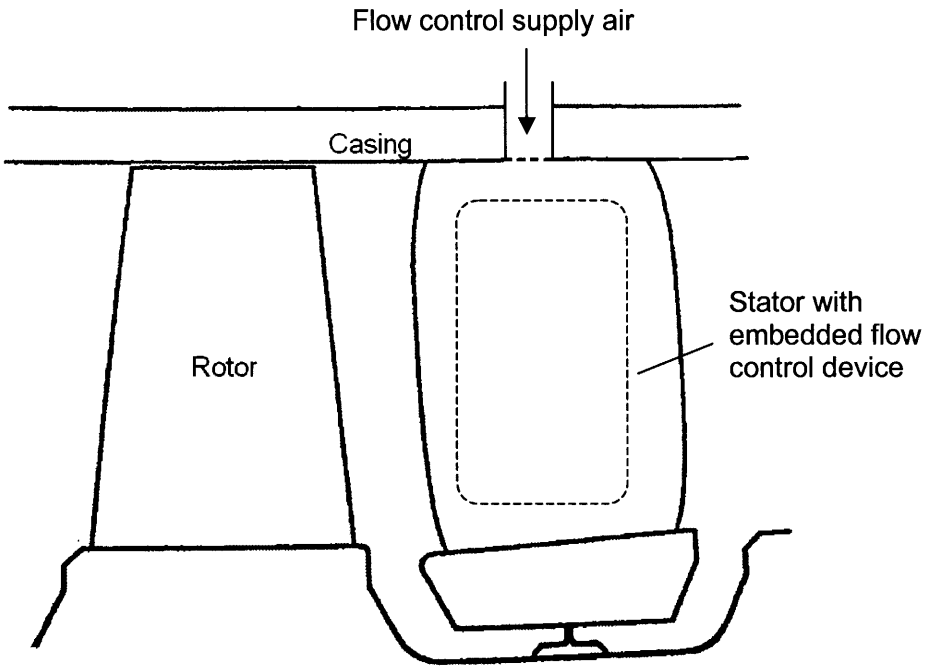

Figure 4.2 Schematic of actuation flow delivery from compressor casing.

A design intended to mitigate hub corner separation by introducing spanwise momentum to alleviate secondary flow as shown in Figure 4.3 was proposed. The flow control device consists of a cavity embedded in a blade with actuation flow fed by a feed channel from the casing. The incoming flow is turned 90° by the feed channel and impinges on the cavity wall adjacent to the blade leading edge, setting up two recirculation zones inside the cavity. Simulation of the blade cavity provides detail of the recirculating flow as depicted in Figure 4.4. Injection can be delivered to the freestream by implementing a slot on the cavity wall. The injection from a slot located near the leading edge side of the cavity has a spanwise velocity component from the recirculating flow. The spanwise momentum of the injection alleviates the secondary flow in a blade passage and mitigates hub corner separation. Besides spanwise momentum, streamwise momentum that energizes the boundary layer on the suction surface to further alleviate flow separation can be imparted to the freestream by pitching the injection slot in the streamwise direction.

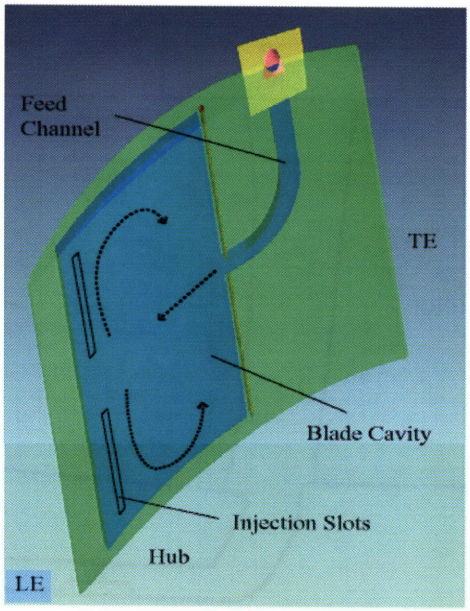

Figure 4.3 Flow control device with an embedded cavity to deliver spanwise momentum to alleviate secondary flow from the blade suction surface. Arrows indicate flow direction inside cavity.

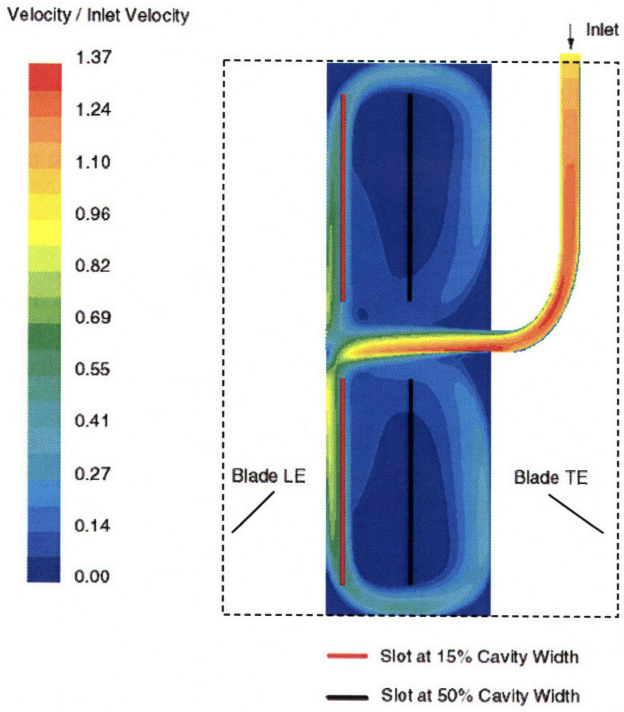

Figure 4.4 CFD calculation showing the recirculation zones inside the blade cavity. Outline of blade is shown in dotted lines.

Simulation of the three-dimensional, steady blade cavity flow was performed to examine the flow uniformity of injection from slots at the two different locations as shown in Figure 4.4. The boundary conditions for the blade cavity model were the mass flow rate at the feed channel inlet and the static pressure at the slot. The computation was performed with an injection flow rate of 1% of the cascade flow (the choice of injection flow rate will be further discussed in Section 4.3). The static pressure drop from the inlet of the feed channel to the slot is 3% of the stagnation pressure at the feed channel inlet. The computation results plotted in Figure 4.5 show that good uniformity of injection flow is achieved at the two locations examined. The standard deviation of the velocity distribution at the slot is less than 5% of the mean value. The blade cavity concept thus has an additional advantage that the location of injection slot has little effect on the flow uniformity of the injected sheet of air. This attribute provides flexibility in the design of flow control schemes in situation that the injection slot location is not known a priori.

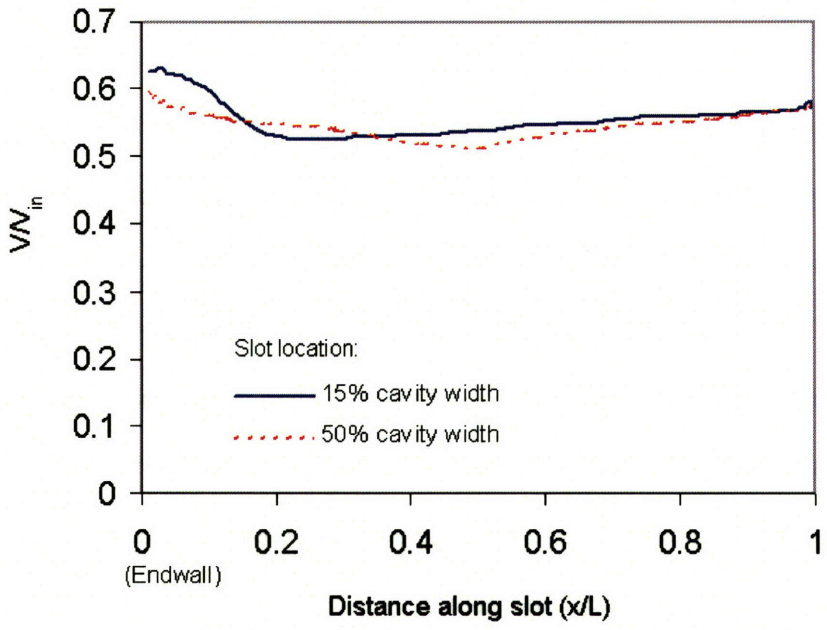

Figure 4.5 Velocity profile across the length of injection slot at two different locations in Figure 4.4. Injection velocity is normalized by the flow velocity at the feed channel inlet. Flow uniformity is not sensitive to the slot location.

4.2 Assessment of Flow Control Concept Using CFD

In accordance with the D criterion of three-dimensional flow separation developed in Chapter 2, the flow control idea was evaluated using a blade passage with hub corner separation as indicated by a D parameter above 20. A linear cascade with a D parameter of 21 on the HCS branch from Section 2.3 was chosen to assess the flow control concept. The design parameters of the linear cascade selected for the analysis are tabulated in Table 4.1.

Solidity	1.5
Aspect ratio	1.36
Camber	42°
Stagger	38°
Inlet flow angle	60.2°
Reynolds number	2.5×10^5

Table 4.1 Design parameters of the test cascade.

Rather than constructing a cascade model with an embedded blade cavity, the flow in the cascade blade passage and the flow inside the blade cavity were modeled separately to simplify the simulation. The compressor cascade was numerically modeled with an injection slot such that the injection velocity could be specified using the solution from the blade cavity simulation as shown in Figure 4.6. The slot was located on the blade suction surface at 21% chord where hub corner separation initiates. Both Culley et al. (2003) and Kirtley et al. (2004) reported using an injection flow rate of 1% of the freestream flow rate in their flow control experiments. With this as a reference, the assessment was performed with an injection flow rate of 1% of the cascade flow.

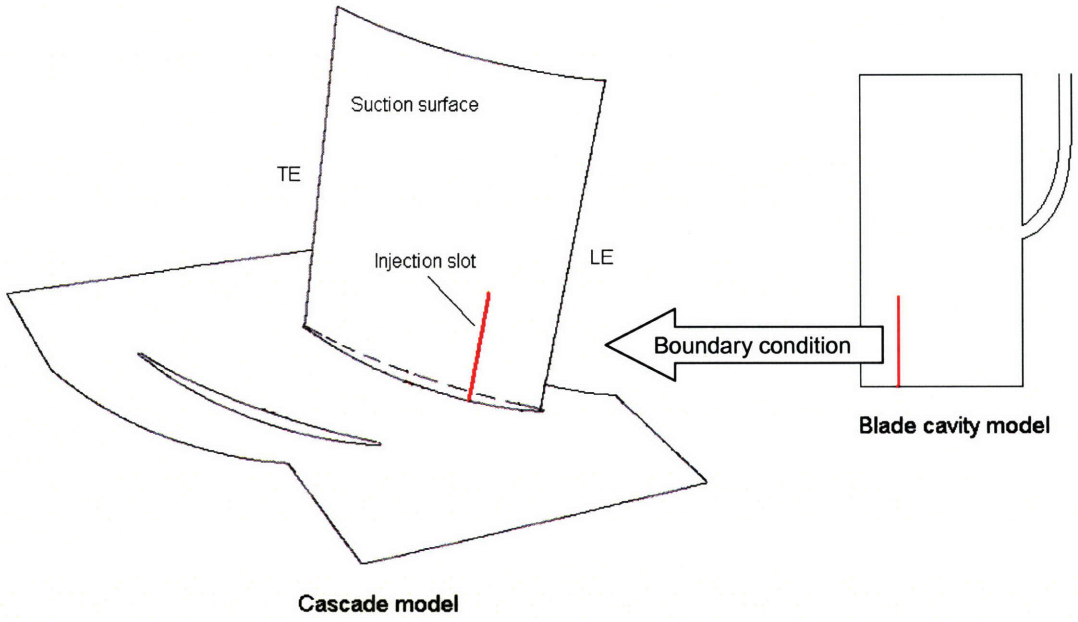

Figure 4.6 Schematic of computation domains with injection slot. Injection velocity from the blade cavity simulation is applied to the cascade model.

In addition to spanwise momentum, the injection slot in this numerical experiment was pitched in the streamwise direction at 24° to the suction surface such that streamwise momentum was also imparted to the freestream. In the flow control experiments of Culley et al. (2003) and Kirtley et al. (2004), the injection was in the streamwise direction only. To compare the effect of the proposed flow control scheme to the strategy with streamwise injection only, a second numerical experiment without spanwise momentum was also performed. In this case, the injection was in the streamwise direction only with the same injection flow rate of 1% of the cascade flow.

The effectiveness of the flow control scheme was assessed by examining the size of the high loss region associated with hub corner separation. Figure 4.7 shows that injection using only streamwise momentum reduces the size of the high loss region, and the size is further reduced with injection in both spanwise and streamwise directions.

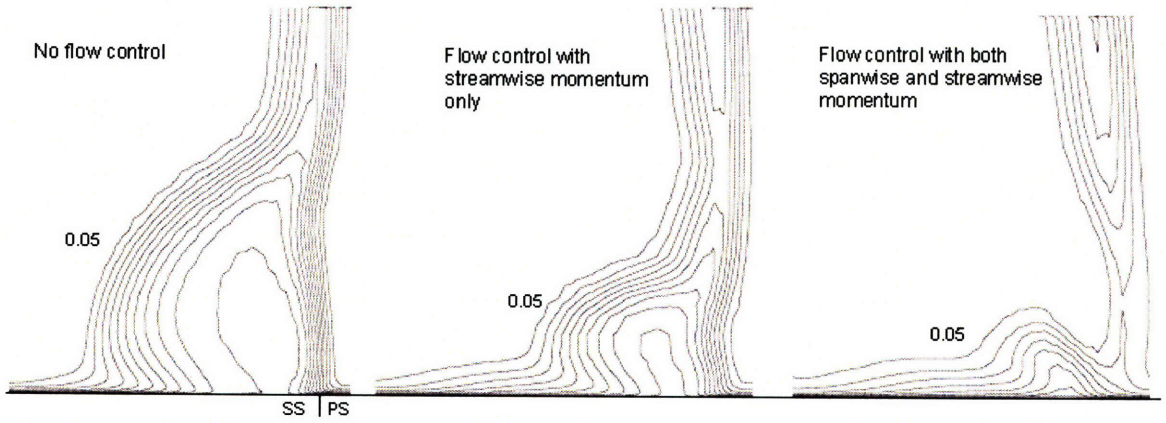

Figure 4.7 Contour of stagnation pressure at cascade exit indicating the size of high loss region. Contour begins at 0.05 with intervals of 0.05.

The advantage of injection with both spanwise and streamwise momentum over that with streamwise momentum only can be further verified by examining the flow field near the endwall as shown in Figure 4.8. With no flow control as in Figure 4.8a, flow separation near the endwall indicates the presence of hub corner separation. For the flow control case with streamwise injection only, hub corner separation is still present as shown in Figure 4.8b but the size of the separation region is reduced. In the flow control case with the injection of both spanwise and streamwise momentum, hub corner separation is absent from the flow field in Figure 4.8c. The results demonstrated the effectiveness of the proposed flow control scheme in the mitigation of hub corner separation.

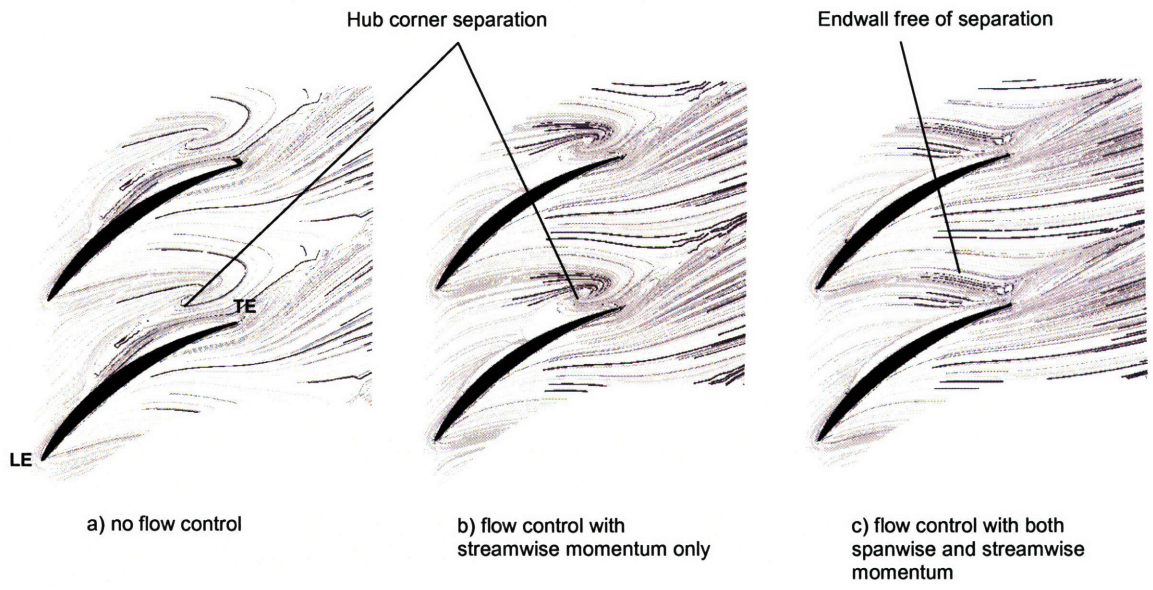

Figure 4.8 Limiting streamlines depicting the flow field near the endwall. From left to right: a) no actuation, presence of hub corner separation is indicated by the flow reversal and a recirculation zone near the endwall; b) actuation without imparting spanwise momentum, hub corner separation is still present; c) actuation with spanwise momentum injected, hub corner separation is eliminated.

Effect of the flow control scheme on hub corner separation can also be shown in terms of the S indicator and the D parameter. Similar to the action of hub cavity leakage discussed in Section 2.4.4, the injection of spanwise momentum from the suction surface causes the boundary layer to become skewed. The alleviating effect of the injection on secondary flow is a function of the skewness of the boundary layer which is captured by the D parameter as discussed in Section 2.4.4. The S indicators and the D parameters for the baseline case and the flow control case are plotted in Figure 4.9. Data from Section 2.3 is also shown for a reference. The drop in the S indicator from the HCS branch level to the SSS branch level concurs with the elimination of the three-dimensional flow separation.

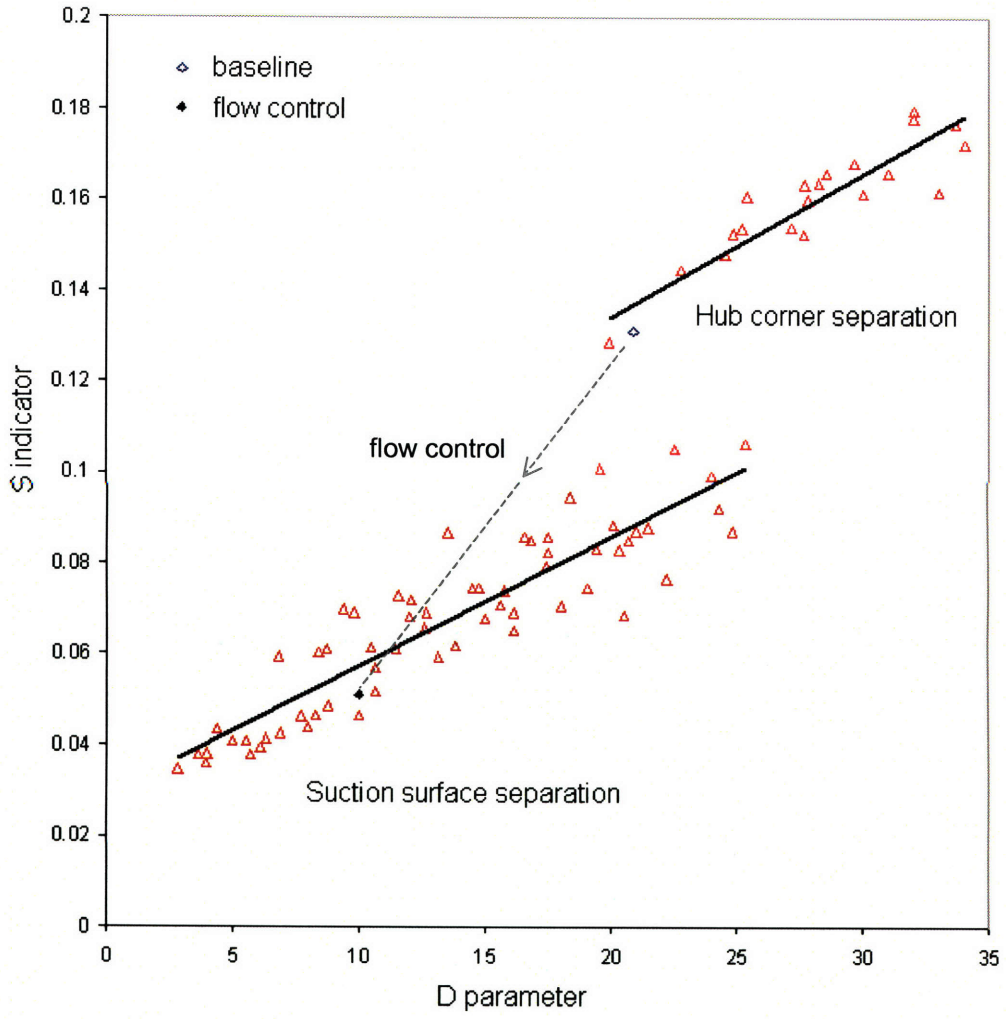

Figure 4.9 Elimination of hub corner separation with flow control.

4.3 Experimental Demonstration of Flow Control Concept

The computation results suggest that the flow control scheme with injection of spanwise momentum from the blade suction surface is capable of eliminating hub corner separation. It is desirable to demonstrate the effectiveness of the flow control design with a proof of concept experiment. Moreover, there are no publications on the application of the FLUENT package, which was used in the assessment of the flow control concept, to turbomachinery problem involving three-dimensional flow separation. A flow control experiment will provide further confidence in the new concept.

4.3.1 Design of Flow Control Experiment

The NASA LSAC compressor was used as a reference for a blade passage geometry representative of a modern compressor design. Barankiewicz and Hathaway (1998) reported that the LSAC operating at the increased loading condition had a moderately sized hub corner separation. To reproduce the flow feature near the endwall region, the flow passage geometry at 20% span of the LSAC stator was chosen for the design of a linear cascade experiment. As the main flow feature in concern is hub corner separation, it is desirable to replicate the adverse pressure gradient near the endwall. Comparison of the static pressure distribution at 5% span, as shown in Figure 4.10, shows that the adverse pressure gradient from the cascade geometry is similar to that in the LSAC stator.

This geometry has a D parameter of 21 and the flow field calculated with CFD indicates that the endwall flow in this geometry is separated in accordance with the flow separation criterion in terms of the D parameter. The design parameters of this cascade geometry are identical to the ones listed in Table 4.1.

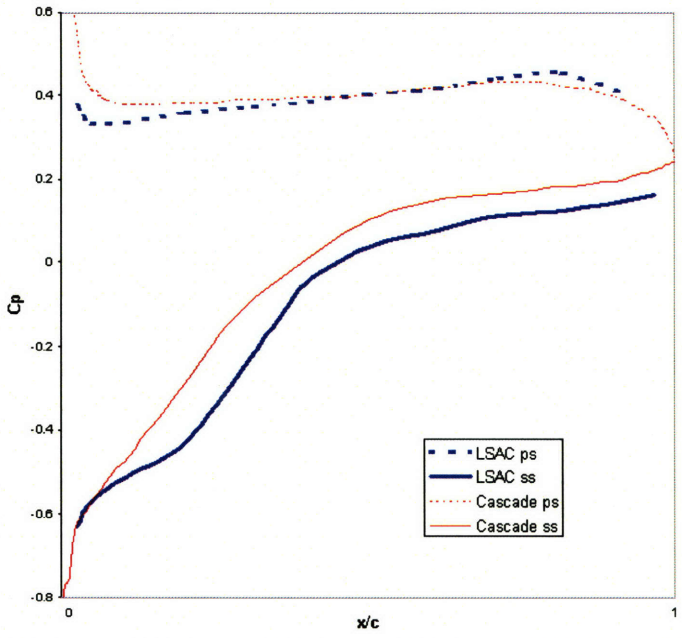

Figure 4.10 Static pressure distributions at 5% span in the LSAC stator from measurement (Barankiewicz and Hathaway, 1998) and in the linear cascade from CFD.

The effectiveness of the flow control scheme with the injection of spanwise momentum from the blade suction surface has been demonstrated in Section 4.2. An actuated blade with an embedded cavity as described in Section 4.1 was designed to deliver the necessary flow actuation. The schematic of the actuated blade is shown in Figure 4.11.

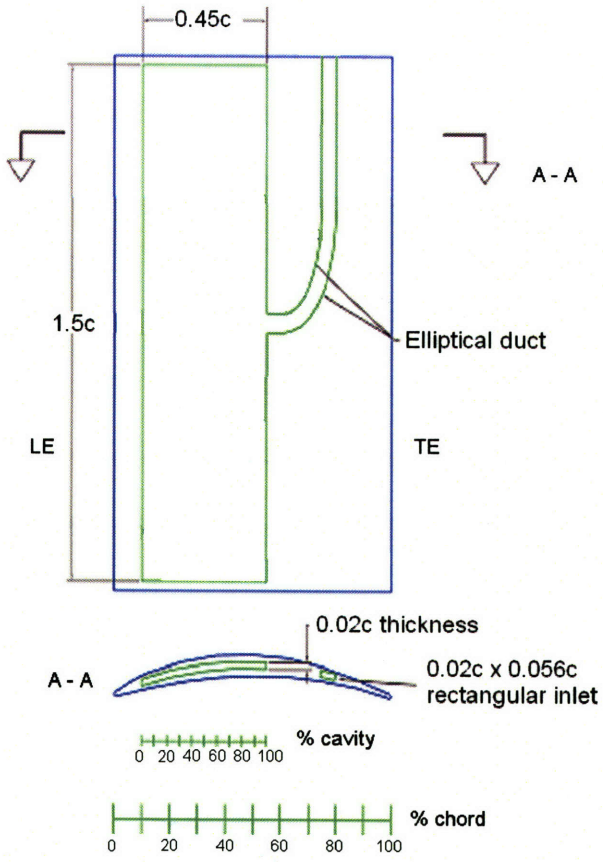

Figure 4.11 Schematic of the actuated blade. The blade cavity is outlined in green.

CFD analysis of the linear cascade indicated the onset of hub corner separation at 21% chord and the injection slot was located at this chordwise position. The slot spanned one third of the blade from the endwall.

In addition to spanwise momentum to alleviate secondary flow, the injection slot was pitched at 24° relative to the blade suction surface to impart streamwise momentum to the flow. Since the blade

cavity was pressurized in the flow control experiment, the actuated blade was designed with a wall thickness of 0.007 of chord to ensure structural integrity. With this wall thickness, the slot width was chosen to be 0.004 of chord such that the depth to width ratio of the angled slot is greater than 4 to make sure the injection flow was properly guided. The choices of slot angle and slot width were limited by the capability of the machine that cuts the injection slot on the actuated blade.

To determine the optimal injection flow rate, a CFD analysis with injection flow rates ranging from 0.4% to 1.5% of the cascade flow rate was performed. To assess the effectiveness of flow control on loss reduction Culley et al. (2003) used the loss coefficient (ω), based on the difference in stagnation pressure across the blade row, as a metric. Using the loss coefficient through the cascade as a measure for the size of the high loss region, the result in Figure 4.12 suggests that a high injection flow rate is always desirable. However, there is work done associated with the delivery of the injection which is not accounted for and the negative loss coefficient at 1.5% injection indicates excessive momentum is injected to the cascade.

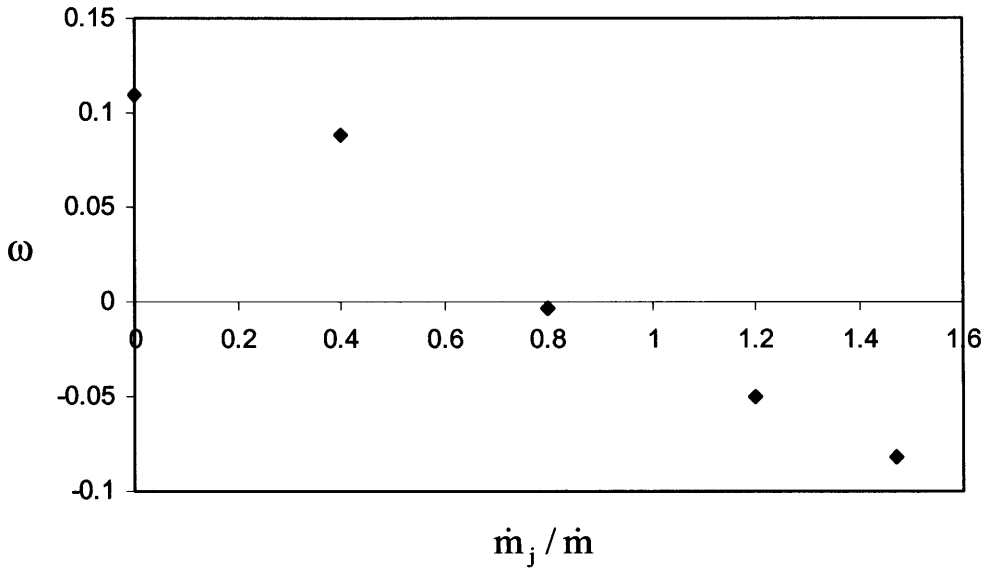

Figure 4.12 Stagnation pressure loss coefficient as a function of injection flow rate.

To better account for the injection such that a fair comparison can be made, a control volume analysis in terms of entropy generation using the second law of thermodynamics was performed. The schematic of the control volume which represents the blade row with injection slot is shown in Figure 4.13.

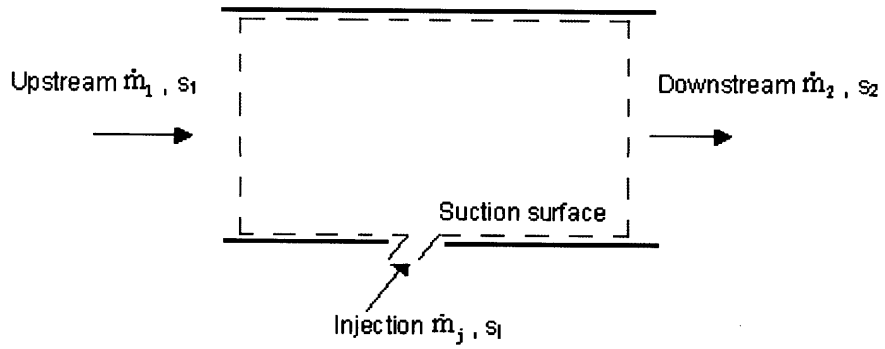

Figure 4.13 Control volume of blade row with injection

As the cascade flow is steady with no heat transfer, the rate of entropy generation $\dot{S}_{gen}$ is

$$\dot{S}_{gen} = \dot{m}_2 s_2 - (\dot{m}_1 s_1 + \dot{m}_j s_j). \tag{4.1}$$

The rate of entropy generation per unit mass flow $\dot{s}_{gen}$ is

$$\dot{s}_{gen} = s_2 - \bar{s}_{in} \tag{4.2}$$

where $\bar{s}_{in}$ is the mass averaged entropy entering the control volume as defined by

$$\bar{s}_{in} = \frac{\dot{m}_1 s_1 + \dot{m}_j s_j}{\dot{m}_1 + \dot{m}_j}. \tag{4.3}$$

For a perfect gas with constant specific heat, the change in entropy as given by the Gibbs equation is

$$ds = \frac{c_p dT_t}{T_t} - \frac{dp_t}{\rho_t T_t}. \tag{4.4}$$

For adiabatic flow $dT_t = 0$, hence

$$\frac{\dot{s}_{gen}}{R} = \frac{s_2 - \bar{s}_{in}}{R} = \ln\frac{p_{t2}}{p_{tin}} \sim \frac{p_{tin} - p_{t2}}{p_{tin}}. \tag{4.5}$$

The entropy generation can thus be expressed in terms of the stagnation pressure loss through the control volume. With the mass averaged stagnation pressure entering the control volume defined as

$$\bar{p}_{tin} = \frac{\dot{m}_1 \bar{p}_{t1}^{\,M} + \dot{m}_j \bar{p}_{tj}^{\,M}}{\dot{m}_1 + \dot{m}_j}, \tag{4.6}$$

the entropy generation in the cascade with flow control can be quantified by a loss coefficient ω_{act} defined as

$$\omega_{act} = \frac{\bar{p}_{tin} - \bar{p}_{t2}^{\,M}}{1/2\rho U_1^{\,2}}. \tag{4.7}$$

Figure 4.14 shows ω_{act} computed at different injection rate using the CFD results. With flow control applied, ω_{act} drops gradually to a minimum at an injection flow rate of about 0.8% and then increases rapidly at higher injection flow rates. The reduction in ω_{act} for injection flow rate below 0.8% is due to reduction of the size of the high loss region as indicated in Figure 4.12. For injection flow rates above 0.8%, the energy expenditure outweighs the benefit of loss reduction and as a result ω_{act} increases.

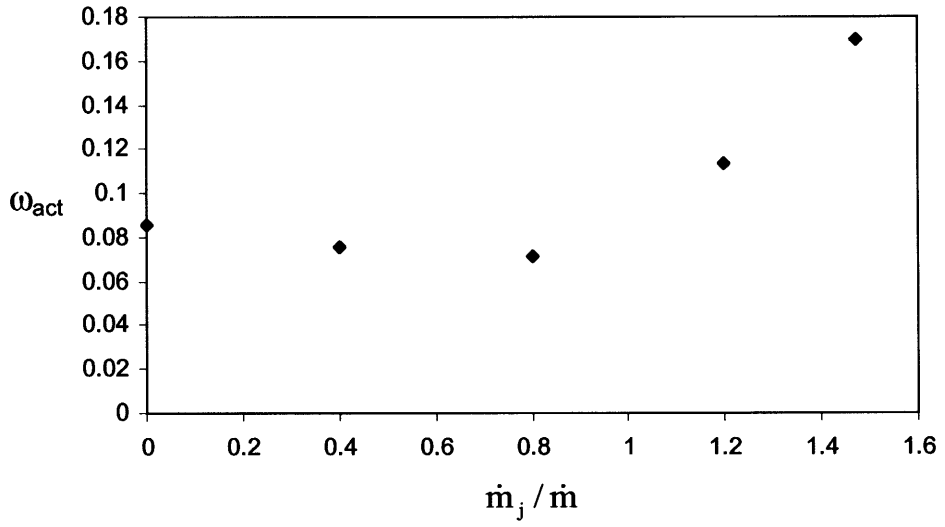

Figure 4.14 Loss coefficient with actuation as a function of injection flow rate.

A simulation of the cascade with flow control shows that hub corner separation is eliminated with the optimal injection flow rate of 0.8%. This injection flow rate was thus tested in the flow control experiment.

4.3.2 Experimental Setup

A linear compressor cascade experiment with parameters shown in Table 4.1 was built. A sketch of the linear cascade is shown in Figure 4.15. The cascade walls were constructed with 3/8 inch thick Plexiglass plates. The five blades in the cascade were fabricated using stereo lithography at the NASA Glenn Research Center. The actuated blade was located in the center of the blade row. An injection slot with a width of 0.04% chord, spanning one third of the blade from the hub, was machined on the suction surface. The slot was located at 21% chord from the blade leading edge and was pitched at an angle of 24° with the suction surface. Tufts were attached to the endwall of the actuated blade passage to visualize the presence of hub corner separation. With no flow control, the presence of hub corner separation was indicated by erratic motion of the tufts.

Periodicity of the cascade shown in Figure 4.15 was achieved by adjusting the amount of sidewall bleed air upstream of the blades and by setting the angles of the sidewalls downstream of the blade row. A screen was installed at the exit of the test section in order to pressurize the cascade such that boundary layers could be bled to the atmosphere.

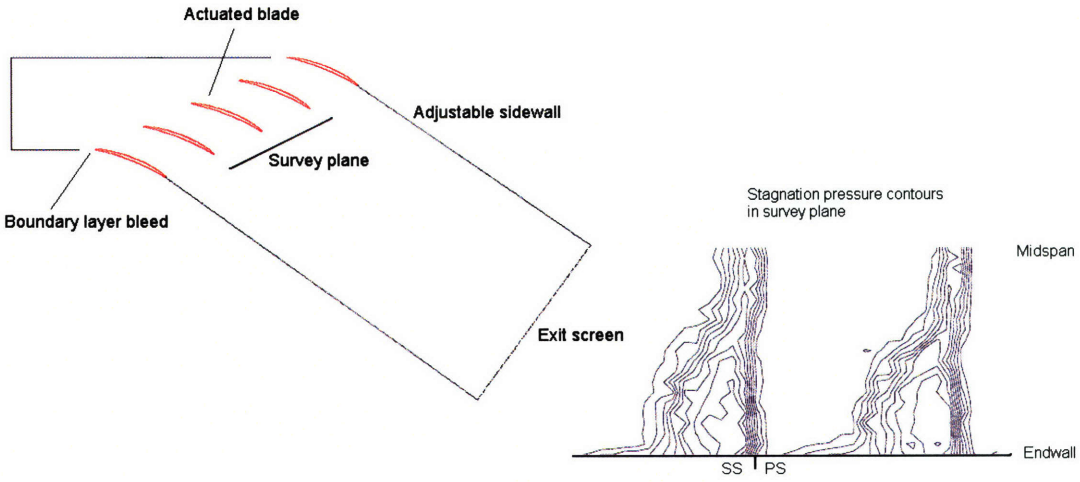

Figure 4.15 Schematic of linear cascade and sample of stagnation pressure survey showing periodic flow conditions.

A Pitot-static probe located at 0.5 axial chord upstream of the blade row was used to monitor the reference dynamic pressure (q_{ref}). To record the size and strength of the loss region caused by hub corner separation, stagnation pressure was surveyed by a Kiel probe located 30% of axial chord downstream of the blade trailing edge. A three-axis TSI traverse table with 0.01mm position resolution was used to control the Kiel probe position in the survey plane. The survey plane measures 1 pitch x 0.5 span with 20 points in both the pitchwise and spanwise directions.

Two Setra 264 pressure transducers with full span of 2.5 inches WC (623Pa) were used to measure the reference dynamic pressure and the stagnation pressure change through the cascade. The pressure transducer has ±0.4% full span accuracy which translates to ±1.5% of reference dynamic pressure at the design Reynolds number. The stagnation pressure coefficient defined by

$$C_{pt} = \frac{p_{t\_ref} - p_{t\_survey}}{q_{ref}} \tag{4.8}$$

has an uncertainty of ±4.8%.

The injection flow rate was measured by a thermal mass flow meter manufactured by Teledyne Hastings Instruments. The model HMF-201 flow meter has a capacity of 300 liters per minute with ±1.0%

full span accuracy. The uncertainty in injection flow rate is ±1.8%. Figure 4.16 shows the linear cascade experiment with the data acquisition system.

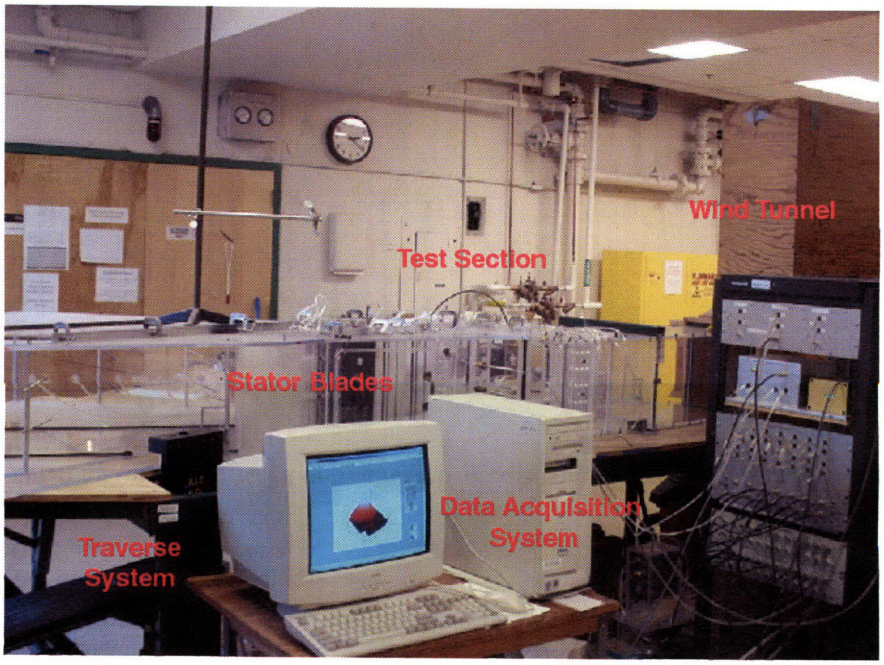

Figure 4.16 The linear cascade experiment.

4.3.3 Characterization of the Actuated Blade

The flow uniformity of the injection air was assessed using a DANTEC single hot-wire (5μm thick) with a DANTEC CTA bridge 56C17. The hot wire was positioned at a distance of three times the slot width from the slot and was oriented such that it was perpendicular to the sheet of injection air. The single hot-wire measures the total magnitude of the streamwise and spanwise velocity components of the injection air together. The hot-wire was traversed along the slot and the measurement is compared with CFD results in Figure 4.17. The measured standard deviation of the velocity distribution was 7% of the mean value. Satisfactory flow uniformity was obtained from the actuated blade.

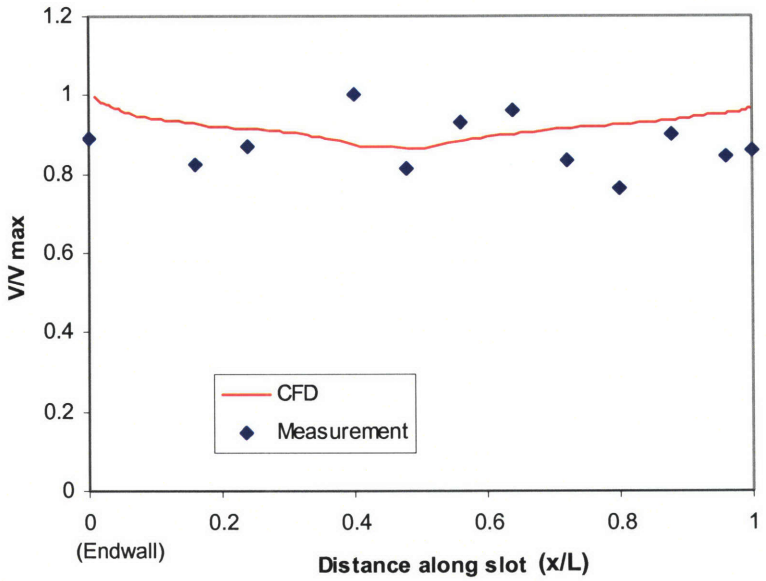

Figure 4.17 Uniformity of injection from measurement and CFD. The flow velocity is normalized by the maximum velocity in the velocity profile.

The actuated blade was characterized with a static pressure coefficient

$$C_{p\,act} = \frac{p_{in} - p_j}{p_{t\,in}} \tag{4.9}$$

and a stagnation pressure coefficient defined as

$$C_{pt\ act} = \frac{p_{t\,in} - p_{t\,j}}{p_{t\,in}}. \tag{4.10}$$

From measurement, $C_{p\,act} = 0.01$ and $C_{pt\,act} = 0.1$. The discharge coefficient, which is the ratio of the actual flow rate to the isentropic flow rate, was estimated to be 0.9.

4.3.4 Flow Control Experimental Results

The objective of the experiments is to assess the effectiveness of the flow control scheme in terms of mitigating hub corner separation. The best parameter to measure the size of the three-dimensional flow separation would be the S parameter. However, the design of the actuated blade consisting of an

embedded cavity prohibited the measurement of static pressure on the suction surface which is necessary to calculate the S indicator. As discussed in Section 2.5, the stagnation pressure loss coefficient can also serve as an indicator of the size and strength of hub corner separation. In addition to the optimal injection flow rate of 0.8% an experiment at a reduced injection flow rate of 0.4% was also conducted to examine the sensitivity of injection flow rate on the size of the hub corner separation. The contours of the measured stagnation pressure coefficients are presented in Figure 4.18 and the corresponding plots from the computations are shown in Figure 4.19.

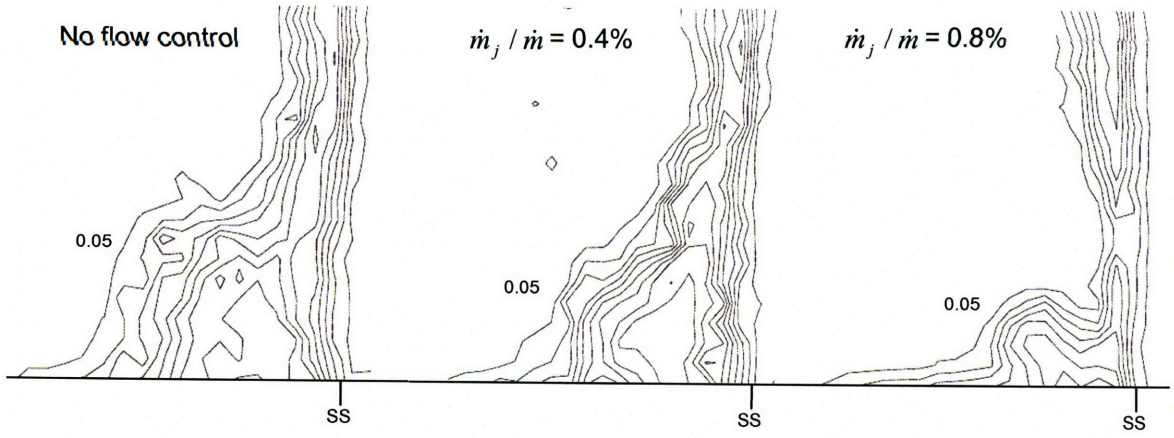

Figure 4.18 Contours of stagnation pressure coefficient from measurement. From left to right: a) Baseline without flow control; b) with flow control at 0.4% flow rate; c) with flow control at 0.8% flow rate. Contours begin at 0.05 with 0.05 intervals.

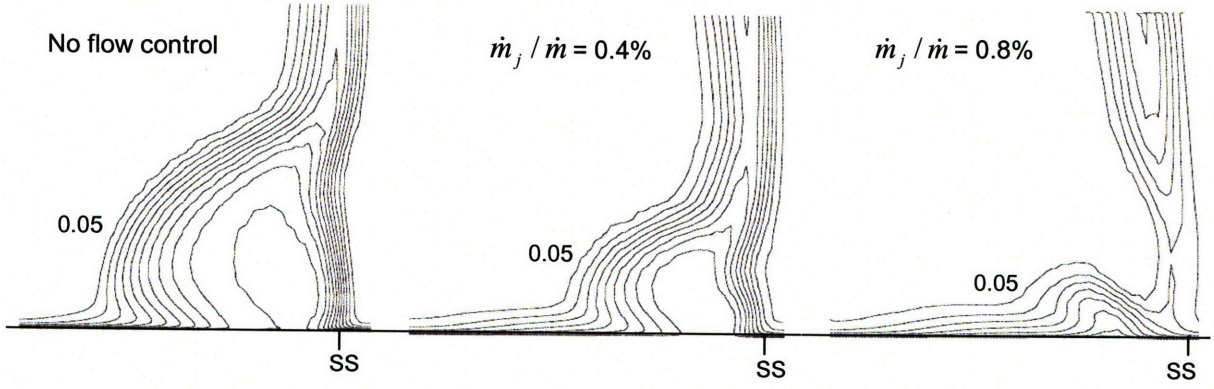

Figure 4.19 Contours of stagnation pressure coefficient from CFD. From left to right: a) Baseline without flow control; b) with flow control at 0.4% flow rate; c) with flow control at 0.8% flow rate. Contours begin at 0.05 with 0.05 intervals.

The measurements compare well with the CFD data for both the datum line and flow control cases. At an injection flow rate of 0.4%, there is a small reduction in the size of the high loss region. Flow visualization at the endwall with tufts confirmed the presence of hub corner separation at this injection flow rate. On the other hand, at the injection flow rate of 0.8%, the size of the high loss region was further reduced and the elimination of hub corner separation was confirmed by endwall tufts pointing in the streamwise direction.

To quantitatively compare the experimental and CFD results, ω and ω_{act} defined in equation (4.7) are tabulated in table Table 4.2.

	CFD		Experiment	
Injection flow rate	ω	ω_{act}	ω	ω_{act}
0 (baseline)	0.086	0.086	0.083	0.083
0.4%	0.076	0.076	0.080	0.080
0.8%	0.046	0.071	0.049	0.076

Table 4.2 ω and ω_{act} from CFD and experiment.

The values of ω and ω_{act} from measurement compare well with the CFD results for the baseline case and the flow control cases. Note that the results from both CFD and experiment at an injection flow rate of 0.4% indicate identical ω and ω_{act}. It appears that the benefit of a reduced high loss region is balanced by the energy expenditure associated with the injection at this particular injection flow rate. To quantify the effectiveness of the flow control scheme, the CFD results predict a 17% reduction in ω_{act} while the measurement shows a 8% reduction at the optimal injection rate of 0.8%.

4.4 Summary

A novel flow control concept to mitigate hub corner separation in axial compressor was proposed. The idea is to alleviate the detrimental effect of secondary flow that promotes three-dimensional flow

separation by imparting spanwise momentum to the blade passage. The actuation is delivered from the blade suction surface which allows easy adaptation to axial compressors.

The effectiveness of the flow control concept was assessed numerically. Hub corner separation in a linear cascade with a D parameter of 21 was eliminated using an optimal injection flow rate of 0.8% of the cascade flow based on a loss analysis. To gain further confidence in the flow control design, a proof of concept experiment in a linear cascade featuring profile of the stator blade of the NASA LSAC compressor was performed. The flow control scheme eliminated hub corner separation with 8% reduction in loss taking the injection flow into consideration.

Chapter 5 Summary and Conclusions

5.1 Summary

A preliminary design method was developed to assess three-dimensional flow separation limits for blade design in axial compressors. The method consists of a parameter that quantifies the tendency toward hub corner separation in terms of the combined effects of adverse pressure gradient and secondary flow. Linear compressor cascades with a wide range of design parameters were assessed with this method and a criterion for three-dimensional flow separation was proposed based on a CFD analysis of the cascades. The generality and limitations of the separation criterion were evaluated with data from the literature and industry.

The idea of mitigating hub corner separation with the injection of spanwise momentum from blade suction surface to alleviate secondary flow was assessed with CFD. A flow control scheme using this concept was designed and its effectiveness was demonstrated in a linear cascade experiment.

5.2 Conclusions

The conclusions from this research are

- Compressor blade design in terms of three-dimensional flow separation can be assessed with a simple parameter which is defined as

$$D = \frac{C_{pi}\varepsilon}{\sigma} \tag{2.18}$$

  The D parameter quantifies the combined effect of adverse pressure gradient and endwall secondary flow that governs the onset of hub corner separation.

- The size and strength of suction surface separation and hub corner separation can be quantified by the S indicator which is defined as

$$S = \psi_z\big|_{z/L=0.5} - \psi_z\big|_{z/c=0.1} \tag{2.6}$$

in terms of the Zweifel coefficient with reference to the inlet dynamic pressure. The onset of hub corner separation is indicated by an abrupt reduction in blade loading as quantified by the S indicator.

- The onset of three-dimensional flow separation occurs when the D parameter is between 20 and 25. It is recommended that compressor blades be designed with D less than 20 to avoid the occurrence of hub corner separation.

- For incompressible, steady and fully turbulent flow, the separation criterion in terms of the D parameter is valid for Reynolds numbers between 2.5×10^4 and 2.5×10^6, blade aspect ratios between 0.5 and 5, incoming endwall boundary layer with thickness up to 20% of chord. The separation criterion in terms of the D parameter is applicable to linear cascades, annular cascades and compressor stages. Nevertheless, the D parameter does not capture the effects of blade sweep or dihedral that affect the onset of hub corner separation because these effects are not quantified and modeled.

- Cross-stream and spanwise momentum associated with boundary layer skew affects the magnitude of the D parameter. With this idea, the D parameter of a blade passage with hub corner separation can be reduced to a lower level such that the separation is mitigated. This reduction in D parameter can be achieved in an axial flow compressor by introducing spanwise momentum to the blade passage from the suction surface in a direction opposite to secondary flow. A proof of

concept experiment demonstrated the elimination of hub corner separation at an injection flow rate of 0.8% of the free stream in a linear compressor cascade.

5.3 Contributions

The major contributions of this research include a simple method to evaluate blade passage design of axial compressors in terms of the onset of three-dimensional flow separation as indicated by the criterion of $D > 20$. The separation criterion provides guidance to the design of flow control schemes that mitigates hub corner separation by suppressing secondary flow in the blade passage. The proposed flow control strategy that mitigates hub corner separation via injection of spanwise momentum from the blade suction surface may have a potential application in axial compressor where physical access to the hub is limited.

5.4 Recommendations for Future Work

- The effect of sweep and dihedral on endwall secondary flow should be quantified and incorporated in the D parameter.

- To use the D parameter in the preliminary design of flow control schemes via injection of cross-stream or spanwise momentum to alleviate secondary flow, a simple analytical model that relates the change in the D parameter with the injection properties should be developed.

- It would be desirable to further assess the effectiveness of the proposed flow control scheme by analyzing its impact on compressor performance at a system level. Depending on the results, the flow control scheme may be implemented in a real axial compressor environment to conduct a proof-of-concept experiment.

References

Barankiewicz, W. S. and Hathaway, M. D., 1998, Impact of Variable-Geometry Stator Hub Leakage in a Low Speed Axial Compressor, ASME paper 98-GT-194.

Breugelmans, F. A. H., Carels, Y. and Demuth, M., 1984, Influence of Dihedral on the Secondary Flow in a Two-Dimensional Compressor Cascade, Journal of Engineering of Gas Turbines and Power, Vol. 106, pp. 578-584.

Culley, D. E., Bright, M. M., Prahst, P. S. and Strazisar, A. J., 2003, Active Flow Separation Control of a Stator Vane Using Surface Injection in a Multistage Compressor Experiment, ASME paper GT2003-38863.

Cumpsty, N. A., 2004, Compressor Aerodynamics, Krieger Publishing Company.

Demargne, A. A. J., and Longley, J. P., 2000, The Aerodynamic Interaction of Stator Shroud Leakage and Mainstream Flows in Compressors, ASME paper 2000-GT-570.

Dixon, S. L., 1978, Fluid Mechanics, Thermodynamics of Turbomachinery, Butterworth Heinemann.

Dong, Y., Gallimore,. S. J. and Hodson, H. P., 1987, Three-Dimensional Flows and Loss Reduction in Axial Compressors, Journal of Turbomachinery, Vol. 109, pp. 354-36.

Gallus, H. E., Hah, C. and Schulz, H. D., 1991, Experimental and Numerical Investigation of Three-Dimensional Viscous Flows and Vortex Motion Inside an Annular Compressor Blade Row, Journal of Turbomachinery, Vol. 113, pp. 198-206.

Gbadebo, S. A., Cumpsty, N. A. and Hynes, T. P., 2004, Three-Dimensional Separations in Axial Compressors, ASME paper GT2004-53617.

Gümmer, V., Wenger, U., Kau, H.-P., 2000, Using Sweep and Dihedral to Control Three-Dimensional Flow in Transonic Stators of Axial Compressors, ASME paper 2000-GT-491.

Hah, C. and Loellbach, J., 1997, Development of Hub Corner Stall and its Influence on the Performance of Axial Compressor Blade Rows.

Hinck, E. C., 1959, Secondary Flow in a Compressor Cascade, MIT GTL Report No. 50.

Horlock, J. H., Percival., P. M. E., Louis, J. F. and Lakshminarayana, B., 1961, Wall Stall in Compressor Cascades., ASEM paper 61-WA/FE-29.

Johnston, J. P., 1957, Three-Dimensional Turbulent Boundary Layer, MIT GTL Report No. 39.

Joslyn, H. D. and Dring, R. P., 1985, Axial Compressor Stator Aerodynamics, Journal of Engineering for Gas Turbines and Power, Vol. 107, pp. 485-493.

Kang, S. and Hirsch, CH., 1991, Three Dimensional Flow in a Linear Compressor Cascade at Design Conditions, ASME paper 91-GT-114.

Kirtley, K. R., Graziosi P., Wood, P., Beacher, B. and Shin, H.-W., 2004, Design and Test of an Ultra-Low Solidity Flow-Controlled Compressor Stator, ASME paper GT2004-53012.

Koch, C. C., 1981, Stalling Pressure Rise Capability of Axial Flow Compressor Stages, Journal of Engineering for Power, Vol. 103, pp. 645-656.

Lieblein, S., 1959, Loss and Stall Analysis of Compressor Cascades, Journal of Basic Engineering, pp. 387-400.

Leishman, B. A., Cumpsty, N. A. and Denton, J. D., 2004, Effects of Bleed Rate and Endwall Location on the Aerodynamic Behaviour of a Circular Hole Bleed Off-Take, ASME paper GT2004-54197.

Lord, W. K., MacMartin D. G. and Tillman. T. G., 2000, Flow Control Opportunities in Gas Turbine Engines, AIAA paper 2000-2234.

Luecke, J. R., Gallus, H. E., Sanz, W., Benetschik, H. and Platzer, M. F., 1996, Numerical Investigation of Transition and Hub Corner Stall Phenomena Inside an Annular Compressor Cascade, AIAA paper 96-2655.

Mertz, C., 1954, A Study of the Effect of Boundary Layer Control on an Axial Flow Compressor Stage, Aeronautical Engineer Thesis, California Institute of Technology.

Peacock, R.E., 1965, Boundary-Layer Suction to Eliminate Corner Separation in Cascades of Airfoils, Reports and Memoranda no. 3663, University Engineering Department, Cambridge.

Schulz, H. D. and Gallus, H. D., 1988, Experimental Investigation of the Three-Dimensional Flow in an Annular Compressor Cascade, Journal of Turbomachinery, Vol. 110, pp. 467-478.

Schulz, H. D., Gallus, H. E. and Lakshminarayana, B., 1990, Three-Dimensional Separated Flow Field in the Endwall Region of an Annular Compressor Cascade in the Presence of Rotor-Stator Interaction: Part 1-Quasi-Steady Flow Field and Comparison with Steady-State Data, Journal of Turbomachinery, Vol. 112, pp. 669-678.

Shang, E., Wang, Z. Q. and Su, J. X., 1993, The Experimental Investigations on the Compressor Cascades with Leaned and Curved Blade, ASME paper 93-GT-50.

Smith, L. H., 1970, Casing Boundary Layers in Multistage Compressors, Flow Research on Blading, L. S. Dzung, Elsevier Publishing Company, Amsterdam, The Netherlands.

Squire, H.B. and Winter, K. G., 1951, The Secondary Flow in a Cascade of Airfoils in a Nonuniform Sream, Journal of the Aeronautical Sciences, pp. 271-277.

Tang, Y.-P. and Chen, M.-Z., 2004, An Experimental Investigation of a Vortex Flow Cascade, ASME paper 88-GT-265.

Tweedt, D. L., Okiishi, T. H. and Hathaway, M. D., 1986, Stator Endwall Leading-Edge Sweep and Hub Shroud Influence on Compressor Performance, ASME paper 86-GT-197.

Weber, A., Schreiber, H.-A., Fuchs, R. and Steinert, W., 2002, 3-D Transonic Flow in a Compressor Cascade with Shock-Induced Corner Stall, Journal of Turbomachinery, Vol. 124, pp. 358-365, 2002.

Weingold, H. D., Neubert, R. J., Behike, R. F. and Potter, G. E., 1995, Reduction of Compressor Endwall Losses Through the Use of Bowed Stators, ASME paper 95-GT-380.

Wellborn, S. R. and Okiishi, T.H., 1996, Effects of Shrouded Stator Flows on Multistage Axial Compressor Aerodynamic Performance, NASA Contractor Report 198536.

Wellborn, S. R., 2005, External Memorandum, Rolls Royce.

Appendix A

Analysis of the Functional Form of the D Parameter

The D parameter developed in section 2.2 is a non-dimensional parameter formed by multiplying the term

$$s(\alpha_1 - \alpha_2) \tag{2.15}$$

that characterizes secondary flow and the term

$$\frac{1-\left(\frac{\cos\alpha_1}{\cos\left(\gamma-\frac{\theta}{2}\right)}\right)^2}{c} \tag{2.14}$$

that characterizes the adverse pressure gradient. The result is a non-dimensional parameter $D=\frac{C_{pi}\varepsilon}{\sigma}$.

Since the three parameters involved in the definition of D are non-dimensional, they can be combined in different ways to form a non-dimensional parameter. However, the D parameter should provide physical insight in terms of the onset of hub corner separation. As the size and strength of hub corner separation is quantified by the S indicator, a correlation between the S indicator and an appropriately formulated D parameter is anticipated.

Assuming the S indicator scales with the D parameter such that $S \propto C_{pi}^{p}\varepsilon^{q}\sigma^{r}$ where p, q and r are the exponents of the C_{pi}, ε and σ terms respectively, a power law analysis was performed to evaluate the exponents. By keeping ε and σ constant while varying C_{pi}, the slope of the log-log plot of S versus C_{pi} gives the value of p. The exponents q and r were obtained similarly.

The different log-log plots are shown in Figure A1 to Figure A3. The results suggest that p = 1, q = 1 and r = -1. This gives $D=\frac{C_{pi}\varepsilon}{\sigma}$.

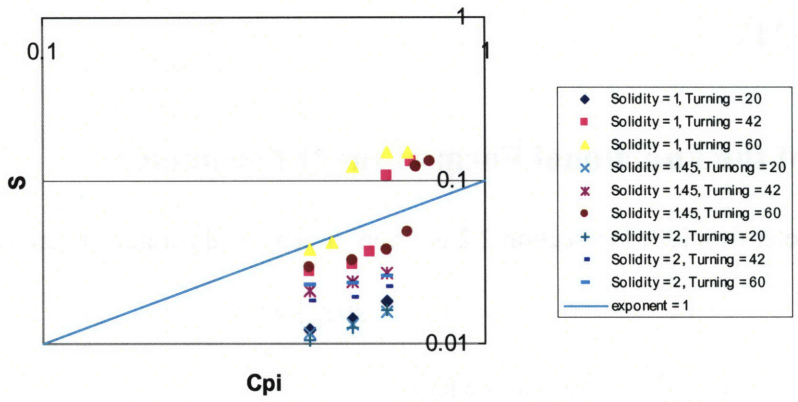

Figure A1 Log-log plot of S versus C_{pi} with ε and σ kept constant. The slope is about 1.

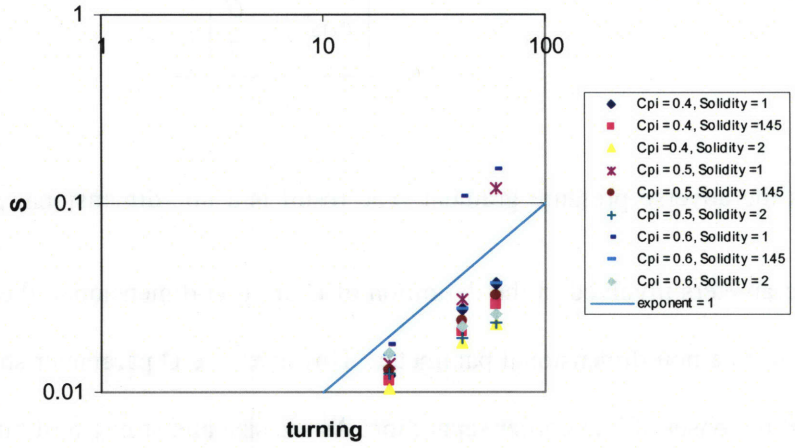

Figure A2 Log-log plot of S versus ε with C_{pi} and σ kept constant. The slope is about 1.

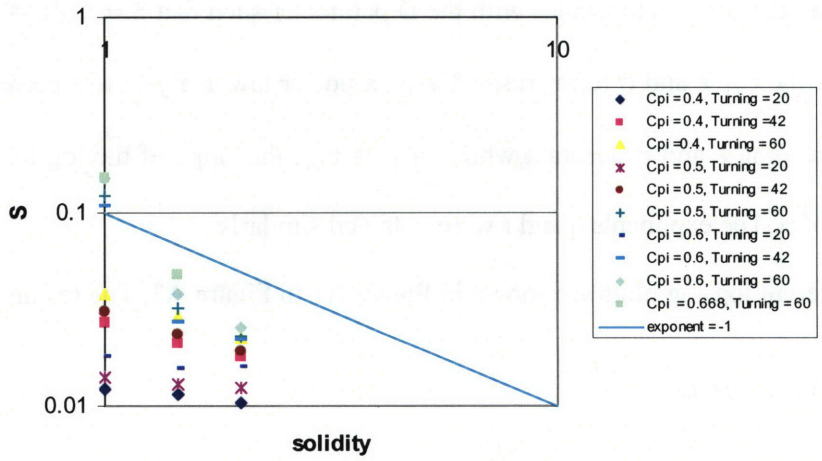

Figure A3 Log-log plot of S versus σ with C_{pi} and ε kept constant. The slope is about -1.

Appendix B

Control Volume Analysis to Model Hub Cavity Leakage Effect

The modified D parameter that accounts for the effect of boundary layer skew was assessed with CFD in Section 2.4.4.1. Results of the analysis showed that the modified D parameter is capable of capturing the effect of hub cavity leakage that mitigates hub corner separation. To design a flow control scheme using hub cavity leakage based on the modified D parameter, a simple analytical model that predicts the B coefficient (see Section 2.4.4 for detail) associated with the skewed boundary layer as a function of the leakage property is needed.

The effect of hub cavity leakage on the skewness of boundary layer is modeled using a simple control volume analysis. Figure B1 illustrates the control volumes used in the analysis. Control volume 1 encompasses both the free stream and the boundary layer while control volume 2 contains the freestream only. The x-axis points in the streamwise direction, the y-axis in the cross stream direction (into page) and the z-axis in the spanwise direction. The following assumptions are made in the control volume analysis:

1. Flow is steady, incompressible and inviscid.
2. $H >> \delta_1$ and δ_2.
3. The edge of boundary layer coincides with the local streamline such that there is no mass transfer between the two control volumes. For the flow over a flat plate, streamlines penetrate into the boundary layer. However, the CFD analysis shows that the leakage flow pushes the streamlines away from the boundary layer and hence the assumption is believed to be sound.
4. The x-component of pressure forces at the edge of the boundary layer is negligible.
5. The boundary layer from upstream is collateral.

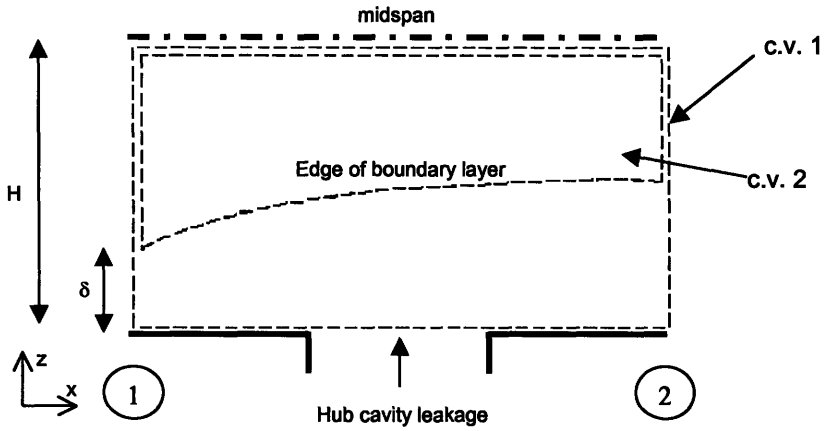

Figure B1 Control volume used in the hub cavity leakage model

Conservation of mass and momentum for control volume 1 gives

$$\rho U_1(H-\delta_1^*)+\dot{m}_j=\rho U_2(H-\delta_2^*) \tag{B1}$$

$$P_1H+\rho U_1^2(H-\delta_1^*-\theta_1)+\dot{m}_j v_{jx}=P_2H+\rho U_2^2(H-\delta_2^*-\theta_2) \tag{B2}$$

$$\dot{m}_j v_{jy}=\rho\int_0^{\delta_2}u_2v_2dz \tag{B3}$$

Conservation of mass and momentum for control volume 2 gives

$$\rho U_1(H-\delta_1)+\dot{m}_j=\rho U_2(H-\delta_2) \tag{B4}$$

$$P_1(H-\delta_1)+\rho U_1^2(H-\delta_1)=P_2(H-\delta_2)+\rho U_2^2(H-\delta_2) \tag{B5}$$

Velocity profiles for the boundary layer are needed to evaluate the integral quantities. Linear velocity profiles are assumed for the streamwise and cross-stream velocities as shown in Figure B2. As the flow is modeled as inviscid, the boundary layer is allowed to slip at the endwall with velocity components u_o and v_o.

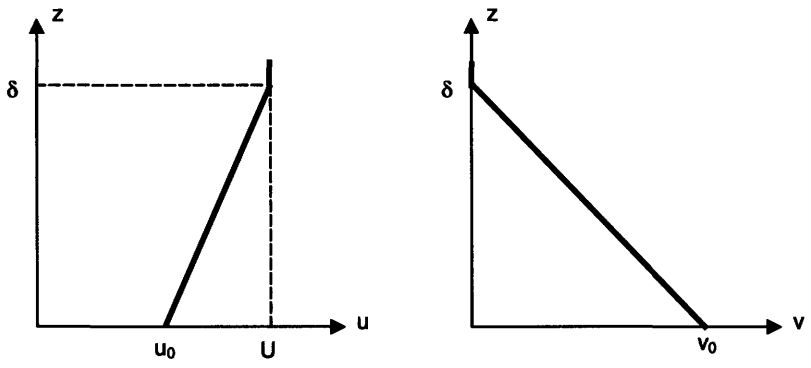

Figure B2 Linear velocity profiles assumed for the velocity in the direction of the freestream (u) and cross stream velocity (v).

The output of interest is the ratio of streamwise vorticity to normal vorticity at station 2. This is essentially the B coefficient required to calculate the D parameter. Since the primary focus is the change in vorticities from station 1 to station 2, these linear profiles are the simplest possible choices suitable for the analysis. The integral quantities of the boundary layer with the linear profiles are

$$\delta^* = \frac{\Omega}{2U}\delta^2 \tag{B6}$$

$$\theta = \delta^*(1 - \frac{2}{3}\frac{\delta\Omega}{U}) \tag{B7}$$

with vorticites in the normal and streamwise directions

$$\Omega = \frac{U - u_0}{\delta} \tag{B8}$$

$$\zeta = \frac{v_0}{\delta}. \tag{B9}$$

A complete system of nine equations with nine unknowns for station 2 is obtained. The system of equations can be reduced to a bi-quadratic equation in δ_2 which can be solved numerically.

Using the same geometry of D = 25 and with the same leakages considered in Section 2.4.4.1, the D parameters with effect of boundary layer skew are calculated and plotted in Figure B3.

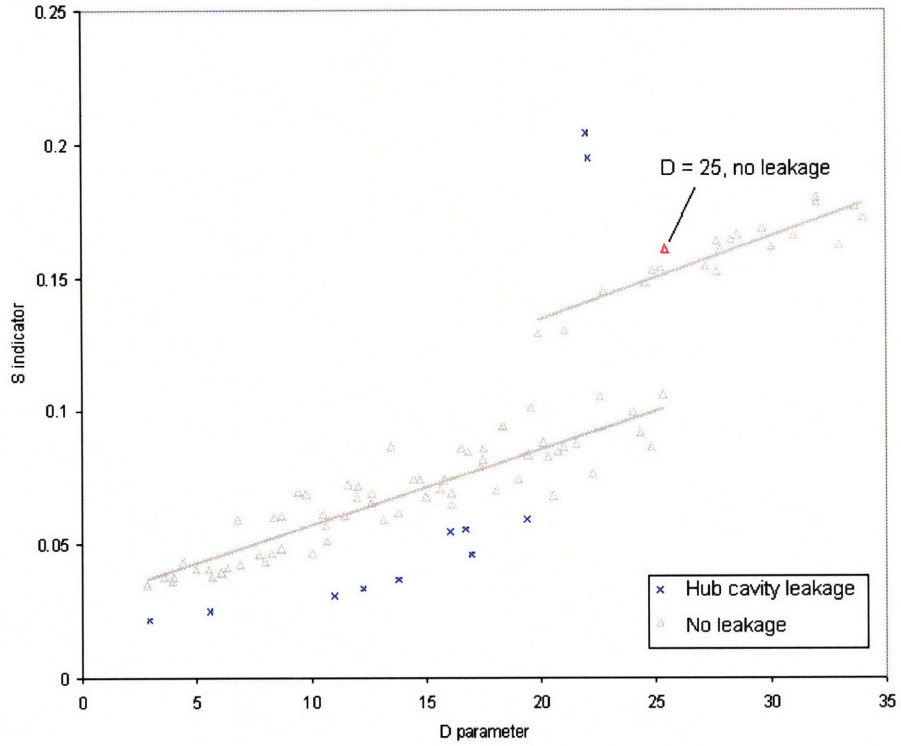

Figure B3 D parameter with cavity leakage effect from model. The baseline data from Section 2.3.3 are shown in grey.

The trend of the results agrees with the CFD results shown in Figure 2.24 but the D parameter calculated by the model is greater than that calculated from CFD data. To investigate the cause of the discrepancy, boundary layer profiles downstream of the leakage slot are examined. The streamwise and cross-stream velocity profiles downstream of the slot from both CFD and the model are compared in Figure B4. From the profiles of the velocity in the freestream direction (u), the boundary layer thickness and normal vorticities (as indicated by the slopes of the velocity profiles) are reasonably well predicted by the model. However, the streamwise vorticity from the model is less than that from CFD. The under-prediction in streamwise vorticity is the reason for the inadequate correction of the D parameter.

It is speculated that the assumption made regarding the distance at which cross-stream velocity gradient is non-zero is responsible for the under prediction of the streamwise vorticity. In the linear profile of the cross-stream velocity, it is assumed that the velocity gradient is zero at the edge of the

boundary layer (Figure B2). However, CFD data indicates that the distance over which the gradient of the cross-stream velocity is non zero is only half of the boundary layer thickness. If this observation is taken into account in the modeling of the velocity profile, the streamwise vorticity predicted will increase and the D parameter will decrease. However, it is unclear how the distance over which the velocity gradient is non zero can be prescribed more appropriately. Further investigation is required to improve the accuracy of the model such that it can be used to guide the design of flow control scheme to mitigate hub corner separation using hub cavity leakage.

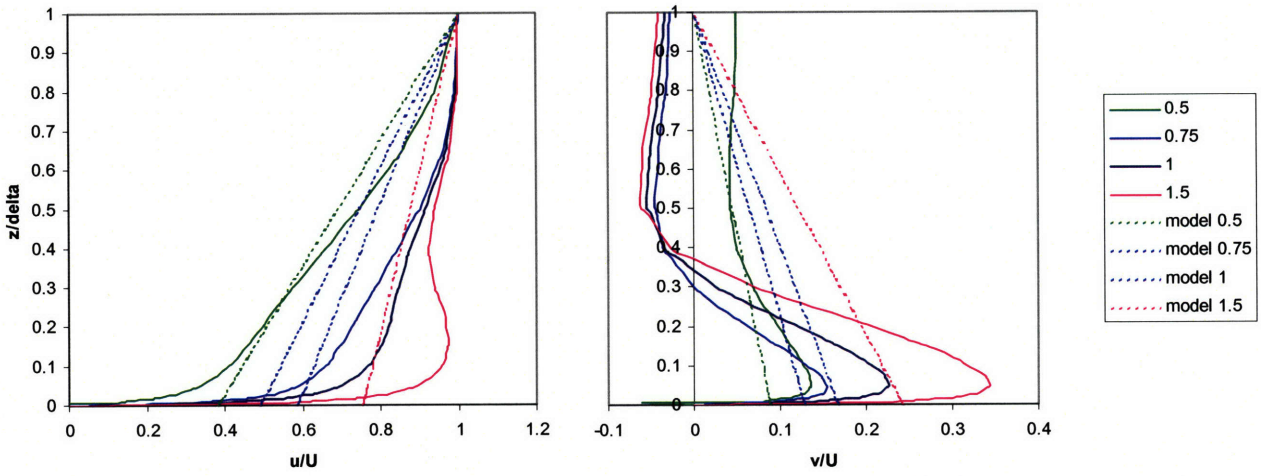

Figure B4 Velocity profiles of boundary layer downstream of leakage slot from CFD and model. Leakage fraction = 0.7% with various v_j/v_y.